INKJET PRINTED CONDUCTIVE INKS FOR THE FABRICATION OF ORGANIC THIN FILM TRANSISTORS

By:

Jason Doggart, B. Eng.

A Thesis

Submitted to the School of Graduate Studies

in Partial Fulfillment of the Requirements

for the Degree

Master of Applied Sciences

INKJET PRINTED CONDUCTIVE INKS FOR THE FABRICATION OF ORGANIC THIN FILM TRANSISTORS

MASTER OF APPLIED SCIENCES McMaster University

(Chemical Engineering) Hamilton, Ontario

TITLE: Inkjet Printed Conductive Inks For The Fabrication Of Organic Thin Film Transistors

AUTHOR: Jason Doggart, B. Eng.

SUPERVISORS: Dr. Shiping Zhu, Dr. Yiliang Wu

NUMBER OF PAGES: xxiv, 138

Abstract

In recent years, there has been a strong interest in the use of drop-on-demand inkjet printing for the fabrication of organic thin-film transistors (OTFTs). This method would allow for roll-to-roll fabrication of low-end, disposable, and large-area electronics such as RFID tags, sensors, and flexible displays at a small fraction of the current costs. A great deal of research has already yielded new materials which are solution processable and have demonstrated excellent performance when incorporated into OTFTs. One of the largest obstacles to the commercialization of this technology is the development of a successful strategy for the inkjet printing process. In order for this printing process to be successful, it must be able to deposit the components of the OTFTs such that they have sufficient resolution, excellent film thickness uniformity and excellent performance.

Here a strategy is developed which allows for high resolution printing of source and drain electrodes with excellent film uniformity. By simultaneously optimizing dot-to-dot spacing and solvent composition, near-perfect film uniformity and very high resolution can be obtained. Resolution is further improved via increasing the viscosity of the ink and decreasing the surface roughness of the substrate.

The inkjet printing system is further investigated and optimized for printing with silver nanoparticle ink. By using the design of experiments method, we determined the independent influence of silver nanoparticle mass fraction, solvent composition, substrate surface energy, substrate temperature and dot-to-dot spacing on printed line width, line thickness and film uniformity. Furthermore, this method also allowed for the

determination of the influence of variable interaction, allowing a complete understanding of the system to be developed. This knowledge was used to develop a non-linear computer optimization program such that optimal variable settings could be determined. As a result of this study, highly conductive silver lines with excellent resolution and film uniformity were inkjet printed and incorporated in high performance OTFTs.

A novel method for printing source and drain electrodes with a very small channel length was also developed. A silver nanoparticle ink with a large concentration of free alkylamine stabilizer was used in this study. The excess alkylamine formed a hydrophobic boundary around printed silver features, which repelled any ink subsequently deposited near the original feature. This allowed for source and drain electrodes to be printed with very narrow channel length with no need for any intermediate processing steps. Furthermore, the self-alignment nature of this technique allowed the process to automatically correct for slight printing errors, resulting in transistor arrays with very narrow channel length distributions.

Acknowledgements

I would like to express great thanks to my supervisors, Dr. Shiping Zhu and Dr. Yiliang Wu, for their constant support, insight, and encouragement. They have both been a tremendous help throughout this project.

I would also like to thank the members of Dr. Zhu's research group – Jerry Chen, Shane Gao, Ping Liu, Mary Jin, Sara Alibeik, Helen Gu, Thomas Kowpak, Mohammad Haj-bed and Mark Machado) for your encouragement and support.

I am grateful for the help I received from the research staff at the Xerox Research Center of Canada including Ping Liu, Yuning Li and the many co-op students who aided in this effort.

I am grateful for the financial support provided by the Natural Science and Engineering Research Council of Canada.

I thank my parents for their unwavering support throughout my whole life. Your love, kind words and encouragement allowed me to believe in myself. Also I would like to thank my sister and brother for their love and support.

Finally I would like to thank my wife, Shari, for her constant support, encouragement and love. This accomplishment was possible because you are in my life. I love you.

To Shari

Table of Contents

Abstract iii

Acknowledgements v

Table of Contents vii

List of Schemes xii

List of Figures xiii

List of Tables xxi

Chapter 1: Introduction 1

1.1 Background on Organic Thin Film Transistors 1

1.2 Materials for OTFT Fabrication 6

1.2.1 Organic Semiconducting Materials 6

1.2.2 Dielectric Materials 9

1.2.3 Conductive Materials 11

1.3 Fabrication of Organic Thin Film Transistors 14

1.3.1 Methods for OTFT Fabrication 14

1.3.2 Mechanics of Inkjet Printing 16

1.3.3 Inkjet Printing for OTFT Fabrication 17

1.4 Current Research 20

1.5 Research Objectives in Current Study 21

1.6 Thesis Outline 22

1.7 References 23

Chapter 2: A Novel Strategy for Improving Resolution and Film Uniformity in Inkjet Printing Silver Electrodes **30**

2.1 Introduction 30

2.1.1 Background on Organic Thin Film Transistors 30

2.1.2 Inkjet Printing 31

2.1.3 Current Challenges to Inkjet Printed Source and Drain Electrodes 32

2.1.4 Purpose of this Study 33

2.2 Materials and Methods 34

2.2.1 Conductive Ink 34

2.2.2 Inkjet Printer Parameters 35

2.2.3 Characterization 36

2.3 Results and Discussion 36

2.3.1 Substrate Surface Energy 37

2.3.2 Dot-to-Dot Spacing 38

2.3.3 Solvent Composition 43

2.3.4 Silver Acetate Concentration 48

2.3.5 Number of Printed Layers 55

2.3.6 Printer Nozzle Size 56

2.4 Fabrication of OTFT Devices 57

2.5 Conclusion 60

2.6 References 61

Chapter 3: Optimization of Inkjet Printing of Silver Nanoparticles Using Design of Experiments Method and Mixed Integer Non-Linear Optimization **65**

3.1 Introduction 65

3.1.1 Engineering the Inkjet Printing Process Using Design of Experiments 65

3.1.2 Optimizing the Inkjet Printing Process Using Non-Linear Programming 72

3.1.3 Purpose of this Study 73

3.2 Materials and Methods 74

3.2.1 Silver Nanoparticles 74

3.2.2 Ink Formulation and Printing 76

3.2.3 Input Variables Selected for Study 76

3.2.4 Output Variables Selected For Study 78

3.2.5 Experimental Design 80

3.3 Results of the DOE Study 81

3.3.1 Ink Properties 81

3.3.2 Conductivity 83

3.3.3 Line Width 84

3.3.4 Line Thickness 90

3.3.5 Center to Edge Height Ratio 93

3.3.6 Final Conclusions Based on DOE Study 96

3.4 Non-Linear Optimization 97

3.4.1 Development of Variables for Optimization Study 98

3.4.2 Development of Constraints for Optimization 98

3.4.3 Development of Objective Equations 102

3.4.4 Full Optimization Schemes 104

3.4.5 Results of Optimization Studies 108

3.4.6 Determining the Optimal Variable Setting 109

3.5 Fabrication of OTFT Devices 110

3.6 Conclusions and Recommendations 113

3.7 References 114

Chapter 4: A Novel Method for the Fabrication of Defect-Free Inkjet Printed Source and Drain Electrodes with >10μm Channel Length 118

4.1 Introduction 118

4.1.1 The Challenge of Decreasing Channel Length 118

4.1.2 Purpose of this Study 120

4.2 Materials and Methods 120

4.3 Results and Discussion 122

4.3.1 Scheme for Self Alignment Technique 122

4.3.2 Verification of Substrate Modification 123

4.3.3 Fabrication of Source and Drain Electrodes with Self Aligned Channel 123

4.3.4 Demonstration of Improved Channel Length Reproducibility 124

4.3.5 Fabrication of OTFT Devices 126

4.4 Conclusion 127

4.5 References 128

Chapter 5: Contributions, Perspective and Recommendations for Future Research **129**

5.1 Contributions to the Field 129

5.1.1 Improved Understanding of the Influence of Dot-to-Dot Spacing, Substrate Temperature, Surface Energy, and Ink Properties on Inkjet Printed Films 130

5.1.2 Optimization of Inkjet Printing Process for Fabrication of Electrodes with Silver Nanoparticle Ink 131

5.1.3 Development of Method for Defect Free Inkjet Printing of Source and Drain Electrodes with Self-Aligned and Very Narrow Channel 132

5.2 Perspective 133

5.3 Recommendations for Future Research 134

5.3.1 Optimization of the Inkjet Printing Process for Fabrication of Dielectric and Semiconductor Components 134

5.3.2 Optimization of Complete Device Fabrication 135

List of Schemes

Scheme 3.1 Optimization of line width using data from DOE study 105

Scheme 3.2 Optimization of line thickness using data from DOE study 106

Scheme 3.3 Optimization of Center to edge height ratio using data from DOE study 107

List of Figures

Figure 1.1: RFID tag (a), inkjet printed backpane for active matrix display (b) and example of e-paper (c). 1

Figure 1.2: Architecture of bottom gate – bottom contact (a), bottom gate – top contact (b) and top gate (c) thin film transistors 3

Figure 1.3: Schematic showing the creation of a channel of high charge carrier concentration. When no voltage is applied, transistor is in the 'off' state (a). Upon the application of a voltage, transistor switches to 'on' state (b). 4

Figure 1.4: Chemical structure of polyacetylene 7

Figure 1.5: Chemical structure of pentacene 8

Figure 1.6: Chemical structure of PQT – 12 9

Figure 1.7: Chemical structure of polyvinylphenol (a), poly(methyl methacrylate) (b) and poly(vinyl alcohol) (c). 11

Figure 1.8: Chemical structure of PEDOT (a) and PSS (b). 12

Figure 1.9: TEM image of silver (a) and gold (b) nanoparticles. 13

Figure 1.10: Illustration showing mechanism of a piezo electric print head 17

Figure 2.1: An OTFT array fabricated by researchers at PARC. This required the use of both additive and subtractive inkjet printing. 32

Figure 2.2: An illustration demonstrating electrode width and channel length measurements for typical OTFT devices. 33

Figure 2.3: Images illustrating silver precursor inkjet printed onto glass microscope slides which have been plasma cleaned (a), plasma cleaned and modified with HMDS (b) and plasma cleaned and modified with OTS (c). Image (a) was taken using a camera built into the Dimatix printer. Images (b) and (c) were taken using an optical microscope. 37

Figure 2.4: Optical micrographs and typical height vs. width profiles for annealed silver precursor inkjet printed using ink with 12.5 wt% silver acetate in n-butanol and 6.57 wt% ethylene glycol as cosolvent at dot-to-dot spacing of

(a) 20μm, (b) 40μm and (c) 80μm. Arrows indicate direction of solute migration. Scale bars indicate 50μm. 39

Figure 2.5: Illustration showing the coffee ring effect. Evaporation rate (represented by upward arrows) is highest at the edges of a drying droplet. Since the contact line is pinned, solvent flows out to edges to compensate for higher evaporation rate, resulting in all of the solute being deposited at the periphery. 40

Figure 2.6: Illustration showing the slip stick behaviour observed at low dot-to-dot spacing. The higher evaporation rate at the edges of the line causes an increased concentration of ethylene glycol (dark blue) which increases the peripheral surface tension. This causes the line to retract to a new, smaller width, depositing only a small amount of silver during the process. This process repeats continuously and results in the bulk of the solute being deposited in the middle of line. 41

Figure 2.7: Typical height vs. width profile illustrating the method for calculating the center to edge height ratio 42

Figure 2.8: Center to edge height ratio (h_c/h_e ratio) (▲,___) and line width (■,- - -) as a function of dot-to-dot spacing. Vertical line at 33μm shows optimal dot-

to-dot spacing ($h_c/h_e = 1$) and horizontal arrow shows corresponding line width. 43

Figure 2.9: Center to edge height ratio and line width as a function of dot-to-dot spacing for silver precursor inks formulated with 6.6% (♦), 13.1% (●), 19.7% (▲) and 26.3% (■) ethylene glycol. It is evident that the hc/he ratio vs. dot-to-dot spacing trend clearly shifts to the right when ethylene glycol concentration reaches 19.7%. 45

Figure 2.10: Optical microscope images of lines printed using inks of increasing ethylene glycol concentration and increasing dot-to-dot spacing. It is evident that as the ethylene glycol concentration increases the direction of the migration of the solute shifts towards the center. 47

Figure 2.11: Viscosity as a function of silver acetate for silver precursor inks. 49

Figure 2.12: Illustration showing the dynamics of droplets impacting a surface. Droplet impacts the surface (a), spreads due to kinetic energy (b) then recedes to some final radius determined by surface tension of the ink, surface energy of the substrate and the influence of contact line pinning. 50

Figure 2.13: The effect of viscosity on printed line width for silver precursor inks inkjet printed onto HMDS modified glass (▲) and HMDS modified silicon wafer (♦) substrates. 52

Figure 2.14: Optical microscope images of lines printed with from inks of different viscosities at different dot-to-dot spacing. 53

Figure 2.15: Center to edge height ratio at various dot-to-dot spacing for silver precursor inks with viscosity of 9.52cp (♦), 13.46cp (■) and 15.84cp (▲). 54

Figure 2.16: Optical microscope images of lines printed using one, two or three layers of 22% silver acetate ink. Only lines printed with three layers were found to be conductive. 56

Figure 2.17: Current vs. voltage curve for electrodes fabricated using a 10pL (a, solid line) and a 1pL (b, dotted line) nozzle. The electrodes were fabricated by printing three layers of 22% silver acetate ink, then annealing. The lines show excellent conductivity. Inset (c) demonstrates the excellent height vs. width profile obtained using a 1pL nozzle. 57

Figure 2.18: Schematic illustration method of fabricating OTFT devices using spin coated PQT–12 (a) and inkjet printed PQT–12 (e) and optical microscope images of actual devices (b and f). The performance of these devices was characterized by analyzing graphs showing drain current as a function of gate voltage (c and f) as well as drain current as a function of drain voltage for a range of gate voltages (d and g). 59

Figure 3.1: Ink viscosity as a function of silver nanoparticle mass fraction for inks with a solvent ratio of 5 (♦), 2 (■) and 1 (▲). 82

Figure 3.2: Ink surface tension as a function of silver nanoparticle mass fraction for inks with a solvent ratio of 5 (♦), 2 (■) and 1 (▲). 83

Figure 3.3: Organic thin film transistor fabricated using printed silver nanoparticle ink for source and drain electrodes. Electrodes were printed onto heavily doped n-type silicon wafer (gate) with a 200nm SiO_2 layer (dielectric). After the printed lines were annealed PQT – 12 was spin coated onto the wafer. 110

Figure 3.4: Drain current vs. gate voltage (a) and drain current vs. drain voltage for a variety of gate voltages (b). Data is for the device shown in figure 3. 111

Figure 3.5: Schematic showing method of fabricating top-gate organic thin film transistors 112

Figure 3.6: Top gate transistor fabricated using all solution processing methods. Silver nanoparticles were inkjet printed for the source, drain and gate electrodes, PQT-12 was inkjet printed for the semiconductor and PVP was spin coated for the dielectric. 112

Figure 4.1: The water contact angle of plasma cleaned glass (a) is shown to increase from 25° to 78° when the surface is modified with hexadecylamine (b). 121

Figure 4.2: Schematic illustrating the method used for self alignment. Droplets ejected from the inkjet printer impact the surface (a) and spread to a maximum radius R_m (b). The surface tension of the ink and the surface energy of the substrate then cause the ink to recede to some final radius R_f during which hexadecylamine is deposited on the substrate (c). Subsequent ink deposited in the proximity of the original feature is repelled by the hydrophobic boundary layer (d). This repulsion is evident in the optical microscope image shown (e). 122

Figure 4.3: To show that free hexadecylamine within the silver nanoparticle ink also modified the surface, two lines were printed 5mm apart and 4μL of water was dropped between them (a). It is evident from the optical microscope image (b) that a 50μm hydrophobic boundary exists around the printed silver. 123

Figure 4.4: When overlapping silver is printed on plasma cleaned glass it is evident that this hydrophobic boundary causes the second electrode to be repelled creating a narrow channel (a). When the same two electrodes are printed on hexadecylamine modified glass no repulsion is seen (b). 124

Figure 4.5: Optical microscope images of 10x10 transistor arrays printed using our new self aligning ink (a) and a commercial ink (b). Histograms showing distribution of channel lengths for transistors printed with new ink (c) and commercial ink (d). Scale bar in (a) and (b) indicates 300μm. 125

Figure 4.6: 10x5 OTFT array fabricated using inkjet printed silver source and drain electrodes and inkjet printed PQT–12 semiconductor (a). When magnified one can see the narrow and consistent channel achieved using this printing method (b). Shown is the drain current vs. gate voltage curve for a device fabricated on OTS–8 modified substrate. Devices fabricated in this manner showed very high mobility and on/off ratio. 127

List of Tables

Table 2.1: Original formulation of silver precursor ink 34

Table 2.2: Typical settings for inkjet printing silver precursor ink. 35

Table 2.3: Mass fraction of various components, surface tension and viscosity of various recipes used to study the effect of ethylene glycol concentration 44

Table 2.4: Mass fraction of various components, surface tension and viscosity of various recipes used to study the effect of ink viscosity 48

Table 3.1: Design matrix of a 2^3 experiment. Actual design matrix is highlighted. 68

Table 3.2: Variables examined along with high and low values used during Study 78

Table 3.3: Runs used for DOE study. +1 indicates high value of variable, -1 indicates low value. 80

Table 3.4: Conductivity of lines printed using various combinations of high and low settings for silver mass fraction, solvent ratio, substrate surface energy, substrate temperature and dot-to-dot spacing. 84

Table 3.5: Raw data showing line width obtained for each experimental run outlined in table 3. 85

Table 3.6: Value of coefficients in the equation describing the effect of silver nanoparticle concentration, solvent ratio, substrate surface energy, substrate temperature and dot-to-dot spacing on printed line width. Numbers associated with coefficients indicate variables or variable interactions. 1 = silver nanoparticle concentration; 2 = solvent ratio; 3 = substrate surface energy; 4 = substrate temperature; 5 = dot-to-dot spacing. 86

Table 3.7: Raw data showing line thickness obtained for each experimental run outlined in table 3. 90

Table 3.8: Value of coefficients in the equation describing the effect of silver nanoparticle concentration, solvent ratio, substrate surface energy, substrate temperature and dot-to-dot spacing on printed line thickness. Numbers associated with coefficients indicate variables or variable

interactions. 1 = silver nanoparticle concentration; 2 = solvent ratio; 3 = substrate surface energy; 4 = substrate temperature; 5 = dot-to-dot spacing. 91

Table 3.9: Raw data showing center to edge height ratio obtained for each experimental run outlined in table 3. 94

Table 3.10: Value of coefficients in the equation describing the effect of silver nanoparticle concentration, solvent ratio, substrate surface energy, substrate temperature and dot-to-dot spacing on center to edge height ratio. Numbers associated with coefficients indicate variables or variable interactions. 1 = silver nanoparticle concentration; 2 = solvent ratio; 3 = substrate surface energy; 4 = substrate temperature; 5 = dot-to-dot spacing. 95

Table 3.11: Conductivity of lines printed using various combinations of high and low settings for silver mass fraction, solvent ratio, substrate surface energy, substrate temperature and dot-to-dot spacing. 99

Table 3.12: Conductivity data for experiments performed with different combinations of variable settings. Variable setting combinations disallowed by constraints are shown shaded in grey. 100

Table 3.13: Optimal variable settings determined by optimizing system for various output variables 108

Table 3.14: Optimal variable setting for inkjet printing silver nanoparticle ink for fabrication of source and drain electrodes of OTFT devices. 110

Chapter 1

Introduction

1.1 Background on Organic Thin Film Transistors

Perhaps one of the most influential inventions of the twentieth century is that of transistor. This device has allowed for the miniaturization of computing devices to a size that was once thought to be utterly impossible. Transistors are now ubiquitous in our world and have been incorporated into cars, cellular telephones, display screens, computers, and an ever expanding list of other applications. As this technology has become further incorporated into society, it has become the hope of researchers that these devices would find their way into more common low end, disposable devices. These include applications such as security features on credit or debit cards, flexible and lightweight display screens, electronic paper and others (figure 1.1). Unfortunately, the cost of fabricating traditional transistors prohibits their use in such inexpensive applications.[1]

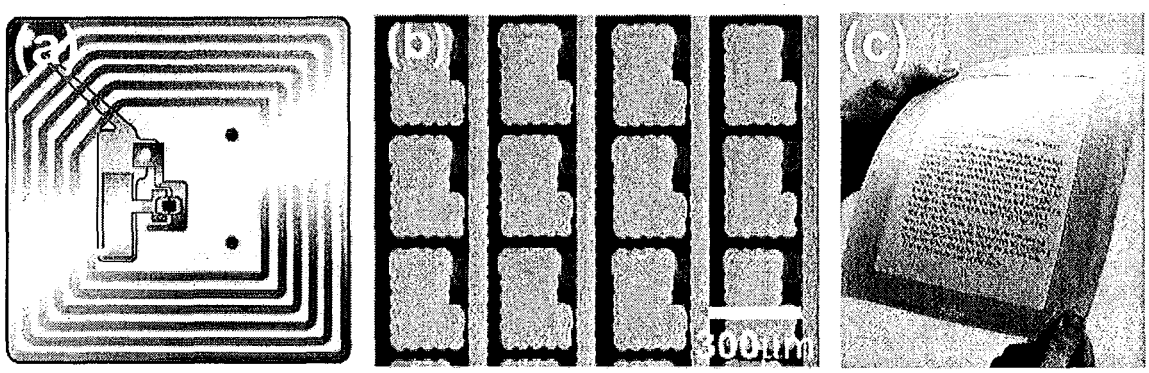

Figure 1.1: RFID tag (a), inkjet printed backpane for active matrix display (b) and example of e-paper (c).

In an effort to overcome this, a great deal of research has recently been devoted to the development of organic thin film transistors (OTFTs). These devices, which fall into the relatively new field of printed organic electronics, replace traditional inorganic semiconductors such as amorphous silicon with organic semiconductors. The benefit of this is found in the dramatically reduced processing costs associated with organic semiconductors. These materials are soluble, allowing for them to be solution processed (spin/spray coating, microprinting, inkjet printing). Furthermore, they require very low annealing temperatures (less than 150 °C) and can be processed in atmospheric conditions, precluding the need for the clean rooms and high temperatures required for inorganic semiconductors.[1, 2]

The mechanism by which organic semiconductors operate is considerably different than that of traditional semiconductors. Inorganic semiconductors are crystalline materials which conduct electricity either through electrons which have jumped to the conduction band or through the holes which remain in the valence band after the jump. Organic semiconductors, on the other hand, rely on electrons or holes 'hopping' between overlapping π bonds.[2] That being said, the basic device architecture of OTFT devices is fairly similar to that of traditional thin film transistors.

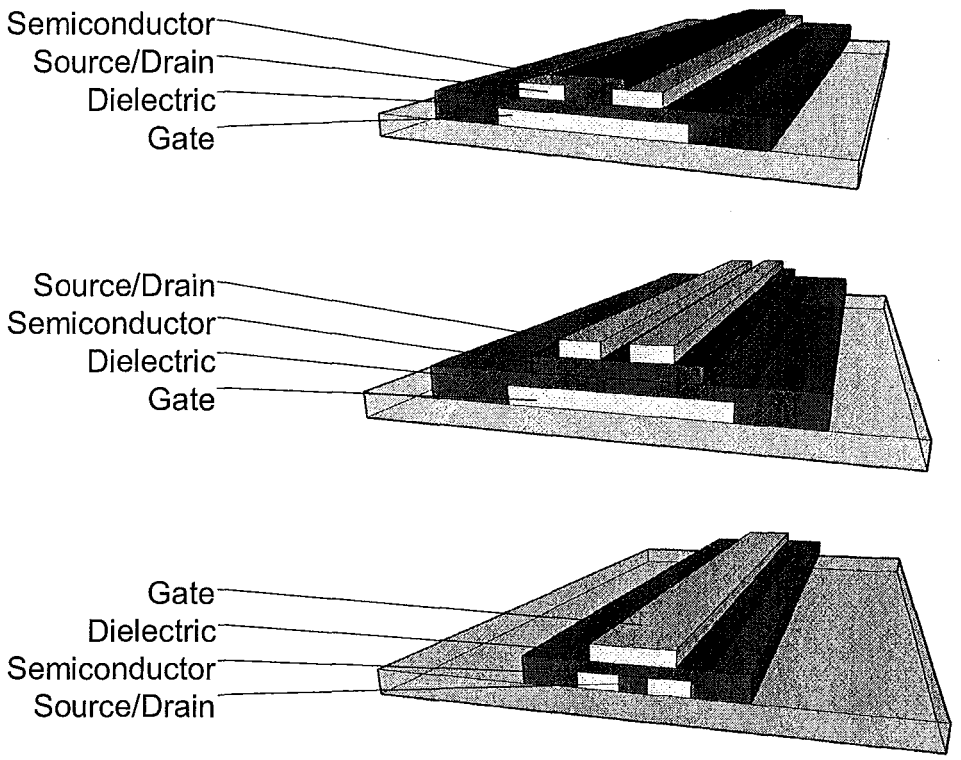

Figure 1.2: Architecture of bottom gate – bottom contact (a), bottom gate – top contact (b) and top gate (c) thin film transistors

There are several different device architectures which may be used. These may be classified into: bottom gate – bottom contact, bottom gate – top contact, and top gate. These can be seen in figure 1.2. Figure 1.3 illustrates the mechanism by which these devices operate. Shown is a bottom gate - bottom contact transistor which uses a p-type organic semiconductor. When a negative voltage is applied to the gate electrode, positive charges are accumulated at the semiconductor/dielectric interface. This creates a conductive channel (a high concentration of holes at the interface of the semiconductor

and the dielectric), allowing for holes injected from the source electrode into the semiconductor to be conducted to the drain electrode.[2]

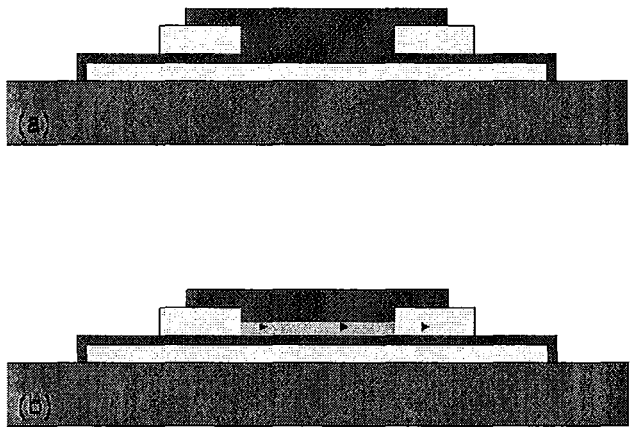

Figure 1.3: Schematic showing the creation of a channel of high charge carrier concentration. When no voltage is applied, transistor is in the 'off' state (a). Upon the application of a voltage, transistor switches to 'on' state (b).

There are two values which are generally used to characterize the performance of thin film transistor devices. The first is the charge carrier mobility (μ), which is the drift velocity of electrons through the semiconductor under a unit electric field. This parameter is used to characterize the speed of the device, and is especially important in devices which require many calculations. A typical inorganic thin film transistor has a mobility of 1 $cm^2/V \cdot s$. The second parameter most often used to benchmark these devices is the current on/off ratio. This is the ratio of the current through the semiconductor when the device is in its "on" state to the current when the device is in its "off" state. A typical on/off current ratio for an inorganic thin film transistor is 10^8.[1]

The architecture described in Figure 1.3 can be deceiving. Although it may appear that the fabrication and optimization of transistor devices is quite simple, the

opposite is in fact true. In order to achieve optimal mobility and on/off current ratio in a device there are many factors that must be considered. This is especially true when working with organic thin film transistors.

First, one must ensure that the material used for the source and drain electrodes is electrically compatible with the organic semiconductor. What this means is that the energy level at which the conductive material releases an electron must be the same or very close to the energy level at which the semiconductor receives an electron. This ensures that the source electrode is able to easily inject charge into the semiconductor.

Secondly, one must ensure that the organic semiconductor is deposited and annealed such that it has optimal molecular orientation. As previously discussed, organic semiconductors conduct charge via electrons 'hopping' between π bonds. In order for this to occur, these π bonds must be properly aligned. Ideally, these π bonds are stacked such that charge can easily move from the source through the semiconductor to the drain electrode.

Thirdly, it is necessary that the dielectric layer be as thin as possible. This minimizes the voltage required to put the device into the "on" state – something very desirable for low-end, low-power applications. However, it is also essential that in decreasing the thickness of this layer one does not induce the presence of "pinholes" in the layer. These tiny holes allow current to leak from the gate electrode to the semiconductor and source and drain electrodes which causes the device to short out. Thus it is necessary to carefully optimize the layer thickness.

Finally, to optimize the performance of these OTFT devices, it is necessary that the channel length (the distance between the source and drain electrodes) be as small as possible. By minimizing this length, one decreases the distance over which the charge carrier must be conducted, which greatly improves the performance of these devices.

Given the above requirements, it is evident that two aspects of device production are key to obtaining high performance transistors. The first is the choice of materials for the device, and the second is the method by which these devices are fabricated. These will be looked at in closer detail in the following sections.

1.2 Materials for OTFT Fabrication

1.2.1 Organic Semiconducting Materials

Organic semiconducting materials are a relatively new discovery. It was previously thought that all organic materials were always, to varying degrees, insulating. This notion began to fade slowly throughout the twentieth century. In 1906, it was discovered that some anthracene crystals possessed photoconductivity.[3, 4] Although this was a great discovery at the time, it nearly fifty years until an organic molecule (the perylene-bromine complex) was found to have any significant electrical conductivity.[5] A major breakthrough was achieved in 1973 when Coleman and coworkers synthesized tetrathiofulvalene-tetracyanoquinodimethane (TTF-TCNQ). This molecule had conductivity close to 8000 S/cm (typical metals have a conductivity of 100,000 S/cm) and an activation energy of nearly zero.[6]

The discovery that initiated the concept of organic semiconductors was made by Heeger *et al.* in 1977. This group discovered that by adding trace amounts of a donor or

an acceptor to polyacetylene they could vary the conductivity by eleven orders of magnitude.[7] This immediately began speculation of the use of organic molecules as semiconductors. This speculation became reality in 1983 when polyacetylene (figure 1.4) was used for the first time as the semiconductor in a functioning organic thin film transistor.[8] The performance of these organic thin film transistors increased dramatically as new materials were developed. These materials can be grouped into several classes based on their structure.

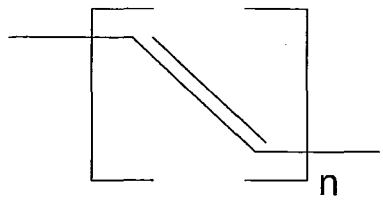

Figure 1.4: Chemical structure of polyacetylene

One of the most researched and most promising classes of organic semiconductor is acene-derived molecules. As has been previously mentioned, anthracene was one of the first organic molecules to show any kind of conductivity. Pentacene (figure 1.5) is currently one of the most promising organic semiconductors. It has shown tremendous charge carrier mobility up to 3 $cm^2/V \cdot s$ and on/off current ratio 10^5.[9] However this molecule is very susceptible to oxygen, is unstable under light, and is not soluble, and thus cannot be solution processed. For these reasons, there has been a recent drive to create soluble pentacene precursors which can be solution deposited then annealed to form pentacene.[10]

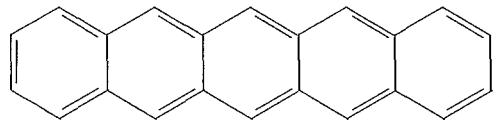

Figure 1.5: Chemical structure of pentacene

Another very popular class of organic semiconductor is polymer semiconductors. This class includes molecules such as polyacetylene [8] (described above) and polythiophene. The most studied polymeric semiconductor is poly(3-substituted thiophene), with poly(3-hexylthiophene) (P3HT) being the most popular.[11] Researchers found that by synthesizing this semiconductor with head-to-tail (regioregular) structure, the mobility could be improved by a factor of 10^4.[12] However, the conductivity of these molecules increased with exposure to air, causing the on/off ratio to decrease dramatically.[13, 14] In 2004, Ong et al. determined that by properly engineering polythiophene such that it had side chains which allowed for proper molecular ordering and atmospheric stability they would achieve a practical, useful organic semiconductor. The result of their work was poly (3-3'''-dialkylquaterthiophene) (PQT) (see figure 1.6). This semiconductor yielded device mobilities of up to 0.14 $cm^2/V \cdot s$ and on/off current ratios of over 10^7.[15]

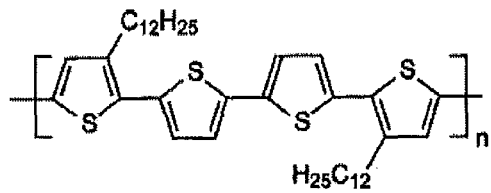

Figure 1.6: Chemical structure of PQT – 12

1.2.2 Dielectric Materials

Although a majority of the materials research associated with developing OTFTs has been devoted to the advancement of organic semiconductor materials, the other components of these devices have an equally important role in determining the final device performance. There has recently been a great push for the development of low cost solution processable dielectric and conductive materials.

Dielectric materials have a major influence on the performance of OTFT devices for several reasons. The purpose of the dielectric material is to insulate the gate electrode from the semiconductor and the source and drain electrodes, thus prevent device shortages and allow for an electric field to build up when the transistor is 'on'. One can immediately see that for adequate device performance the material chosen for the dielectric must have a suitably high dielectric constant. Furthermore, since many applications for OTFTs (such as RFID tags) have little voltage available, these dielectrics must be able to applied as a fairly thin film, allowing for the device to be in the 'on' state at a low threshold voltage. When a bottom gate architecture is used, the dielectric also directly influences the molecular ordering of the organic semiconductor. Recent work has found that including a layer of alkyl-trichlorosilane on top of the dielectric (which lowers the surface energy) drastically improves the molecular order of the semiconductor, which in turn greatly improves carrier mobility and on/off ratio.[16]

Materials which have been used for dielectric materials can be grouped into two different classes. First, there are inorganic materials. Typically these come into play for material testing. Typically new semiconductors are tested by building a device on

heavily doped n-type silicon (gate) with a thermally grown silicon oxide layer (dielectric).[9, 17, 18] Although this is clearly not a feasible solution for real-world applications, some groups have shown that there is some promise for inorganic dielectrics. Groups have shown that Al_2O_3, TiO_2, Ta_2O_5 and others can be sputtered onto devices at fairly low temperatures.[19-21] Unfortunately, this sputtering is costly and complex and this method requires fairly thick films to eliminate device shorting.

The second class of materials often used for dielectrics is polymeric materials. Most polymeric materials are known to be excellent insulators and to be generally soluble and thus solution processable. Furthermore, methods such as living radical polymerization allow for the synthesis of tailor-made polymers containing desirable functional groups. These materials can either be 'grown' from the surfaces using an in-situ polymerization, or they can be deposited via spin coating or another solution processing method. Often these materials are further crosslinked to improve performance. Polymers which have been previously investigated include polyimide,[22, 23] polyvinylphenol,[24] poly(methyl methacrylate),[25] poly(vinyl alcohol),[26] and many others (see figure 1.7).

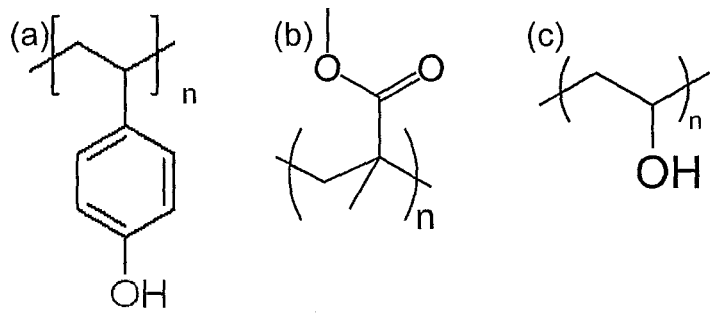

Figure 1.7: Chemical structure of polyvinylphenol (a), poly(methyl methacrylate) (b) and poly(vinyl alcohol) (c).

1.2.3 Conductive Materials

A great deal of recent research has also focused on the development of conductive materials for use as the source, drain and gate electrodes. These conductive components have a large influence on the performance of the OTFT, and thus the material and the fabrication method must be chosen with care. First, the material must obviously be able to yield highly conductive films. This is especially true for large area devices such as liquid crystal displays, where source electrodes are required to carry current over large distances. Secondly, the electrodes must be able to adequately inject charge carriers (electrons or holes) into the semiconductors. In order for this to occur, the work function of the electrode must match that of the semiconductor. The work function describes the energy necessary for a charge carrier to be discharged from the electrode or accepted into the semiconductor. If these work functions are not aligned, large charge injection barrier is induced so that little charge flows from the electrode to the semiconductor, giving poor transistor performance. Thirdly, the material must be easily solution processed to yield very uniform films which can be annealed at very low temperatures. Finally, to maintain the economic advantage that OTFTs pose over traditional thin film transistors, the material must be inexpensive and be solution processable. Given these requirements, researchers have developed several different materials which have shown varying degrees of promise.

One type of material which has been widely investigated is conductive polymers, the most popular and well-studied being a blend of poly(3,4-ethylenedioxythiophene) and polystyrene sulfonic acid (PEDOT-PSS) (see figure 1.8). PEDOT is a conductive

polymer which has been used extensively in various applications (antistatic coatings, conducting layers and hole-injecting layers). When this polymer is blended with PSS, the result is a stable complex which can be easily dispersed in aqueous solutions. This allows for easy solution processing at low temperatures.[27, 28] Unfortunately, the conductivity of these materials has yet to reach a level which makes them suitable for large area applications.

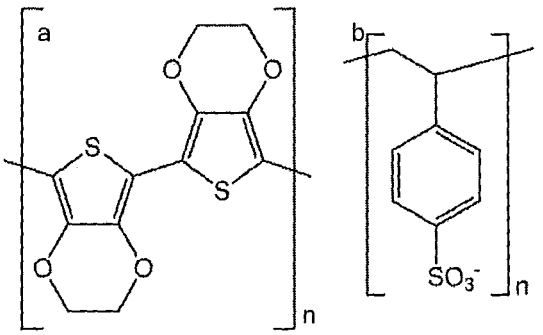

Figure 1.8: Chemical structure of PEDOT (a) and PSS (b).

An alternative material which has been developed is the use of metal precursors. These precursor solutions are typically synthesized by combining a metallic salt with a weak reducing agent and some form of stabilizer. When this solution is spread into a thin film and heated, the salt is reduced to form a highly conductive film of the elemental metal. These solutions have been developed for silver, gold, and gold-copper blends.[29-32] Although these are easily solution processed and yield excellent films, they tend to be unstable at room temperature and can yield non-uniform films. Work still continues in the development of these materials.

Another conductive material which has gained a great deal of popularity recently is metal nanoparticles. These nanoparticles can range in size from 1nm up to 100nm, and

are fabricated using a strong reduction agent in the presence of a stabilizer which remains on the nanoparticles to prevent aggregation. These nanoparticles have been synthesized using gold, silver, copper and other metals (see figure 1.9 as examples).[33-41] It has been shown that the stabilizer molecules have a large effect on the performance of OTFT devices fabricated using these nanoparticles. Furthermore, the choice of metal has a large effect on both cost and performance of the OTFT device.[35]

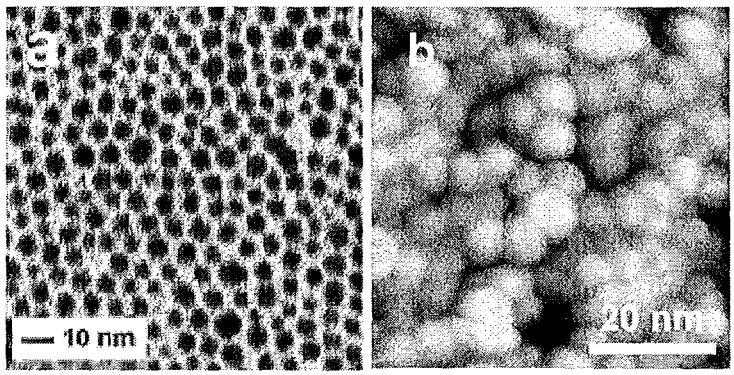

Figure 1.9: TEM image of silver (a) and gold (b) nanoparticles.

1.3 Fabrication of Organic Thin Film Transistors

1.3.1 Methods for OTFT Fabrication

Inasmuch as the choice of material for the semiconductive, dielectric and conductive components is essential to the performance of the OTFT, so to is the method of fabrication. Unfortunately this area has generated a disproportionately small amount of research.

The choice of fabrication method determines the attainable device dimensions. In order to improve the performance it is desired that one be able to fabricate these devices

such that they are as small as possible. Furthermore, the fabrication method used also determines the morphology of the resulting components. This influences not only the performance of the individual components but also how effectively these components can be integrated together.

In order to take advantage of the economic advantage presented by the use of organic semiconductors, it is essential that the method of fabrication chosen possess the following qualities:

- It must be a solution processing technique. This greatly reduces the cost of fabrication as well as the energy required to do so.
- It must allow for low temperature, low pressure processing in atmospheric conditions. This significantly reduces both capital and operating costs for device fabrication.
- It must allow for roll-to-roll continuous processing. This greatly reduces the cost and increases the device output rate.
- It must allow for production on a variety of substrates – including flexible polymeric substrates.
- It must result in high performance, high resolution devices.

There are a number of technologies which have been shown to possess some or all of these properties to varying degrees. Spin casting, for example, is a solution processing method in which a solution is dripped on to substrate which is being spun at a high rate. The shear force of the spinning drives the solution off the surface leaving only a very thin film. Although this method allows for excellent film uniformity, requires no high

temperature or pressure and can be performed in any environment, there is no method for patterning the solution – thus it cannot be used for complete fabrication of these devices.

Gravure printing is another fabrication method which has received some attention. In this method, a long roll of substrate is run in between two rotating cylinders. One of these cylinders contains a pattern of recessed areas. This cylinder is rotated through an ink bath, after which a razor runs over it to remove all ink except that held in the recessed areas. The second cylinder then impresses the substrate onto the first cylinder causing the ink to be transferred to the substrate.[2] This process is very fast, and allows for roll-to-roll continuous fabrication, however it has low resolution. Furthermore, a separate cylinder system is required for each component, which results in greatly increased capital costs.

Other methods which have generated some attention include flexography (in which a flexible relief of the pattern is used to deposit ink onto a substrate), screen printing or offset printing. Although all of these techniques possess some of the required properties, they are often lacking in one or more. Additionally, these processes are all performed using stencils or plates or cylinders, making a change in pattern very expensive and time consuming. These also require contacting the surface, which can cause damage to components which had been previously deposited.[1, 2]

In light of the shortcomings of the above processes, inkjet printing has recently arisen as a very promising fabrication method for OTFT devices. This method, which will be discussed in greater depth in the following section, allows for roll-to-roll continuous fabrication with high resolution and is performed at room temperature with no

high pressure or modified environments required. Furthermore, this process is performed without contacting the substrate, allowing for the integrity of previously deposited layers to remain intact. The patterns printed using inkjet printing are also created digitally using a computer, which means changes to these patterns are quick and easy to achieve.

1.3.2 Mechanics of Inkjet Printing

Inkjet printing is a fairly commonplace technology that was first developed in the early 1960's, and has since become ubiquitously used as a desktop printer for both commercial and residential purposes. Although this technology has been and continues to be widely used for graphic printing, in the past decade it has also been widely researched as a tool for 3D solution based fabrication. This has been demonstrated for fabricating models and small parts on the macro-scale, and also for the fabrication of small micro-scale devices, including OTFTs.

Typically inkjet printers used for fabrication use what is known as a drop-on-demand piezoelectric actuated print head for depositing ink. In this mechanism, ink is stored in a reservoir which is kept above a print head. A small volume of ink is drawn into the print head, which is a small channel typically made of glass and surrounded by a piezoelectric material. When a voltage is applied to this material it contracts, which squeezes the ink in the channel and forces it to be expelled out from the channel through the nozzle and down onto the substrate (See figure 1.10). This piezoelectric activity also acts to draw the next drop from the reservoir into the channel. Inkjet printers typically use anywhere from 1 – 256 channels and nozzles simultaneously, which allows for very high speed

printing. By printing multiple times in the same area, this method can be used to build up a three dimensional structure composed of one or many different inks.[42].

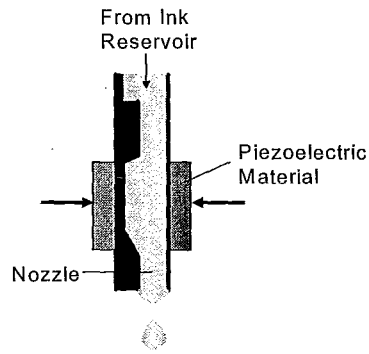

Figure 1.10: Illustration showing mechanism of a piezo electric print head

1.3.3 Inkjet Printing for OTFT Fabrication

There are many aspects of drop-on-demand piezoelectric inkjet printing which make it an ideal fabrication method for OTFTs. Inkjet printing is fast, highly resolute, requires little energy input, works well with any substrate and can incorporate a wide variety of inks. Furthermore the inkjetting process is very customizable. One can control voltage amplitude and waveform, temperature of ink, temperature of substrate, drop frequency, drop volume, and dot-to-dot spacing (distance between drops on a substrate). By controlling and optimizing these variables, one a gains great deal of control over the attainable resolution and the quality of the films deposited.[42]

Many groups have investigated the use of inkjet printing for fabricating both individual components of OTFTs and complete OTFTs. For each component (semiconductor, dielectric and conductive) there are separate challenges which must be addressed and overcome.

In order to inkjet print organic semiconductor such that high performance devices can be fabricated, the inkjet printing process must result in a thin film of semiconductor with sufficient molecular alignment to induce a high charge carrier mobility.[43] This has proven to be a cause of great difficulty, and a great deal of research has been devoted to improving the performance of inkjet printed semiconductors. This research has resulted in successful inkjet printing of a number of semiconductors including triisopropylsilylethynyl pentacene (a pentacene precursor).[43] and poly(3''-dialkylquaterthiophene) (PQT – 12).[44]

The dielectric component of OTFTs has proven to be difficult to inkjet print. This difficulty arises from the need for a very thin defect free layer. Where methods such as spin – casting allow for such a layer to be formed easily, this becomes very difficult when inkjet printing is employed. The reason for this is the presence of various drying effects which cause the solute contained within the ink to be selectively deposited during the drying or annealing process. This results in a layer with variable thickness and many defects. To overcome this obstacle, some groups have suggested simultaneously printing semiconductor and dielectric layers. This ink would separate once it had been deposited due to differences in surface tension (much like an oil and water mixture), resulting in a thin layer of semiconductor on the surface. Other groups continue to investigate methods for independently inkjet printing the dielectric. This remains an area of active research.

The inkjet printing of conductive components is a particularly interesting subject, as the width of the source and drain electrodes and the distance between them (the channel length) determine the overall dimensions of the transistor. Thus by improving the

resolution of the printer, one is able to simultaneously improve the performance of each individual transistor (by narrowing the channel) and fit more transistors in a device (by reducing the dimension). This is clearly desirable. In order for this fabrication method to be successful, however, the process must result in printed electrodes which have excellent film thickness uniformity. The improvement of both the film uniformity and the printing resolution has been the focus of a great deal of research. Many different inks have been successfully inkjet printed including PEDOT/PSS blends,[45, 46] metal precursors,[30, 32] and metal nanoparticles.[35, 36, 41, 44, 47] These inks have yielded highly conductive lines, however there remains a great deal of work to be performed in optimizing this printing process.

Some groups have investigated the use of inkjet printing for fabrication of complete OTFTs. This, however, has proven to be very difficult, and a completely inkjet printed OTFT device which uses only additive steps and requires no intermediate processing has yet to be reported. A group at PARC has demonstrated the fabrication of OTFTs which use inkjet printing for both additive and subtractive techniques.[44] However, their technique is costly and wasteful and requires many intermediate steps. Other groups have demonstrated all solution processed OTFTs with some components (usually the dielectric or the semiconductor) spin-cast, instead of inkjet printed. However this requires steps which hinder the desired roll-to-roll continuous processing. This is still a very active area of research.

1.4 Current Research

The field of inkjet printed organic thin film transistors is at a transition stage. Already materials have been developed which have been shown to yield high performance and excellent integration into devices. What remains to be developed is an effective method for fabrication. Although inkjet printing has been shown to be an ideal candidate for this fabrication, there remains a great deal to be discovered regarding methods for controlling resolution and film morphology. Furthermore if this method is to be successfully used in a commercial setting it must be completely optimized for each component.

It is evident that this field is moving from a stage of material science into a more engineering – focused fabrication and optimization phase. This phase will determine the feasibility of fabricating all solution processed OTFTs using inkjet printing, and will also be instrumental in determining the viability of this technology in a commercial setting.

1.5 Research Objectives In Current Study

Organic thin film transistors are in a position to radically change the microelectronics industry. Although there has been a great deal of successful materials research in this field, one of the major obstacles preventing the commercialization of this technology is fabrication. Inkjet printing has demonstrated a great deal of promise for this purpose, however there remains a great to be understood about the process. Although many groups have demonstrated that the materials which make up an OTFT can be inkjet printed, there has been little literature which describes methods for optimizing and

improving the process. This is particularly relevant for inkjet printed source and drain electrodes, as these features determine the overall dimensions of the device and have a significant influence over device performance.

The purposes of this thesis are:

1) To determine novel strategies for increasing the resolution and film morphology of inkjet printed source and drain electrodes such that these electrodes can be successfully integrated into OTFT devices;
2) Having determined the variables relevant to successful inkjet printing of source and drain electrodes, to perform a thorough optimization of these variables such that optimal printing conditions can be determined;
3) To develop novel methods for inkjet printing source and drain electrodes with a very narrow gap between them (small channel length).

1.6 Thesis Outline

Five chapters are presented in this thesis. The following is an outline of these chapters.

Chapter one is an introduction to the field of printed organic thin film transistors. Here a brief description of OTFTs is presented, including applications and the mechanism by which the devices operate. A review of recent advances in materials is also presented, including new developments in organic semiconductors, dielectrics and conductive materials. An overview of inkjet printing for fabrication of OTFTs is also presented including a description of the inkjet printing process and an overview of the

current state of research. Finally the purpose of the current project and an outline of this thesis is presented.

Chapter two presents a novel strategy for improving both the printing resolution and the film uniformity of inkjet printed silver electrodes. Silver precursor ink is investigated for the fabrication of source and drain electrodes. The effect of dot-to-dot spacing, solvent composition of the ink, ink viscosity and surface roughness on the printing resolution and film uniformity are investigated.

Chapter three depicts a complete optimization of the inkjet printing process for fabrication of source and drain electrodes using silver nanoparticle ink. The influence of five input variables on printing resolution, film uniformity, film thickness and conductivity was investigated using a design of experiments method. The results were then used to derive a non-linear optimization such that optimal variable settings could be determined.

Chapter four presents a novel and highly effective method for reducing the channel length that can be obtained using inkjet printing. A low surface energy agent present in silver nanoparticle ink causes a hydrophobic boundary to be present around all inkjetted features. This boundary repels any ink subsequently deposited resulting in a well defined, very narrow channel.

Chapter five presents the author's contribution to the field as well as their recommendations for future research.

1.7 References

1. Klauk, H. Organic Electronics. , 428 (2006).

2. Gamota, D. R., Brazis, P., Kalyanasundaram, K. & Zhang, J. Printed Organic and Molecular Electronics. , 695 (2004).

3. Koenigsberger, J. & Schilling, K. Über Elektrizitätsleitung in festen Elementen und Verbindungen. I. Minima des Widerstandes, Prüfung auf Elektronenleitung, Anwendung der Dissoziationsformeln. *Annalen der Physik* **337**, 179 (1910).

4. Pochettino, A. Sul comportamento foto-elettrico dell' antracene. *Academy of Lincei Rendic* **15**, 355 (1906).

5. Akamatu, H., Inokutchi, H. & Matsunaga, Y. Electrical conductivity of the perylene-bromine complex. *Nature* **173**, 168 (1954).

6. Coleman, L. B. *et al.* Superconducting fluctuations and the peierls instability in an organic solid. *Solid State Communications* **12**, 1125 (1973).

7. Chiang, C. K. *et al.* Electrical conductivity in doped polyacetylene. *Physical Review Letters* **39**, 1098 (1977).

8. Ebisawa, F., Kurokawa, T. & Nara, S. Electrical properties of polyacetylene/polysiloxane interface. *Journal of Applied Physics* **54**, 3255 (1983).

9. Klauk, H. *et al.* High-mobility polymer gate dielectric pentacene thin film transistors. *J. Appl. Phys.* **92**, 5259-5263 (2002).

10. Afzali, A., Dimitrakopoulos, C. D. & Breen, T. L. High-Performance, Solution-Processed Organic Thin Film Transistors from a Novel Pentacene Precursor. *J. Am. Chem. Soc.* **124**, 8812-8813 (2002).

11. Pron, A. & Rannou, P. Processible conjugated polymers: from organic semiconductors to organic metals and superconductors. *Progress in Polymer Science* **27**, 135-190 (2002).

12. Sirringhaus, H. *et al.* Two-dimensional charge transport in self-organized, high-mobility conjugated polymers. *Nature* **401**, 685-688 (1999).

13. Sirringhaus, H., Tessler, N. & Friend, R. H. Integrated, high-mobility polymer field-effect transistors driving polymer light-emitting diodes. *Synth Met* **102**, 857-860 (1999).

14. Bao, Z., Feng, Y., Dodabalapur, A., Raju, V. R. & Lovinger, A. J. High-Performance Plastic Transistors Fabricated by Printing Techniques. *Chemistry of Materials* **9**, 1299-1301 (1997).

15. Ong, B. S., Wu, Y., Liu, P. & Gardner, S. High-Performance Semiconducting Polythiophenes for Organic Thin-Film Transistors. *J. Am. Chem. Soc.* **126**, 3378-3379 (2004).

16. Wu, Y. *et al.* Controlled orientation of liquid-crystalline polythiophene semiconductors for high-performance organic thin-film transistors. *Appl. Phys. Lett.* **86**, 142102 (2005).

17. Tsumura, A., Koezuka, H. & Ando, T. Macromolecular electronic device: Field-effect transistor with a polythiophene thin film. *Appl. Phys. Lett.* **49**, 1210-1212 (1986).

18. Lin, Y. -., Gundlach, D. J., Nelson, S. F. & Jackson, T. N. Stacked pentacene layer organic thin-film transistors with improved characteristics. *Electron Device Letters, IEEE* **18**, 606-608 (1997).

19. Baude, P. F. *et al.* Pentacene-based radio-frequency identification circuitry. *Appl. Phys. Lett.* **82**, 3964-3966 (2003).

20. Stassen, A. F., de Boer, R. W. I., Iosad, N. N. & Morpurgo, A. F. Influence of the gate dielectric on the mobility of rubrene single-crystal field-effect transistors. *Appl. Phys. Lett.* **85**, 3899-3901 (2004).

21. L. A. Majewski, R. Schroeder,M.Grell,. One Volt Organic Transistor. *Adv Mater* **17**, 192-196 (2005).

22. Kato, Y. *et al.* High mobility of pentacene field-effect transistors with polyimide gate dielectric layers. *Appl. Phys. Lett.* **84**, 3789-3791 (2004).

23. Rogers, J. A., Bao, Z., Dodabalapur, A. & Makhija, A. Organic smart pixels and complementary inverter circuits formed on plastic substrates by casting and rubber stamping. *Electron Device Letters, IEEE* **21**, 100-103 (2000).

24. Gundlach, D. J., Lin, Y. Y., Jackson, T. N., Nelson, S. F. & Schlom, D. G. Pentacene organic thin-film transistors-molecular ordering and mobility. *Electron Device Letters, IEEE* **18**, 87-89 (1997).

25. Servet, B. *et al.* Polymorphism and Charge Transport in Vacuum-Evaporated Sexithiophene Films. *Chemistry of Materials* **6**, 1809-1815 (1994).

26. Parashkov, R. *et al.* All-organic thin-film transistors made of poly(3-butylthiophene) semiconducting and various polymeric insulating layers. *J. Appl. Phys.* **95**, 1594-1596 (2004).

27. Crispin, X. *et al.* The Origin of the High Conductivity of Poly(3,4-ethylenedioxythiophene)-Poly(styrenesulfonate) (PEDOT-PSS) Plastic Electrodes. *Chem. Mater.* **18**, 4354-4360 (2006).

28. Kirchmeyer, S. & Reuter, K. Scientific importance, properties and growing applications of poly(3,4-ethylenedioxythiophene). *JOURNAL OF MATERIALS CHEMISTRY}* **15}**, 2077-2088} (2005}).

29. Nur, H. M., Song, J. H., Evans, J. R. G. & Edirisinghe, M. J. Ink-jet printing of gold conductive tracks. **13**, 213-219 (2002).

30. Wu, Y., Li, Y. & Ong, B. S. A Simple and Efficient Approach to a Printable Silver Conductor for Printed Electronics. *J. Am. Chem. Soc.* **129**, 1862-1863 (2007).

31. Wu, Y., Li, Y. & Ong, B. S. Printed Silver Ohmic Contacts for High-Mobility Organic Thin-Film Transistors. *J. Am. Chem. Soc.* **128**, 4202-4203 (2006).

32. Gamerith, S. *et al.* Direct Ink-Jet Printing of Ag-Cu Nanoparticle and Ag-Precursor Based Electrodes for OFET Applications. *Advanced Functional Materials* **17**, 3111-3118 (2007).

33. Mallick, K., Witcomb, M. J. & Scurrell, M. S. Directional assembly of polyaniline functionalized gold nanoparticles. *Journal of Physics: Condensed Matter*, 196225 (2007).

34. Sanaur, S., Whalley, A., Alameddine, B., Carnes, M. & Nuckolls, C. Jet-printed electrodes and semiconducting oligomers for elaboration of organic thin-film transistors. *Organic Electronics,* **7**, 423-427 (2006).

35. Wu, Y., Li, Y., Liu, P., Gardner, S. & Ong, B. S. Studies of Gold Nanoparticles as Precursors to Printed Conductive Features for Thin-Film Transistors. *Chem. Mater.* **18**, 4627-4632 (2006).

36. Szczech, J. B., Megaridis, C. M., Zhang, J. & Gamota, D. R. INK JET PROCESSING OF METALLIC NANOPARTICLE SUSPENSIONS FOR ELECTRONIC CIRCUITRY FABRICATION. *Nanoscale and Microscale Thermophysical Engineering* **8**, 327 (2004).

37. Kim, D., Jeong, S., Park, B. K. & Moon, J. Direct writing of silver conductive patterns: Improvement of film morphology and conductance by controlling solvent compositions. *Appl. Phys. Lett.* **89**, 264101 (2006).

38. Noguchi, Y., Sekitani, T. & Someya, T. Organic-transistor-based flexible pressure sensors using ink-jet-printed electrodes and gate dielectric layers. *Appl. Phys. Lett.* **89**, 253507 (2006).

39. Li, Y., Wu, Y. & Ong, B. S. Facile Synthesis of Silver Nanoparticles Useful for Fabrication of High-Conductivity Elements for Printed Electronics. *J. Am. Chem. Soc.* **127**, 3266-3267 (2005).

40. Chong-an Di, Gui Yu, Yunqi Liu, Yunlong Guo, Ying Wang, Weiping Wu,Daoben Zhu,. High-Performance Organic Field-Effect Transistors with Low-Cost Copper Electrodes. *Adv Mater* **9999**, NA (2008).

41. Sunho Jeong, Kyoohee Woo, Dongjo Kim, Soonkwon Lim, Jang Sub Kim, Hyunjung Shin, Younan Xia,Jooho Moon,. Controlling the Thickness of the Surface

Oxide Layer on Cu Nanoparticles for the Fabrication of Conductive Structures by Ink-Jet Printing. *Advanced Functional Materials* **18**, 679-686 (2008).

42. Calvert, P. Inkjet Printing for Materials and Devices. *Chem. Mater.* **13**, 3299-3305 (2001).

43. Lim, J. A. *et al.* Self-Organization of Ink-jet-Printed Triisopropylsilylethynyl Pentacene via Evaporation-Induced Flows in a Drying Droplet. *Advanced Functional Materials* **9999**, NA (2008).

44. Arias, A. C. *et al.* All jet-printed polymer thin-film transistor active-matrix backplanes. *Appl. Phys. Lett.* **85**, 3304-3306 (2004).

45. Kawase, T., Shimoda, T., Newsome, C., Sirringhaus, H. & Friend, R. H. Inkjet printing of polymer thin film transistors. *Thin Solid Films,* **438-439**, 279-287 (2003).

46. Wang, J. Z., Zheng, Z. H., Li, H. W., Huck, W. T. S. & Sirringhaus, H. Dewetting of conducting polymer inkjet droplets on patterned surfaces. *Nat Mater* **3**, 171-176 (2004).

47. Zhao, N. *et al.* Self-aligned inkjet printing of highly conducting gold electrodes with submicron resolution. *J. Appl. Phys.* **101**, 064513 (2007).

Chapter 2

A Novel Strategy for Improving Resolution and Film Uniformity in Inkjet Printed Silver Electrodes

A part of this chapter is based on:

Doggart, J., Wu, Y. and Zhu, S. Inkjet printing narrow electrodes with < 50 μm line width and channel length for organic thin film transistors. *Applied Physics Letters*. **94**, 16.

2.1 Introduction

2.1.1 Background on Organic Thin Film Transistors

The past decade has witnessed tremendous progress in the field of organic electronics. Researchers have developed semiconductor materials with performance that rivals that of amorphous silicon and are solution processable in atmospheric conditions,[1] dielectric materials with exceptionally high dielectric constants which can be easily solution processed,[2-6] and conductive inks which can be solution processed and annealed at very low temperatures to yield films with conductivity equal to that of bulk metals.[7-19] These materials have been used to fabricate devices such as organic thin film transistors (OTFTs) with excellent performance and stability. In fact, groups have already demonstrated OTFTs fabricated using all solution processable materials.[20] These developments demonstrate the need for a shift in focus from materials research to fabrication research.

The main advantage of these OTFT devices is economic. These devices promise to drastically reduce the required capital investment, energy costs and fabrication expenses associated with thin film transistor production. In order for this technology to be commercialized, it is thus necessary to develop and optimize methods of fabrication which will deliver this economic incentive. One of the most promising methods for this is inkjet printing.

2.1.2 Inkjet Printing

Inkjet printing, known for decades in the graphic printing industry, has recently been shown to be an excellent method for three dimensional layer by layer fabrication. This method would allow for roll-to-roll continuous production of OTFTs on any substrate. Furthermore, inkjet printing allows for the use of inks with wide ranging properties, and can print these inks with a range of droplet velocity, temperature, and volume. Putting it succinctly, inkjet printing allows for many degrees of freedom in the fabrication process.[21]

As discussed in Chapter 1 of this work, inkjet printing has already been demonstrated as an excellent method for device fabrication. Researchers have shown that semiconductors,[22] dielectrics [20] and conductive materials [8, 10, 13, 14, 19, 20, 23-25] alike can be printed to yield high performance components. In fact, researchers at PARC have demonstrated that through the use of additive and subtractive inkjet printing all inkjet printed transistors can indeed be fabricated (see figure 2.1).[20] This process, however, still requires etching and is not roll to roll. Thus, although these components have been

shown to be successfully printed independently, the ability to fabricate an all inkjet printed OTFT with no etching, lithography, or other intermediate processing step, remains elusive. One of the greatest obstacles towards obtaining this all inkjet printed device is a lack of understanding regarding method of controlling the morphology, resolution and performance of inkjet printed films. Specifically, there is a strong void of information regarding methods of controlling printing resolution and printed film uniformity.

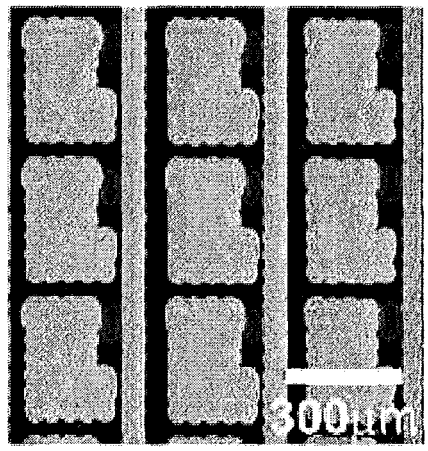

Figure 2.1: An OTFT array fabricated by researchers at PARC. This required the use of both additive and subtractive inkjet printing.[20]

2.1.3 Current Challenges to Inkjet Printed Source and Drain Electrodes

In order for OTFT devices to be commercially relevant, they must offer not only an economic advantage but also performance which is at least equal to that of traditional thin film transistors. This performance is largely governed by two properties: resolution and film uniformity. This is especially true for the fabrication of the source and drain electrodes of these devices. The space between these electrodes is called the device channel. To optimize device performance, it is desired that this channel be as narrow as

possible (See figure 2.2). Furthermore, to increase the number of transistors that can be fabricated within a certain area, it is desired that the width of the electrodes themselves be as small as possible. One can also imagine that the uniformity of these electrodes will have a strong influence on their conductivity, and in turn on the final device performance.

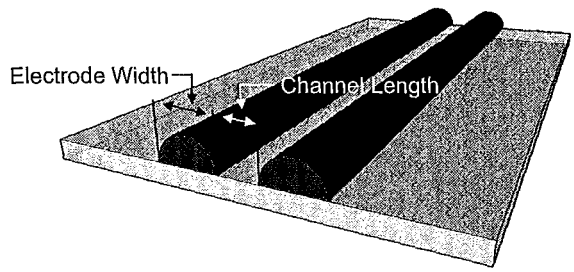

Figure 2.2: An illustration demonstrating electrode width and channel length measurements for typical OTFT devices.

2.1.4 Purpose of this Study

In this portion of this work, the inkjet printing of source and drain electrodes for OTFT devices was investigated. The influence of numerous ink properties and printer parameters was examined. The goal through this portion was to develop a novel strategy for both ink formulation and inkjet printing which would yield electrodes with both excellent film uniformity and very high resolution.

2.2 Materials and Methods

2.2.1 Conductive Ink

For this study, a silver precursor ink was used as the conductive material. This material had been previously developed by the Xerox Research Center of Canada (XRCC). This ink has previously been shown to yield films with excellent conductivity ($2x10^4$S cm^{-1}) when annealed at very low temperatures.[8] To anneal the films, they were simply placed on a 180°C hot plate for 10 minutes in atmospheric conditions. The ink comprises silver acetate, ethanolamine (weak reducing agent), lauric acid (homogenizes the silver film), and ethylene glycol (improves printability) all dissolved in n-butanol. The composition of the original formulation can be seen in table 2.1. This ink was chosen because it was readily available, inexpensive, simple to synthesize and, most importantly, has been shown to yield high performance when incorporated into OTFT devices.

Table 2.1: Original formulation of silver precursor ink

Material	Mass Fraction
n-butanol	0.66
Ethylene glycol	0.07
Silver acetate	0.13
Ethanolamine	0.13
Lauric acid	0.01

This silver precursor ink was printed using a Dimatix DMP 3200 material inkjet printer. This printer uses a refillable piezoelectric drop on demand inkjet print head to deposit material. It allows for control over many of the printing properties including substrate temperature, nozzle temperature, voltage amplitude and waveform, dot-to-dot

spacing and distance from nozzle to substrate. This printer also allowed for easily customizable printing patterns.

2.2.2 Inkjet Printer Parameters

A series of preliminary studies was performed to determine the optimal settings for printing the silver precursor ink. The printer allowed for real time adjustment of the waveform and voltage to optimize droplet shape and velocity. The voltage waveform was adjusted such that the droplets ejected from the printer were spherical and had no satellite droplets. The voltage amplitude was set such that the droplets were leaving the nozzle at a velocity of 5m/s. This velocity was recommended by the Dimatix corporation to yield optimal printing. These settings can be seen clearly in table 2.2.

Table 2.2: Typical settings for inkjet printing silver precursor ink.

Property	Setting
Typical voltage amplitude	14V
Waveform used	Dimatix Model Ink Waveform (default)
Nozzle Temperature	Room Temperature
Substrate Temperature	Room Temperature
Distance from print head to substrate	0.5mm
Jetting Frequency	1kHz
Droplet Velocity	5m/s

Because the silver precursor ink in use contains a weak reducing agent, increases in temperature at any stage of printing were avoided. Although it has been shown by other groups that increased substrate temperature results in higher resolution, it was

found that any increase in temperature reduced the quality of the printed films. Also, increasing the temperature of the nozzle during printing was found to adversely affect the stability of the ink. Although for some formulations some temperature increase was necessary for printing, this was avoided where possible.

During this study both 10pL and 1pL print heads were used. These print heads have nozzle diameters of 23μm and 13μm, respectively.

2.2.3 Characterization

Each ink formulation was studied by printing three lines on the same substrate. Each line was then studied at two separate locations. Lines were characterized using a Dektak – 6 surface profilometer. This device uses a stylus which moves across the lines to measure their width and height. Film morphology was also viewed using an optical microscope. Conductivity was tested using a Keithly two point probe. Transistor device characterization was performed using a Keithly three point probe system.

2.3 Results and Discussion

During the course of this study several variables were analyzed. These include substrate surface energy, dot-to-dot spacing, solvent composition and silver acetate concentration. Below is a discussion of the influence of these variables on the resolution and film morphology of inkjet printed silver precursor electrodes.

2.3.1 Substrate Surface Energy

The substrate onto which the ink was printed was also an important consideration. As an initial study, ink was printed onto three different glass microscope surfaces. The first surface was washed in ethanol, dried, plasma cleaned, then washed in water and ethanol, and air dried. The second was treated similarly, then soaked in a 1% hexamethyldisalizane (HMDS) solution for 20 minutes to decrease the surface energy of the substrate. This modification has been shown to yield surfaces with a water contact any of about 67° (compared to 30° for plasma cleaned glass). Finally the third substrate was plasma cleaned like the first, then soaked in a 1% octyltrichlorosilane (OTS) solution for 15 minutes at 60°C. This modification has been shown to yield glass with a water contact angle of 95°.

Figure 2.3: Images illustrating silver precursor inkjet printed onto glass microscope slides which have been plasma cleaned (a), plasma cleaned and modified with HMDS (b) and plasma cleaned and modified with OTS (c). Image (a) was taken using a camera built into the Dimatix printer. Images (b) and (c) were taken using an optical microscope.

Figure 2.3 shows images of these lines taken using a camera built into the Dimatix printer (a) and using an optical microscope (b and c). From these images, it is evident that ink printed onto the plasma cleaned surface was seen to wet the surface very easily. In fact, a single printing pass yielded a line which was over 500μm wide – much too wide for any practical use. Ink printed on the second surface yielded lines which were drastically improved – lines of about 300μm were obtained. The third surface was

found to have too low of a surface energy, which caused the ink to become discontinuous and aggregate into droplets on the substrate. Given the results of this study, it was decided that HMDS modification would be used for all substrates in this study.

2.3.2 Dot-to-Dot Spacing

Previous work in this field has demonstrated that dot-to-dot spacing during printing has a strong influence on printed line width.[26] Dot-to-dot spacing describes the linear distance between drops during printing. One can intuitively observe that decreasing the distance between adjacent drops increases the volume deposited per unit length. This additional volume causes the line to spread to a wider width, decreasing the resolution. Thus, to decrease the line width, one must increase the dot-to-dot spacing.

Using this previous work as a starting point, we printed silver lines with the original silver precursor developed by the XRCC at varying dot-to-dot spacings. After annealing, these lines were analyzed by both an optical microscope and a Dektak-8 surface profilometer.

Figure 2.4 shows the optical micrographs along with typical height vs. width profiles for silver lines printed with the original ink formulation at increasing dot-to-dot spacing. It was immediately apparent from both the images from the optical microscope and the results of the surface profilometer that the dot-to-dot spacing did indeed have a strong influence over the line width. In fact, increasing the dot-to-dot spacing from 20μm to 80μm decreased the line width from 480μm to 171μm – a 64% decrease. However, there was also another, more surprising effect. It was observed that the dot-to-dot

spacing also had a very powerful influence on the direction of solute migration during line annealing. These results showed that at lower dot-to-dot spacing, solute tended to move towards the center of the line, forming a center heavy triangular shaped line. At higher dot-to-dot spacing, however, this trend was reversed, and it was seen that the solute moved entirely to the edge of the line during annealing, resulting in a hollow center.

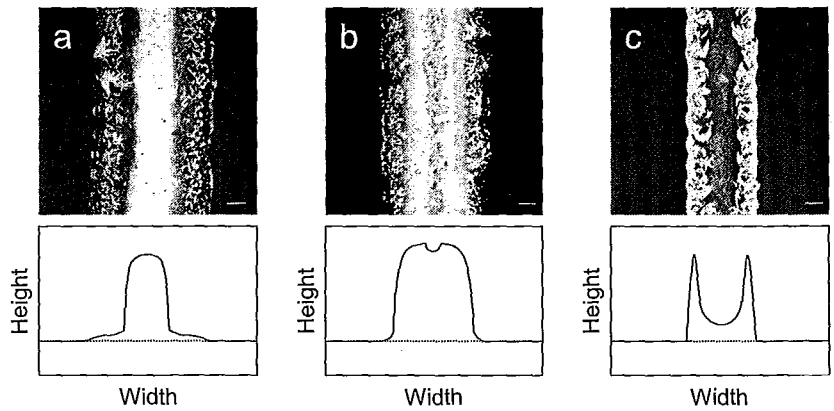

Figure 2.4: Optical micrographs and typical height vs. width profiles for annealed silver precursor inkjet printed using ink with 12.5 wt% silver acetate in n-butanol and 6.57 wt% ethylene glycol as cosolvent at dot-to-dot spacing of (a) 20μm, (b) 40μm and (c) 80μm. Arrows indicate direction of solute migration. Scale bars indicate 50μm.

This surprising result can be explained through an investigation of the behavior of drying droplets. A great deal of research has been performed in this field as it has many wide ranging applications (printing, paints, coatings, etc). One of the most studied phenomena in this field is the 'coffee ring' effect. This describes the propensity of solute to migrate towards the edge of the droplet during drying. It has been shown that the evaporation rate at the edge of drying droplet is higher than the evaporation rate at the center.[27-31] Furthermore, it has been found that surface roughness and chemical homogeneities found on most surfaces cause the boundary of a droplet to be pinned – that

is to say the diameter of the droplet does not change as it dries.[27] Because of this contact line pinning, solvent from the center of the droplet flows to the perimeter to compensate for the higher evaporation rate. This flow brings solute with it and can cause nearly all of the solute to be deposited at the periphery. This effect can be seen graphically in figure 2.5.

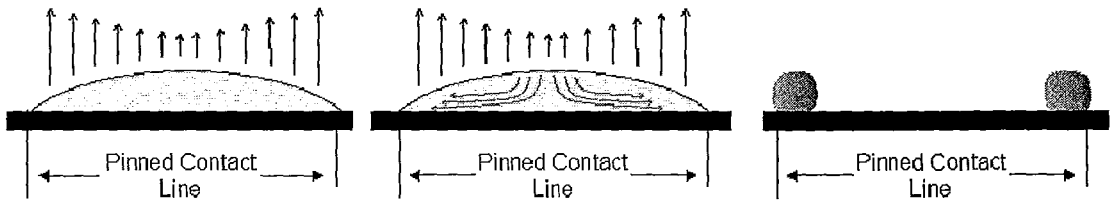

Figure 2.5: Illustration showing the coffee ring effect. Evaporation rate (represented by upward arrows) is highest at the edges of a drying droplet. Since the contact line is pinned, solvent flows out to edges to compensate for higher evaporation rate, resulting in all of the solute being deposited at the periphery.

The coffee ring effect explains the behaviour observed at high dot-to-dot spacing for our system. However, it does not explain why the solute actually moved towards the center for low dot-to-dot spacing. To explain this, one must observe that at low dot-to-dot spacing, the resulting printed line is much wider. This causes the evaporation rate gradient to be spread over a large distance, which weakens the driving force compelling solvent to move towards the edge.

Furthermore, the added volume found in these wider lines causes them to dry more slowly than their thinner counterparts. As they dry, the edges become more concentrated with ethylene glycol due to its higher boiling point. Ethylene glycol also has a significantly higher surface tension that n-butanol. Thus, as the concentration of the edge

shifts, the surface tension rises. This causes the line to contract to a new width, where this pattern will happen again. This slip-stick pattern is similar to those that have been previously reported for self assembly studies using dip coating.[32] The result in this case is little deposition at the edges and a majority of deposition at the center. This behavior is illustrated in figure 2.6.

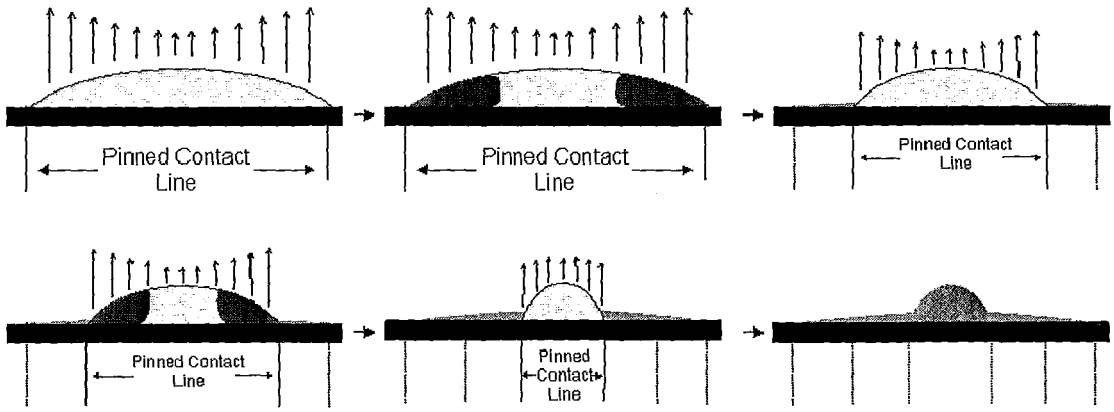

Figure 2.6: Illustration showing the slip stick behaviour observed at low dot-to-dot spacing. The higher evaporation rate at the edges of the line causes an increased concentration of ethylene glycol (dark blue) which increases the peripheral surface tension. This causes the line to retract to a new, smaller width, depositing only a small amount of silver during the process. This process repeats continuously and results in the bulk of the solute being deposited in the middle of line.

The benefit of this trend in solute migration is that there is a possible dot-to-dot spacing at which there is no solute migration – that is to say the film thickness is uniform across the entire width of the line. To determine what this dot-to-dot spacing is, the migration of solute was quantified using a center to edge height ratio. This ratio was defined as the ratio of the average of the center fifty percent of the line to the average height of the outer fifty percent of the line (see figure 2.7). A high center to edge height ratio indicates then that the majority of the solute has moved into the center, whereas a

low center to edge ratio height ratio indicates that most of the solute has moved towards the edge. Ideally one would desire a center to edge height ratio of one, as this would indicate uniform film thickness across the entire line.

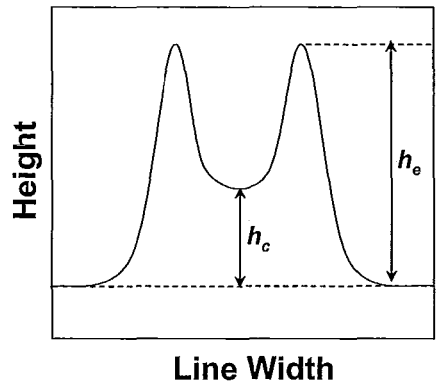

Figure 2.7: Typical height vs. width profile illustrating the method for calculating the center to edge height ratio

When this center to edge height ratio was calculated and plotted against the corresponding dot-to-dot spacing a clear trend emerged (See figure 2.8). From this trend it was evident that for the original silver precursor formulation the ideal center to edge height ratio was achieved using a dot-to-dot spacing of about 33μm. Unfortunately, this dot-to-dot spacing resulted in a printed line width of 350μm. This is much too wide for practical use in OTFT devices, where we desire a line width of less than 100μm. Furthermore, this line width would result in a very thin electrode, which would in turn severely degrade its conductivity.

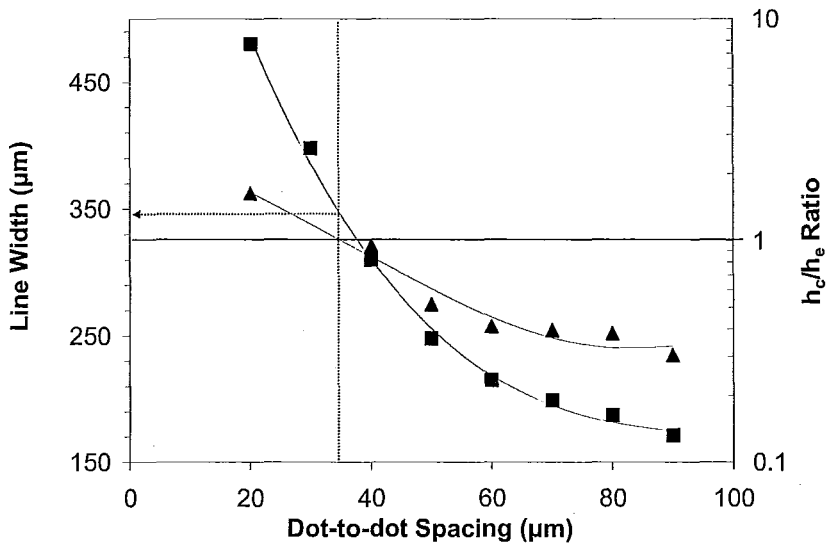

Figure 2.8: Center to edge height ratio (h_c/h_e ratio) (▲,___) and line width (■,- - -) as a function of dot-to-dot spacing. Vertical line at 33µm shows optimal dot-to-dot spacing ($h_c/h_e = 1$) and horizontal arrow shows corresponding line width. Center to edge height ratio data has error of ±0.35. Line width data has error of ±23.4µm.

2.3.3 Solvent Composition

In an effort to decrease the attainable line width, the concentration of ethylene glycol in the ink was modified. Previous studies have shown that printed line morphology is greatly affected by the addition of a high boiling point cosolvent.[29, 33] It was expected that modifying this concentration would shift the center to edge height ratio versus dot-to-dot spacing curve to the right. This would allow the optimal dot-to-dot spacing to be higher, resulting in thinner lines.

The concentration of ethylene glycol was varied between 6.6% and 26.3%. The exact formulations of the inks are shown in table 2.1. When formulating these inks, it was desired that only the ratio of ethylene glycol to n-butanol change and that the concentration of silver acetate, ethanolamine and lauric acid remain constant. Thus as the

concentration ethylene glycol was increased, the concentration of n-butanol was correspondingly decreased.

The recipes used for the ink formulations can be seen in table 2.3. In an effort to better understand the effect of ethylene glycol concentration on ink properties, the viscosity and surface tension were measured for each recipe. These values are also displayed in the table. From this data, it is evident that ethylene glycol concentration has only a small effect on the surface tension, whereas it has a very substantial effect on the viscosity. The increase in viscosity with higher ethylene glycol concentration did not hinder the printing process, however.

Table 2.3: Mass fraction of various components, surface tension and viscosity of various recipes used to study the effect of ethylene glycol concentration. Measurements were taken at 25°C. Error in surface tension measurements is ± 1mN/m. Error in viscosity measurements is ± 0.03cp.

Recipe	n-butanol	Ethylene Glycol	Lauric Acid	Silver Acetate	Ethanol-amine	Surface Tension (mN/m)	Viscosity (cp)
1	0.66	0.07	0.01	0.13	0.13	25.96	7.88
2	0.59	0.13	0.01	0.13	0.13	26.44	8.85
3	0.52	0.20	0.01	0.13	0.13	26.82	9.52
4	0.46	0.26	0.01	0.13	0.13	27	12.02

Lines were printed at various dot-to-dot spacing for each of the ink formulations, and the resulting line widths and center to edge height ratios were plotted against the dot-to-dot spacing (Figure 2.9). From this graph, it was evident that the inks with ethylene glycol concentration of 6.6% and 13.2% behaved drastically different that those with ethylene glycol concentration of 19.7% and 26.3%. It is clear that when the ink was formulated using these higher concentrations of ethylene glycol, the center to edge height ratio versus dot-to-dot spacing curve was shift towards the right, with the optimal dot-to-

dot spacing now being found to be close to 80μm. The change in ethylene glycol concentration was found to have minor impact on the line width, especially beyond dot-to-dot spacing of 60μm. Thus, using these new high ethylene glycol concentration ink formulations, line width of 190μm can be obtained – a 45% increase in resolution.

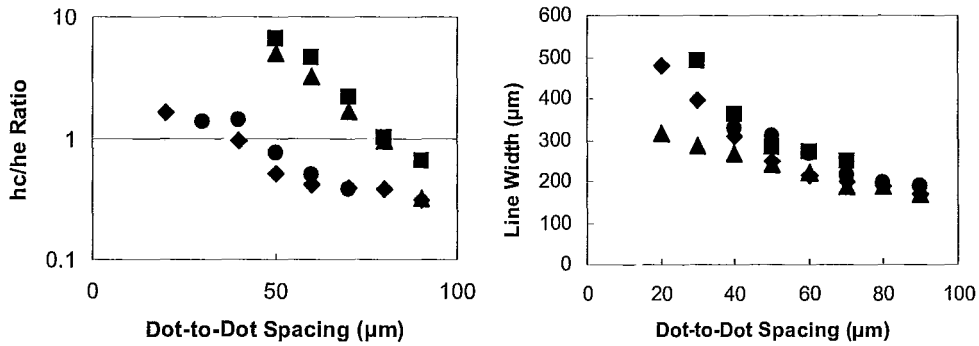

Figure 2.9: Center to edge height ratio and line width as a function of dot-to-dot spacing for silver precursor inks formulated with 6.6% (♦), 13.1% (●), 19.7% (▲) and 26.3% (■) ethylene glycol. It is evident that the hc/he ratio vs. dot-to-dot spacing trend clearly shifts to the right when ethylene glycol concentration reaches 19.7%. Center to edge height ratio has error of ±0.43. Line width data has error of ±25.3μm.

This shift in center to edge height ratio with changing ethylene glycol concentration indicates that the ink solvent composition has a strong influence on solute migration during annealing and drying. As described above, ethylene glycol has been seen to cause solute to deposit in the center of the printed line. This was suspected to be caused by increases in surface tension during drying. As the concentration of ethylene glycol was increased, the change in surface tension would have improved strength, and thus would have an impact even at higher dot-to-dot spacing. Note that this increase in surface tension is dynamic, and is not related to surface tensions shown in Table 2.3. This would cause the center to edge height ratio to be higher that was previously seen, shifting this

trend to the right. Images taken using an optical microscope allow one to confirm visually that as the concentration of ethylene glycol increases solute tended to migrate towards the center. This can be seen in figure 2.10, which shows optical microscopic images for inks of various ethylene glycol concentration printed with various dot-to-dot spacing.

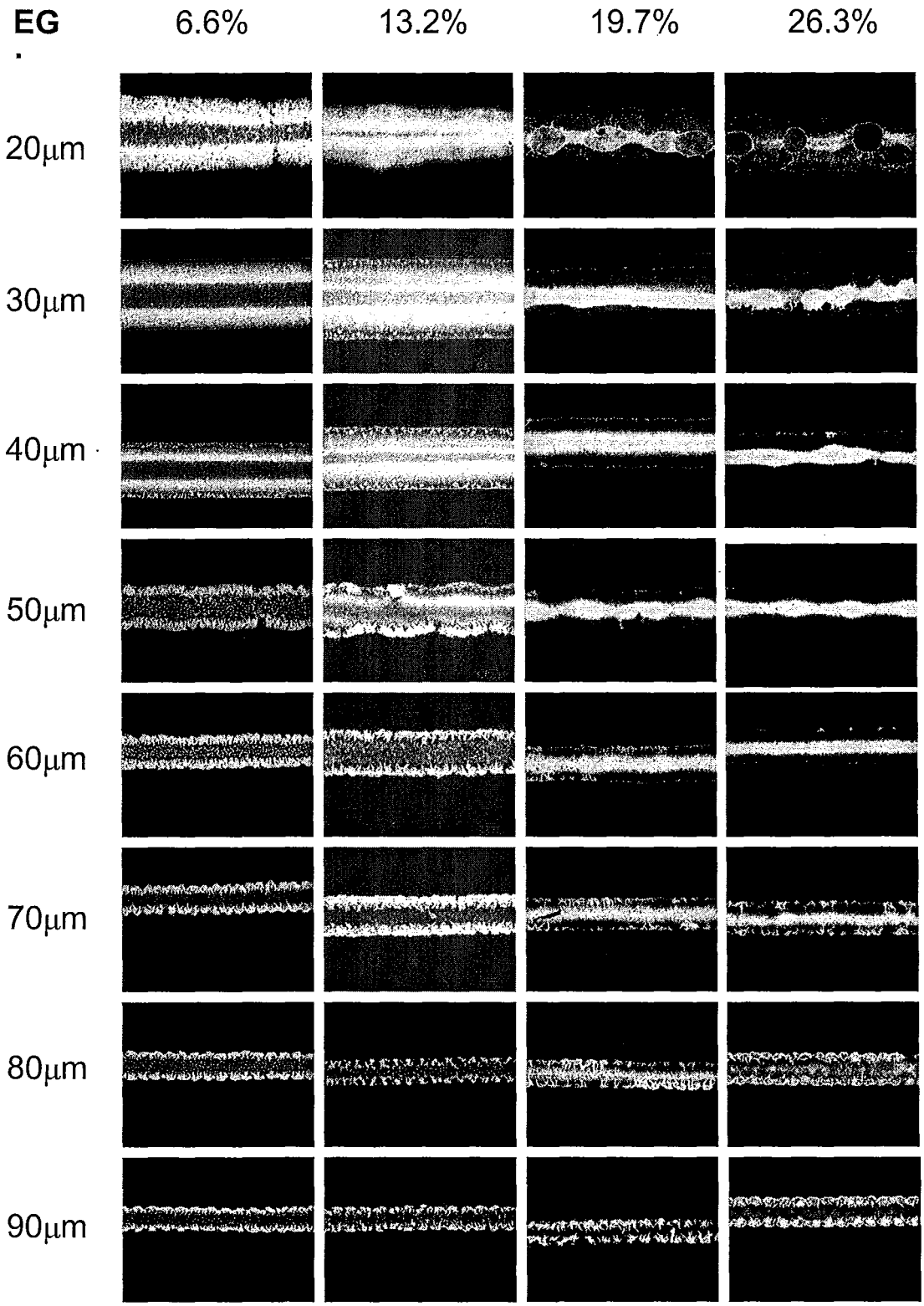

Figure 2.10: Optical microscope images of lines printed using inks of increasing ethylene glycol concentration and increasing dot-to-dot spacing. It is evident that as the ethylene glycol concentration increases the direction of the migration of the solute shifts towards the center.

2.3.4 Silver Acetate Concentration

Although this increase in ethylene glycol concentration has shown tremendous results, a line width of nearly 200μm is still too large for practical use. In an effort to further reduce the printed line width, the viscosity of the ink was manipulated. This was accomplished by increasing the silver acetate concentration in the ink (see figure 2.11). To ensure that the silver salt would indeed react to form elemental silver upon heating, the concentration of ethanolamine (the reducing agent) was correspondingly increased. A constant butanol to ethylene glycol ratio of 2.65 (by mass) was used. Recipes used and their corresponding surface tension and viscosity can be seen in table 2.4.

Table 2.4: Mass fraction of various components, surface tension and viscosity of various recipes used to study the effect of ink viscosity. Measurements were taken at 25°C. Error in surface tension measurements is ± 1mN/m. Error in viscosity measurements is ± 0.03cp.

Recipe	n-butanol	Ethylene Glycol	Lauric Acid	Silver Acetate	Ethanol-amine	Surface Tension (mN/m)	Viscosity (cp)
1	0.53	0.20	0.01	0.13	0.13	26.82	9.52
2	0.48	0.18	0.02	0.16	0.16	27.12	13.46
3	0.45	0.17	0.02	0.18	0.18	27.31	15.84
4	0.38	0.14	0.02	0.23	0.23	27.76	24.57

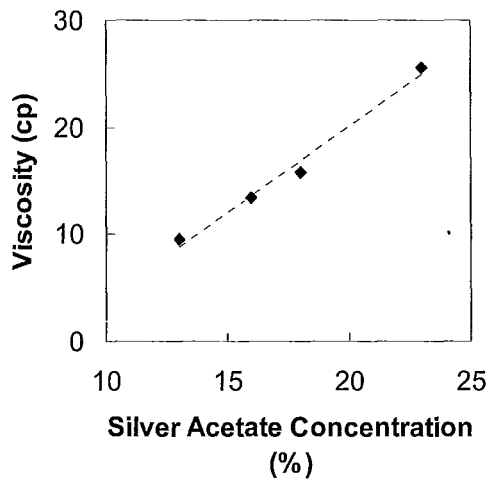

Figure 2.11: Viscosity as a function of silver acetate for silver precursor inks. Error is ± 0.03cp.

To understand the influence of viscosity on printing resolution, one must understand the dynamics of droplets impacting a solid, non-porous substrate. Droplets are released from the print head at a certain viscosity, which allows the droplets to build up kinetic energy as the fall towards the substrate. Upon impact, this kinetic energy drives the droplets to spread out to a maximum radius (R_m), reached when all kinetic energy has been converted or expelled. This maximum radius has been shown to be independent of both the surface tension of the ink and the surface energy of the substrate. However, once the droplet has reached this maximum radius, these energies then cause it to contract, which causes the droplet's edges to recede. This causes some oscillation to occur until the droplet finally settles at its final radius (R_f). This final radius is determined by the surface energies associated with the ink and the substrate and by contact line pinning – which as described earlier occurs due to chemical heterogeneities

and surface roughness on the substrate.[34] An illustration of this behaviour can be seen in figure 2.12. Since this system is being printed onto glass slides, there is a significant amount of roughness, and thus it can be assumed that contact line pinning is indeed occurring. Given this assumption, it is apparent that one way to decrease the final drop radius is to decrease the maximum radius. This is done by increasing the viscosity of the ink. Increased viscosity causes the kinetic energy stored within the droplet to be eliminated more quickly through viscous dissipation, thus decreasing the maximum radius.

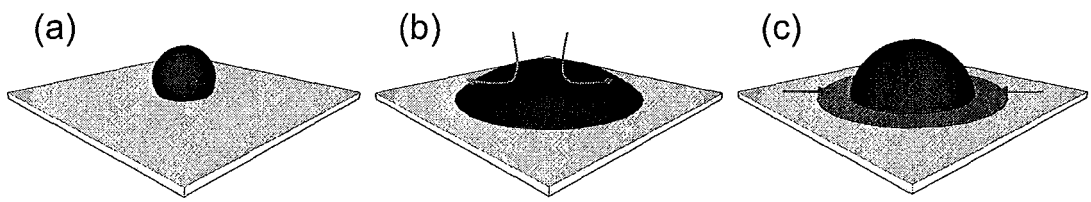

Figure 2.12: Illustration showing the dynamics of droplets impacting a surface. Droplet impacts the surface (a), spreads due to kinetic energy (b) then recedes to some final radius determined by surface tension of the ink, surface energy of the substrate and the influence of contact line pinning.

Lines were printed using various dot-to-dot spacing for each ink formulation. Printed lines were annealed and subjected to the same analysis as those in the previous study. It was found through this study that as the viscosity of the ink increases the printed line width decreases significantly. In fact, as figure 2.13 shows, as viscosity

increased from 9.5cp to 25.6cp the line width decreased from 190μm to 100μm – decrease of 48%. Figure 2.16 shows optical microscope images of lines printed using inks of increasing viscosity with increasing dot-to-dot spacing. It is evident from these images that line width decreases and film morphology and uniformity improve as the viscosity increases.

To determine whether the effect of viscosity was truly dependent on contact line pinning due to surface roughness, the same experiment was carried out using silicon wafer (an extremely smooth surface) as the substrate. It was expected that contact line pinning would have less of an influence on the droplet, allowing for narrower lines to be printed. This was indeed observed and is shown in figure 2.13. When silicon wafer was used as the substrate, the line width decreased a further 40% to only 60μm. This line width is very useful for OTFT applications, as it would allow for a pixel size of only 300μm in display applications.

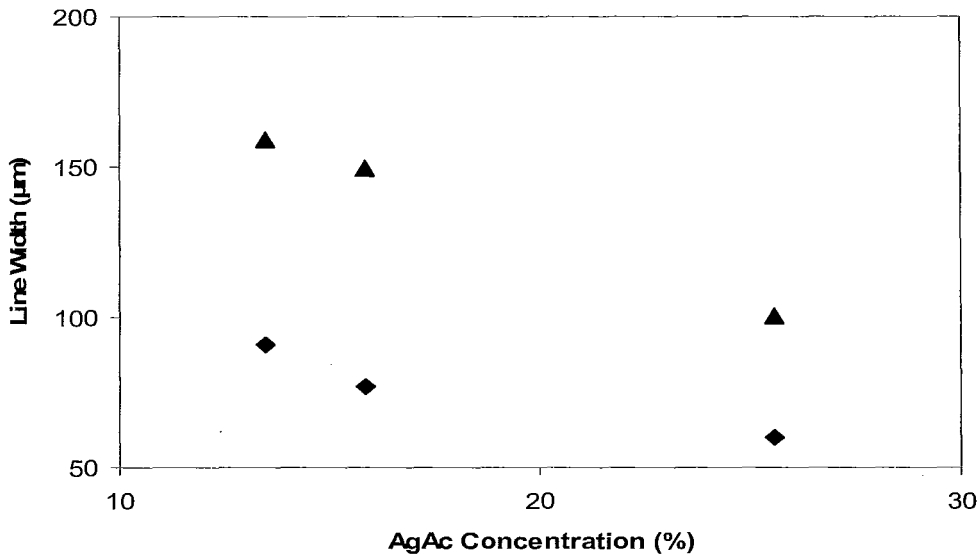

Figure 2.13: The effect of silver acetate concentration on printed line width for silver precursor inks inkjet printed onto HMDS modified glass (▲) and HMDS modified silicon wafer (♦) substrates. Data has error of ±28.5µm.

Not only does increased viscosity allow for decreased electrode line width, it also allows for electrodes to be printed closer together – that is with decreased channel length. As described earlier, droplets impacting a surface spread to a certain maximum radius before contracting. This spreading creates a fundamental limit as to how close electrodes can be printed together. Increasing the viscosity causes droplets to spread less upon impact, thus allowing for a decreased channel length. In fact, when ink with a viscosity of 25.6cp was used, channel lengths as low as 40µm were obtained. Figure 2.14 shows optimal micrographs of lines printed using a range of dot-to-dot spacing for different viscosities.

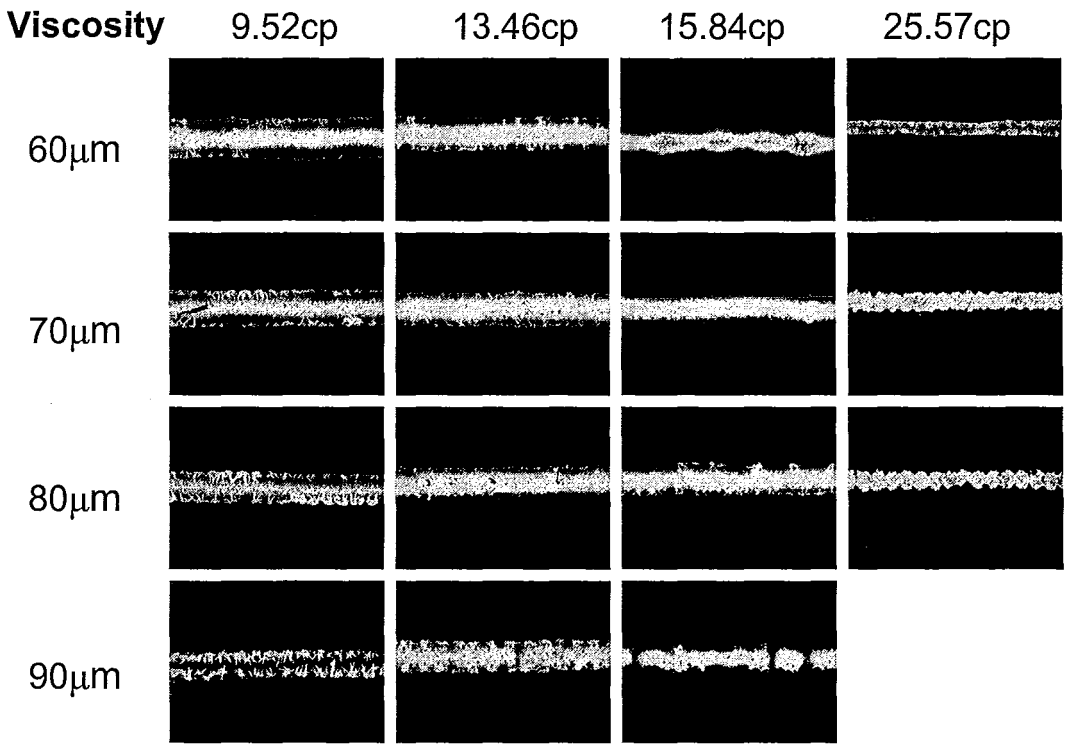

Figure 2.14: Optical microscope images of lines printed with from inks of different viscosities at different dot-to-dot spacing.

Another effect observed when viscosity was increased was a decrease in the influence of dot-to-dot spacing on center-to-edge height ratio. Figure 2.15 shows that at higher viscosities the center to edge height ratio remained fairly constant regardless of dot-to-dot spacing used. This is due to decreased solute diffusion and solvent flow rate caused by increased viscosity. This very useful property allows for lines with excellent film uniformity (center to edge height ratio between 1 and 2) to be printed over a large range of dot-to-dot spacing, which allows for a large operating window.

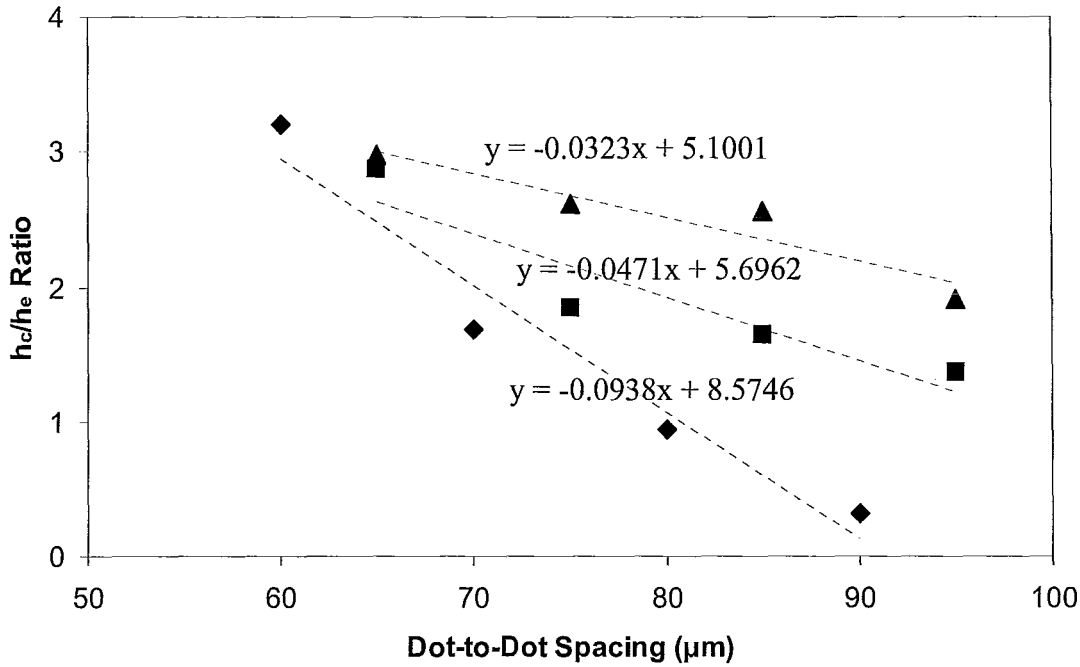

Figure 2.15: Center to edge height ratio at various dot-to-dot spacing for silver precursor inks with viscosity of 9.52cp (♦), 13.46cp (■) and 15.84cp (▲). Data has error of ±0.43.

Although the observed trends would indicate that a further increase in viscosity would be beneficial, there is a limit to the viscosity imposed by the inkjet printer and the ink stability. The printer requires the ink being printed to have a viscosity less than 10cp. Although ours is higher than this, we overcome this obstacle by heating the printing nozzles to 45°C in order to lower the viscosity during printing. However, because our ink is thermally annealed, it becomes unstable if it is heated more than 45°C before annealing. Because of this limit, a viscosity of 25.6cp is the highest possible. While we recognize that heating only one of the ink formulations may introduce some unwanted variation, we were confident that due to the small size of the droplets, all of the added

heat would be dissipated by the time the droplet impacted the surface. For this reason any additional error was thought to be negligible.

This limit is important as it indicates the highest concentration of silver acetate attainable. Unfortunately, at this concentration, lines printed with a single pass of the printer and annealed are not conductive. Given the limit on viscosity, silver acetate concentration cannot be raised to remedy this. Thus it was determined that to create conductive lines multiple passes of the printer would be required.

2.3.5 Number of Printed Layers

It was thought that multiple passes by the printer would increase the change of printing errors, and thus decrease the printing resolution. This was not observed, however. It was found that printing multiple layers of the same line served only to increase the thickness of the printed line, and had no effect on the line width. Furthermore, by printing three layers it was found that the lines became conductive once annealed. Figure 2.16 shows optical microscopic images of lines printed with one, two and three layers. Upon viewing these images, it is evident that the subsequent layers serve to fill in the gaps left by previous layers, thus creating a conductive path.

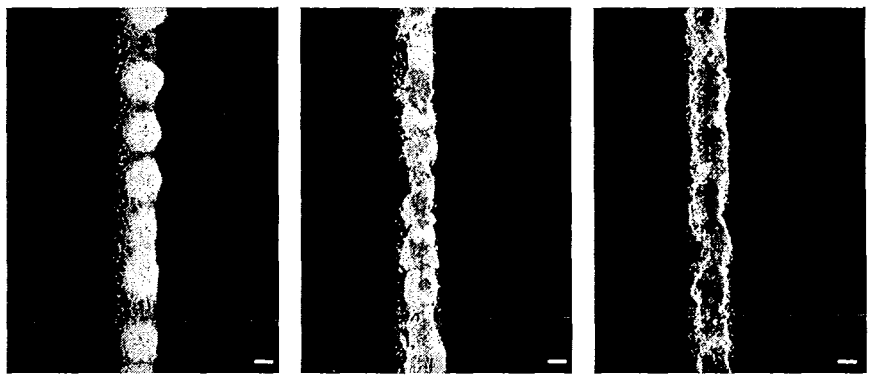

Figure 2.16: Optical microscope images of lines printed using one, two or three layers of 22% silver acetate ink. Only lines printed with three layers were found to be conductive.

2.3.6 Printer Nozzle Size

In a final attempt to further reduce the printed line width, the print head nozzle size was decreased. Previous studies had used a 10pL nozzle. Here, a 1pL nozzle was used instead. The use of this nozzle had been previously shown by others to yield very narrow electrodes when used with silver nanoparticle inks. In this study, using this nozzle yielded electrodes with printed line width of 40μm. Figure 2.17 shows optical images of lines printed with a 10pL nozzle (a) and a 1pL nozzle (b), as well as the current – voltage curves associated with each of these electrodes. It is evident that both yield very high conductivity.

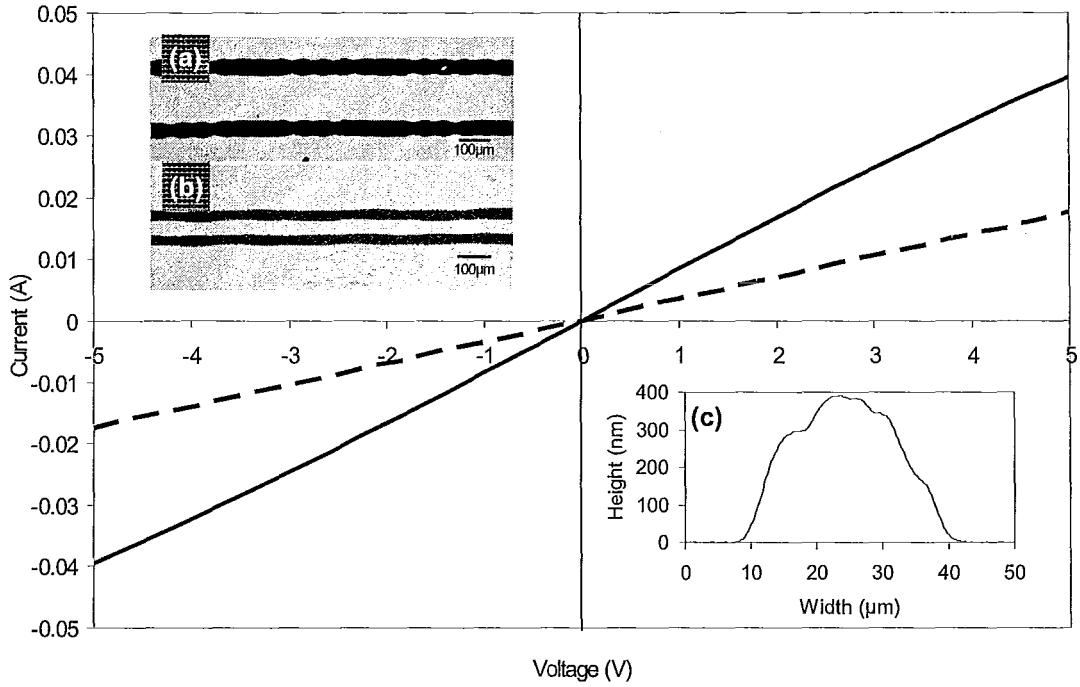

Figure 2.17: Current vs. voltage curve for electrodes fabricated using a 10pL (a, solid line) and a 1pL (b, dotted line) nozzle. The electrodes were fabricated by printing three layers of 22% silver acetate ink, then annealing. The lines show excellent conductivity. Inset (c) demonstrates the excellent height vs. width profile obtained using a 1pL nozzle.

2.4 Fabrication of OTFT Devices

Having now shown that very narrow conductive electrodes with very small channel width and excellent film uniformity could be printed by simultaneously optimizing ink solvent composition, ink viscosity and dot-to-dot spacing, these electrodes were then incorporated into an organic thin film transistor device.

OTFTs have been described earlier. Here, a heavily doped n-type silicon wafer was used as the gate electrode. A thermally annealed 200µm silicon oxide layer was used as the dielectric. The wafer was modified with HMDS to create an optimal printing substrate. Silver precursor ink with 19.5% ethylene glycol and 22% silver acetate was

printed onto the substrate to form 2 electrodes. Each electrode was printed with three layers, and the substrate was subsequently place on a 180°C hotplate to anneal the silver. Once annealed, the substrate was modified with octyltrichlorosilane (OTS) and the electrodes were modified with octanethiol. The OTS modification has been previously shown to drastically improve the molecular ordering of the organic semiconductor subsequently deposited, and the octanethiol modification has been shown to improve the electronic compatibility between the silver electrodes and the semiconductor. After these modifications, PQT – 12 was deposited directly on top of the wafer using either inkjet printing or spin coating.

OTFTs fabricated using spin coated PQT–12 yielded excellent performance. The mobility of these devices was $0.1 cm^2V^{-1}s^{-1}$ and the on/off current ratio was 10^7. This performance is similar to that previously obtained using spin coated silver precursor, indicating that there is no additional contact resistance added through the inkjet printing process. Devices fabricated using inkjet printed PQT–12 were also found to yield excellent performance. The mobility of these devices was $0.05 cm^2V^{-1}s^{-1}$ and the on/off ratio was 10^6. This value is similar to that previously reported for inkjet printed PQT–12 on evaporated gold electrodes. The decrease in performance associated with the inkjet printed PQT–12 may be a result of poorer molecular alignment attained with inkjet printing. Figure 2.18 shows a schematic for the fabrication of these devices along with micrographs of complete devices and drain current vs. gate voltage curves for devices fabricated using both spin coated PQT and inkjet printed PQT.

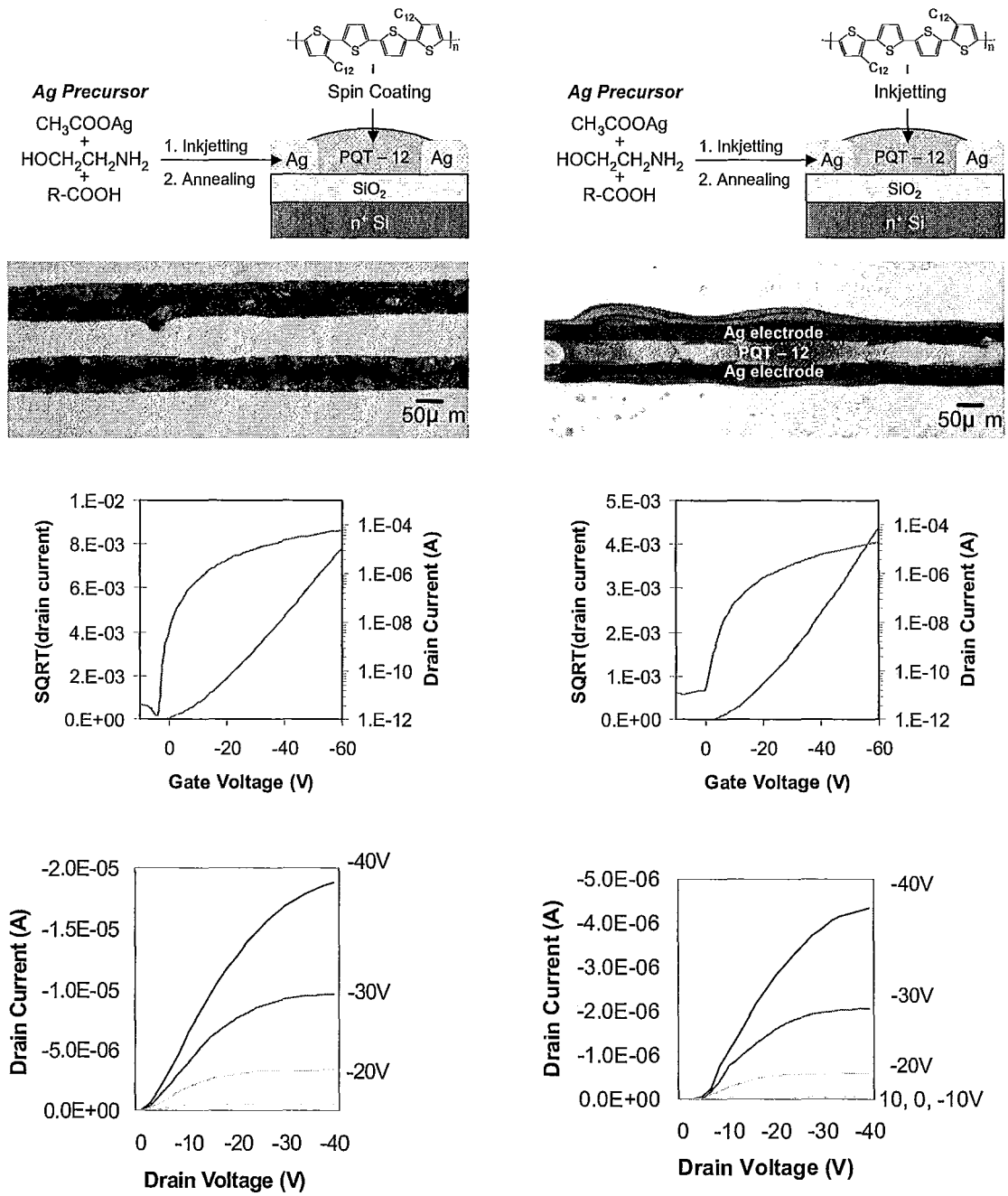

Figure 2.18: Schematic illustration method of fabricating OTFT devices using spin coated PQT–12 (a) and inkjet printed PQT–12 (e) and optical microscope images of actual devices (b and f). The performance of these devices was characterized by analyzing graphs showing drain current as a function of gate voltage (c and f) as well as drain current as a function of drain voltage for a range of gate voltages (d and g).

2.5 Conclusion

This study has resulted in the development of a novel strategy for inkjet printing silver electrodes for use in OTFT devices. It has been shown that both the solvent composition and the dot-to-dot spacing used during printing have a strong influence on the film uniformity. By increasing the concentration of a high boiling point, high surface tension cosolvent (ethylene glycol), we were able to significantly decrease the width of printed electrodes while simultaneously improving their uniformity. Furthermore, by increasing the viscosity of the ink we were able to further reduce the line width and decrease the channel length of transistor devices. Finally by using a 1pL cartridge we demonstrated that this strategy allowed for source and drain electrodes to be printed with line width of 40μm and channel length of 50μm. These electrodes were incorporated into OTFT devices using either inkjet printed or spin coated PQT–12 to yield high performance devices.

2.6 References

1. Klauk, H. *et al.* High-mobility polymer gate dielectric pentacene thin film transistors. *J. Appl. Phys.* **92**, 5259-5263 (2002).

2. Kato, Y. *et al.* High mobility of pentacene field-effect transistors with polyimide gate dielectric layers. *Appl. Phys. Lett.* **84**, 3789-3791 (2004).

3. Rogers, J. A., Bao, Z., Dodabalapur, A. & Makhija, A. Organic smart pixels and complementary inverter circuits formed on plastic substrates by casting and rubber stamping. *Electron Device Letters, IEEE* **21**, 100-103 (2000).

4. Gundlach, D. J., Lin, Y. Y., Jackson, T. N., Nelson, S. F. & Schlom, D. G. Pentacene organic thin-film transistors-molecular ordering and mobility. *Electron Device Letters, IEEE* **18**, 87-89 (1997).

5. Servet, B. *et al.* Polymorphism and Charge Transport in Vacuum-Evaporated Sexithiophene Films. *Chemistry of Materials* **6**, 1809-1815 (1994).

6. Parashkov, R. *et al.* All-organic thin-film transistors made of poly(3-butylthiophene) semiconducting and various polymeric insulating layers. *J. Appl. Phys.* **95**, 1594-1596 (2004).

7. Nur, H. M., Song, J. H., Evans, J. R. G. & Edirisinghe, M. J. Ink-jet printing of gold conductive tracks. **13**, 213-219 (2002).

8. Wu, Y., Li, Y. & Ong, B. S. A Simple and Efficient Approach to a Printable Silver Conductor for Printed Electronics. *J. Am. Chem. Soc.* **129**, 1862-1863 (2007).

9. Wu, Y., Li, Y. & Ong, B. S. Printed Silver Ohmic Contacts for High-Mobility Organic Thin-Film Transistors. *J. Am. Chem. Soc.* **128**, 4202-4203 (2006).

10. Gamerith, S. *et al.* Direct Ink-Jet Printing of Ag-Cu Nanoparticle and Ag-Precursor Based Electrodes for OFET Applications. *Advanced Functional Materials* **17**, 3111-3118 (2007).

11. Mallick, K., Witcomb, M. J. & Scurrell, M. S. Directional assembly of polyaniline functionalized gold nanoparticles. *Journal of Physics: Condensed Matter*, 196225 (2007).

12. Sanaur, S., Whalley, A., Alameddine, B., Carnes, M. & Nuckolls, C. Jet-printed electrodes and semiconducting oligomers for elaboration of organic thin-film transistors. *Organic Electronics,* **7**, 423-427 (2006).

13. Wu, Y., Li, Y., Liu, P., Gardner, S. & Ong, B. S. Studies of Gold Nanoparticles as Precursors to Printed Conductive Features for Thin-Film Transistors. *Chem. Mater.* **18**, 4627-4632 (2006).

14. Szczech, J. B., Megaridis, C. M., Zhang, J. & Gamota, D. R. Ink jet processing of metallic nanoparticle suspensions for electronic circuitry fabrication. *Nanoscale and Microscale Thermophysical Engineering* **8**, 327 (2004).

15. Kim, D., Jeong, S., Park, B. K. & Moon, J. Direct writing of silver conductive patterns: Improvement of film morphology and conductance by controlling solvent compositions. *Appl. Phys. Lett.* **89**, 264101 (2006).

16. Noguchi, Y., Sekitani, T. & Someya, T. Organic-transistor-based flexible pressure sensors using ink-jet-printed electrodes and gate dielectric layers. *Appl. Phys. Lett.* **89**, 253507 (2006).

17. Li, Y., Wu, Y. & Ong, B. S. Facile Synthesis of Silver Nanoparticles Useful for Fabrication of High-Conductivity Elements for Printed Electronics. *J. Am. Chem. Soc.* **127**, 3266-3267 (2005).

18. Chong-an Di, Gui Yu, Yunqi Liu, Yunlong Guo, Ying Wang, Weiping Wu,Daoben Zhu,. High-Performance Organic Field-Effect Transistors with Low-Cost Copper Electrodes. *Adv Mater* **9999**, NA (2008).

19. Sunho Jeong, Kyoohee Woo, Dongjo Kim, Soonkwon Lim, Jang Sub Kim, Hyunjung Shin, Younan Xia,Jooho Moon,. Controlling the Thickness of the Surface Oxide Layer on Cu Nanoparticles for the Fabrication of Conductive Structures by Ink-Jet Printing. *Advanced Functional Materials* **18**, 679-686 (2008).

20. Arias, A. C. *et al.* All jet-printed polymer thin-film transistor active-matrix backplanes. *Appl. Phys. Lett.* **85**, 3304-3306 (2004).

21. Calvert, P. Inkjet Printing for Materials and Devices. *Chem. Mater.* **13**, 3299-3305 (2001).

22. Lim, J. A. *et al.* Self-Organization of Ink-jet-Printed Triisopropylsilylethynyl Pentacene via Evaporation-Induced Flows in a Drying Droplet. *Advanced Functional Materials* **9999**, NA (2008).

23. Kawase, T., Shimoda, T., Newsome, C., Sirringhaus, H. & Friend, R. H. Inkjet printing of polymer thin film transistors. *Thin Solid Films,* **438-439**, 279-287 (2003).

24. Wang, J. Z., Zheng, Z. H., Li, H. W., Huck, W. T. S. & Sirringhaus, H. Dewetting of conducting polymer inkjet droplets on patterned surfaces. *Nat Mater* **3**, 171-176 (2004).

25. Zhao, N. *et al.* Self-aligned inkjet printing of highly conducting gold electrodes with submicron resolution. *J. Appl. Phys.* **101**, 064513 (2007).

26. T. H. J. van Osch, J. Perelaer, A. W. M. de Laat,U.S.Schubert,. Inkjet Printing of Narrow Conductive Tracks on Untreated Polymeric Substrates. *Adv Mater* **20**, 343-345 (2008).

27. Deegan, R. D. Pattern formation in drying drops. *Phys Rev E.* **61**, 475 (2000).

28. Deegan, R. D. *et al.* Contact line deposits in an evaporating drop. *Phys Rev E.* **62**, 756 (2000).

29. Park, J. & Moon, J. Control of Colloidal Particle Deposit Patterns within Picoliter Droplets Ejected by Ink-Jet Printing. *Langmuir* **22**, 3506-3513 (2006).

30. Hu, H. & Larson, R. G. Evaporation of a Sessile Droplet on a Substrate. *J. Phys. Chem. B* **106**, 1334-1344 (2002).

31. Hu, H. & Larson, R. G. Analysis of the Microfluid Flow in an Evaporating Sessile Droplet. *Langmuir* **21**, 3963-3971 (2005).

32. Jiaxing Huang, Rong Fan, Stephen Connor,Peidong Yang,. One-Step Patterning of Aligned Nanowire Arrays by Programmed Dip Coating13. *Angewandte Chemie International Edition* **46**, 2414-2417 (2007).

33. Hu, H. & Larson, R. G. Marangoni Effect Reverses Coffee-Ring Depositions. *J. Phys. Chem. B* **110**, 7090-7094 (2006).

34. Dong, H., Carr, W. W., Bucknall, D. G. & Morris, J. F. Temporally-resolved inkjet drop impaction on surfaces. *AICHE J.* **53**, 2606-2617 (2007).

Chapter 3

Optimization of Inkjet Printing of Silver Nanoparticles Using Design of Experiments Method and Mixed Integer Non-Linear Optimization

3.1 Introduction

3.1.1 Engineering the Inkjet Printing Process Using Design of Experiments

As has been shown in the previous chapters, and by many other groups, the technology required for the development of organic thin film transistors is currently in existence. High performance organic semiconductors,[1] dielectrics,[2-6] and conductive materials [7-19] have been developed and shown to yield devices with excellent properties. Furthermore inkjet printing has been shown to be an excellent method for the fabrication of these devices.[20] Our work, along with the work of many other groups, has demonstrated that inkjet printing is customizable and can be optimized in order to yield high performance devices.

A great challenge to the commercialization of these devices is the optimization of the inkjet printing process. Because this process is highly complex and influenced by many variables, it can be difficult to control, and even more difficult to fully understand. For this reason, the issue of inkjet printing fabrication of OTFTs has taken a step from the realm of material science into the realm of engineering. It is now necessary to develop a full understanding of the influence of relevant input variables on relevant output variables. This understanding will lead to a heightened ability to optimize the entire

process so that one is able to fabricate devices with a great deal of efficacy and efficiency.

An excellent technique for discovering the influence of several variables on a process is the design of experiments (DOE) method. This method involves selectively setting the value of different variables of interest such that one is able to perform a regression on the output data that determine the independent influence of each variable on the process as well as the influence of all variable interactions. This variable interaction is very relevant in a complex system such as inkjet printing where the influence of one variable on the process may be different depending on the setting of a separate variable. As an example, it could be that the influence of dot-to-dot spacing on center to edge height ratio may change depending on the solvent composition used. Clearly the ability to understand both the independent influence of each variable and the influence of all variable interactions is essential to a proper optimization.

The DOE method works under the assumption that a linear model is sufficient for a mathematical description of the influence of a variable on the system. Working under this assumption, only two levels are required for each variable – that is to say one can obtain all necessary information about the system while only requiring each variable of interest to be set at two different levels throughout the entire experiment. To allow for easy calculations, these levels are chosen to be the extremes of the total range of each variable – one level is the highest possible value, while the other is the lowest possible value. To further ease the calculations, these two levels are scaled using equation (1).

This scaling results in the value of the high and low levels of each variable being +1 and -1, respectively.

$$x = \frac{x^* - \bar{x}}{range/2}$$

$$\begin{aligned} &where \\ &x = scaled \quad variable \\ &x^* = unscaled \quad variable \\ &\bar{x} = mid - point \quad of \quad range \\ &range = high \quad level - low \quad level \end{aligned} \qquad (1)$$

Having now scaled the variables of interest, one must then determine how many experimental runs will be required such that all combinations of variable settings will be included. This number grows exponentially as the number of variables increases and can be calculated using equation (2).

$$\begin{aligned} &runs = l^v \\ &where \\ &l = number \quad of \quad levels \\ &v = number \quad of \quad varaibles \end{aligned} \qquad (2)$$

As an example, let us look at a system of three variables where two levels are used. For this system, we would require 2^3 (or 8) experimental runs to examine all combinations of variable settings. The design matrix which describes all these settings can be seen in table 3.1.

Table 3.1: Design matrix of a 2^3 experiment. Actual design matrix is highlighted.

Run	x_0	x_1	x_2	x_3	$x_4 = x_1x_2$	$x_5 = x_1x_3$	$X_6 = x_2x_3$	$x_7 = x_1x_2x_3$
1	1	1	1	1	1	1	1	1
2	1	1	1	-1	1	-1	-1	-1
3	1	1	-1	1	-1	1	-1	-1
4	1	1	-1	-1	-1	-1	1	1
5	1	-1	1	1	-1	-1	1	-1
6	1	-1	1	-1	-1	1	-1	1
7	1	-1	-1	1	1	-1	-1	1
8	1	-1	-1	-1	1	1	1	-1

In the above table, the design matrix is shown highlighted. The variable x_0 is a dummy variable used for the calculation of the "intercept" in the model that will be developed. Variables $x_4 - x_7$ are interaction variables which show the combined effect of two variables. The entire matrix, from $x_0 - x_7$ is known as the variable matrix. It is important to note that all of the columns in this matrix are orthogonal to one another. This trait is what allows for the influence of each variable and each interaction to be seen independently.

The values of the output variables obtained by performing the above described eight runs can be used to create a mathematical model of this system. We can see that since we will have one output variable value for each run, we can create a system of eight equations with eight unknowns, as shown in equations (3).

$$y_1 = \beta_0 + \beta_1 x_{1,1} + \beta_2 x_{1,2} + \beta_3 x_{1,3} + \beta_4 x_{1,4} + \beta_5 x_{1,5} + \beta_6 x_{1,6} + \beta_7 x_{1,7}$$
$$y_2 = \beta_0 + \beta_1 x_{2,1} + \beta_2 x_{2,2} + \beta_3 x_{2,3} + \beta_4 x_{2,4} + \beta_5 x_{2,5} + \beta_6 x_{2,6} + \beta_7 x_{2,7}$$
$$y_3 = \beta_0 + \beta_1 x_{3,1} + \beta_2 x_{3,2} + \beta_3 x_{3,3} + \beta_4 x_{3,4} + \beta_5 x_{3,5} + \beta_6 x_{3,6} + \beta_7 x_{3,7}$$
$$y_4 = \beta_0 + \beta_1 x_{4,1} + \beta_2 x_{4,2} + \beta_3 x_{4,3} + \beta_4 x_{4,4} + \beta_5 x_{4,5} + \beta_6 x_{4,6} + \beta_7 x_{4,7}$$
$$y_5 = \beta_0 + \beta_1 x_{5,1} + \beta_2 x_{5,2} + \beta_3 x_{5,3} + \beta_4 x_{5,4} + \beta_5 x_{5,5} + \beta_6 x_{5,6} + \beta_7 x_{5,7}$$
$$y_6 = \beta_0 + \beta_1 x_{6,1} + \beta_2 x_{6,2} + \beta_3 x_{6,3} + \beta_4 x_{6,4} + \beta_5 x_{6,5} + \beta_6 x_{6,6} + \beta_7 x_{6,7}$$
$$y_7 = \beta_0 + \beta_1 x_{7,1} + \beta_2 x_{7,2} + \beta_3 x_{7,3} + \beta_4 x_{7,4} + \beta_5 x_{7,5} + \beta_6 x_{7,6} + \beta_7 x_{7,7}$$
$$y_8 = \beta_0 + \beta_1 x_{8,1} + \beta_2 x_{8,2} + \beta_3 x_{8,3} + \beta_4 x_{8,4} + \beta_5 x_{8,5} + \beta_6 x_{8,6} + \beta_7 x_{8,7}$$

where

$$x_{i,4} = x_{i,1} x_{i,2}$$
$$x_{i,5} = x_{i,1} x_{i,3}$$
$$x_{i,6} = x_{i,2} x_{i,3}$$
$$x_{i,7} = x_{i,1} x_{i,2} x_{i,3}$$

$$\beta_4 = \beta_1 \beta_2 \qquad (3)$$
$$\beta_5 = \beta_1 \beta_3$$
$$\beta_6 = \beta_2 \beta_3$$
$$\beta_7 = \beta_1 \beta_2 \beta_3$$

$x_{4,3}$ = value of x_3 in run 4

This system of equations can be rewritten in matrix form, which is shown in equation (4). Because our X matrix contains all orthogonal columns, the β matrix can be solved easily using equation (5). This equation is applicable to systems of any number of input variables.

Because the values of the β's obtained using this method are found using regression methods, they contain a certain amount of error. The size of this error depends on the

number of repeats performed for each run and the accuracy of the instruments used for output variable. When reporting the coefficients which describe the influence of the variables and variable interactions involved in a system, it is important that a 95% confidence interval also be included. If this interval includes 0, the influence of the variable can be considered negligible. This 95% confidence interval can be calculated using equation (6). Also, when using the DOE method, it is common practice to regard the coefficient describing the interaction of all five variables as the error term. Thus any term less significant than this term would also be deemed insignificant.

$$y = X\beta + e$$

where

$$y = \begin{bmatrix} y_1 \\ y_2 \\ \vdots \\ y_8 \end{bmatrix}$$

$$X = \begin{bmatrix} x_{1,0} & x_{1,1} & \cdots & x_{1,7} \\ x_{2,0} & \ddots & & \\ \vdots & & \ddots & \\ x_{8,0} & \cdots & \cdots & x_{8,7} \end{bmatrix} \qquad (4)$$

$$\beta = \begin{bmatrix} \beta_0 \\ \beta_1 \\ \vdots \\ \beta_7 \end{bmatrix}$$

$$\beta_i = \frac{\sum_{j=0} x_{i+1,j} y_{j+1}}{\sum_{j=0} x_{i+1,j}^{\ 2}} \tag{5}$$

$$95\%CI = \beta_i \pm t_{v,0.025} \sqrt{\frac{s^2}{\sum x_i^{\ 2}}} \tag{6}$$

Having determined the coefficients describing the influence of each variable and interaction on the process, one now has a mathematical model of system. This model, which is shown in equation (7), can be used to optimize the variable settings such that an optimal output value can be obtained.

$$y_1 = \beta_0 + \beta_1 x_1 + \beta_2 x_2 + \beta_3 x_3 + \beta_{12} x_1 x_2 + \beta_{13} x_1 x_3 + \beta_{23} x_2 x_3 + \beta_{123} x_1 x_2 x_3 \tag{7}$$

One can see that this is in fact a very difficult process to optimize, as each variable is present in four separate terms of the equation. Furthermore the coefficients of these terms may be of different sign, making the prediction of a variable's influence on the output very difficult to make. This difficulty becomes even greater as the number of input variables under study increases. Furthermore, one can use this method to examine the influence of these variables on several different output variables. For instance, in reference to the previous study, one could have looked at the influence of several variables and their interactions on center to edge height ratio and printed line width. The inclusion of several output variables adds even more difficulty to the optimization problem[21].

3.1.2 Optimizing the Inkjet Printing Process Using Non-Linear Programming

One very effective method of optimizing this type of problem is the use of computer software to run optimization algorithms on this equation. Since equation (7) is non-linear, one can use non-linear programming algorithms which will determine the optimal variable setting such that the output is either maximized or minimized, depending on what is desired.

A full discussion of algorithms used for non-linear programming is well beyond the scope of this project. Briefly non-linear programming seeks to find variable settings which result in an optimization equation being minimized or maximized. These variables are subject to a set of constraints which may be equalities or inequalities.

When this optimization is used for the purpose of optimizing variables involved in a DOE study, the process is slightly more complex. In this case the variables can only have values of -1 or +1, making this an integer problem. Furthermore, since these variables can be set only to one of two levels, this type of problem can be further categorized into a binary integer problem. Although binary problems involve variables which can be set to 0 or 1, these values can be mapped to -1 and +1 using equation (8).

$$x = 2b - 1 \qquad (8)$$

where

$$b \in [0,1]$$
$$x \in [-1,1]$$

In order to successfully optimize the problem one must also include all (if any) relevant constraints. These constraints can arise from physical situations, ie. when one variable is at its high level it is unsafe for another to also be at a high level, or from observations made while performing the experiment. The development of constraints for an inkjet printing system will be explored further later in this chapter.

There are many software packages available for optimization problems. In this work software called GAMS (General Algebraic Modeling System) was used. This software was developed by the world bank and is widely used in industry. It is available for free from the supplier. Using GAMS, one is able to select a variety of solvers which use different algorithms for optimization[22].

3.1.3 Purpose of this Study

The purpose of this work was to optimize the process of inkjet printing conductive lines using fundamental engineering optimization methods. To accomplish this, a number of variables were first selected as most relevant to process. These variables were selected based on our previous work (chapter 2) and the work reported by other groups. The design of experiments method was used to determine the influence of these variables, as well as the influence of variable interaction, on the width, thickness, center to edge height ratio and conductivity of printed lines. Having mathematically modeled these influences, mixed integer non-linear programming was employed to optimize the input variable settings for each output variable. The results of this study allowed us to gain a complete understanding of how various input variables affect the inkjet printing process.

This study also allowed for the inkjet printing process to be optimized such that high resolution printing of highly conductive and uniform electrodes could be performed.

3.2 Materials and Methods

3.2.1 Silver Nanoparticles

Although the silver precursor ink used in the previous study has been shown to yield excellent results, it also has several drawbacks. One of the major challenges facing this ink is the issue of stability. Printed silver precursor becomes unstable upon exposure to ambient conditions, hence yields electrodes with poor conductivity and film uniformity. Although this is not an issue when fabricating a single device, it becomes a great challenge when fabricating large area devices such as transistor arrays. In this case the ink deposited at the beginning of the pattern becomes unstable by the time the rest of the pattern is completely printed. Given this difficulty, we sought to apply the ink formulation strategy gained through the previous study to an alternative conductive ink with greater stability.

One of the most promising materials for this purpose is metal nanoparticles. Nanoparticles have been fabricated using gold, silver and platinum and have been shown to have many properties which make them very useful for OTFT fabrication. These nanoparticles are typically capped with organic molecules (so called stabilzers) to prevent aggregation and flocculation. These stabilizers can be functionalized easily to allow the nanoparticles to be soluble in a wide range of solvents. This functionality can also improve the electrical compatibility of the nanoparticles with the organic semiconductor,

allowing for improved OTFT device performance[13]. Another property of metal nanoparticles which is very useful for this application is the very high surface area to volume ratio. This property allows the melting point of these nanoparticles to be drastically lower than that of bulk metals. Silver nanoparticles, for instance, can have a melting point as low as 120°C, whereas the melting point of bulk silver is nearly 1000°C. This low melting point combined with excellent conductivity and easy solution processability makes these metal nanoparticles an excellent option for the fabrication of conductive components of OTFT devices. Although gold and platinum have recently become prohibitively expensive for this use, silver remains inexpensive and has thus been the subject of a great deal of research.

For this study silver nanoparticles synthesized at the Xerox Research Center of Canada were used[17]. These nanoparticles have an average diameter or 7nm and are capped with oleic acid molecules to prevent aggregation. These stabilizer molecules allow the nanoparticles to be soluble in organic solvents. Inks formulated using these nanoparticles were printed using a Dimatix DMP-2800 drop-on-demand inkjet printer equipped with a 10pL print head. The waveform and voltage applied to the print head was adjusted to yield spherical droplets with no satellite drops. The velocity of the ejected droplets was held at about 5m/s.

3.2.2 Ink Formulation and Printing

Ink was formulated using a mixture of dodecane and terpineol as the solvent. This mixture was found in previous studies to yield excellent printing. Exact composition of the solvent was studied as one of the variables in this chapter.

Ink was printed onto glass microscope slides which had been modified with either hexamethyldisilizane (HMDS) or octyltrichlorosilane (OTS – 8). To accomplish these modifications, the glass was first cleaned with isopropyl alcohol (IPA) and dried with compressed air. The glass was then plasma cleaned under air for 3 minutes, then washed with water and subsequently with IPA. The glass was then dried using compressed air. Following this, the glass was submersed in either a 1% solution of HMDS in toluene for 20 minutes at room temperature or a 1% solution of OTS – 8 in toluene for 15 minutes at 60°C. After modification the glass was rinsed with toluene, then with IPA and dried using compressed air.

The variables chosen for this optimization study were dot-to-dot spacing, solvent composition, substrate surface energy, substrate temperature and silver nanoparticle concentration. Below is an explanation as to why these variables were chosen. Also included is an explanation of the range of values used for each variable.

3.2.3 Input Variables Selected for Study

Dot-to-dot spacing was shown in our previous study to have a significant influence on both line width and film uniformity. These findings have also been shown by other groups[23]. For this reason this was chosen to be one of the variables investigated in this

study. To determine an acceptable range of study, various lines were printed onto glass substrates with increasing dot-to-dot spacing. It was found that lines printed with at dot-to-dot spacing of less than 20μm yielded lines which were much too wide for practical use, and that lines printed at dot-to-dot spacing of greater than 40 μm exhibited a large amount of edge roughness. Thus 20μm and 40μm were chosen as the low and high value for this variable, respectively.

Solvent composition was also shown to have a strong influence on film uniformity in the previous study, and so it was selected to be a variable of interest in this study. The solvent used for ink formulation in this study was a mixture of dodecane and terpineol. It was found that inks with a dodecane to terpineol ratio greater than 5 exhibited poor printing and large coffee ring effect, thus this was then high value. Also when the ratio was less than one, solubility of the silver nanoparticles in the solvent became an issue – thus this was selected as the low value.

Our previous work has also demonstrated that solute concentration in the ink has a significant role in line width and film uniformity. Furthermore it was expected that this would have a large influence over printed line conductivity. Preliminary studies indicated that the silver nanoparticles were soluble up to about 40% - thus this was chosen as the high value. It was suspected that inks with a silver concentration of less than 25% would not yield conductive lines due to the fact of small thickness. This was then chosen as the low value.

Substrate temperature has been shown by other groups to have a significant impact on film morphology[16]. It was also expected to have a strong influence over line width. A

low value of 30°C was chosen as this was the lowest controllable temperature available on the printed. A high value of 60°C was chosen as this was the maximum temperature of the printed platen.

Substrate surface energy has been previously shown to have a large impact on line width. In preliminary studies it was found that continuous lines could be printed on glass substrates which had been modified with hexamethyldisilazane (HMDS), octyltrichlorosilane (OTS – 8), or surfaces which had simply been plasma cleaned.. OTS – 8 was thus chosen as the low value for substrate surface energy. HMDS was chosen as the high value instead of plasma cleaned surfaces at it allowed for a more reproducible surface energy.

A complete list of all variables investigated in this study along with the high and low values used can be seen in table 2. This table also includes the symbol used for each variable throughout all equations in the rest of this chapter.

Table 3.2: Variables examined along with high and low values used during study

Variable	High Value	Low Value	Symbol
Silver Mass Fraction	40%	25%	x_1
Dodecane:Terpineol Ratio	5:1	1:1	x_2
Substrate Surface Energy	HMDS Modified	OTS Modified	x_3
Substrate Temperature	60°C	30°C	x_4
Dot-to-Dot Spacing	40μm	20μm	x_5

3.2.4 Output Variables Selected For Study

In order to optimize the settings of the above input variables, one must select measurable output variables which will be used to determine the performance of the inkjet printing process. The goal of this optimization was to inkjet print silver

nanoparticle ink to form highly resolute conductive lines with excellent film morphology. Given this goal the following four output variables were measured for each experimental run.

Printed line width was measured for each printed line. This was accomplished using a Dektak – 6 surface profilometer. This profilometer used a stylus in order to achieve its measurements. In order to improve the attainable printing resolution it was desired that this line width be as small as possible.

Printed line thickness was also measured using the Dektak – 6 surface profilometer. This thickness was taken as the average thickness across the entire line. It was expected that line thickness would affect line conductivity, since very thin lines with voids would not be conductive. Therefore, it was desired that this optimization would result in lines which showed sufficient thickness to ensure high conductivity.

Center to edge height ratio was also measured for each line. This value (described in chapter 2) is used to quantify the film uniformity. Since it is desired that printed electrodes have uniform thickness across their entire width, it was hoped that this optimization would result in a center to edge height ratio as close to unity as possible.

Conductivity was measured for each line using a two point probe attached to an optical microscope. It was found that lines were generally highly conductive or not conductive at all. Given this conductivity was treated as a binary variable, with lines which were conductive given a value of 1 and lines which were not conductive given a value of 0. The conductivity data was also used to create constraints for the non-linear programming problem. This shall be discussed in detail further in the chapter.

3.2.5 Experimental Design

Given that there were five input variables investigated in this study with two levels used for each, equation (2) reveals that 32 runs were required to fully investigate this system. These runs were set up such that all combinations of variable levels were encountered in the study. The complete experimental design matrix can be seen in table 3.3. For each run, two lines were printed, and the average values of each of these lines was reported.

Table 3.3: Runs used for DOE study. +1 indicates high value of variable, -1 indicates low value.

Run	Silver Concentration	Dodecane : Terpineol	Surface Energy	Substrate Temperature	Dot-to-Dot Spacing
1	+1	+1	+1	+1	+1
2	+1	+1	+1	+1	-1
3	+1	+1	+1	-1	+1
4	+1	+1	+1	-1	-1
5	+1	+1	-1	+1	+1
6	+1	+1	-1	+1	-1
7	+1	+1	-1	-1	+1
8	+1	+1	-1	-1	-1
9	+1	-1	+1	+1	+1
10	+1	-1	+1	+1	-1
11	+1	-1	+1	-1	+1
12	+1	-1	+1	-1	-1
13	+1	-1	-1	+1	+1
14	+1	-1	-1	+1	-1
15	+1	-1	-1	-1	+1
16	+1	-1	-1	-1	-1
17	-1	+1	+1	+1	+1
18	-1	+1	+1	+1	-1
19	-1	+1	+1	-1	+1
20	-1	+1	+1	-1	-1
21	-1	+1	-1	+1	+1
22	-1	+1	-1	+1	-1
23	-1	+1	-1	-1	+1

24	-1	+1	-1	-1	-1
25	-1	-1	+1	+1	+1
26	-1	-1	+1	+1	-1
27	-1	-1	+1	-1	+1
28	-1	-1	+1	-1	-1
29	-1	-1	-1	+1	+1
30	-1	-1	-1	+1	-1
31	-1	-1	-1	-1	+1
32	-1	-1	-1	-1	-1

3.3 Results of the DOE Study

3.3.1 Ink Properties

In an effort to gain a complete understanding of the inkjet printing system the impact of solvent ratio and silver nanoparticle concentration on the surface tension and viscosity of the ink was first investigated. It was thought that this knowledge would allow for a deeper understanding of why these variables would have certain effects on the resulting printed electrode. Figures 3.1 and 3.2 show the effect of both silver nanoparticle concentration and solvent ratio on surface tension and viscosity.

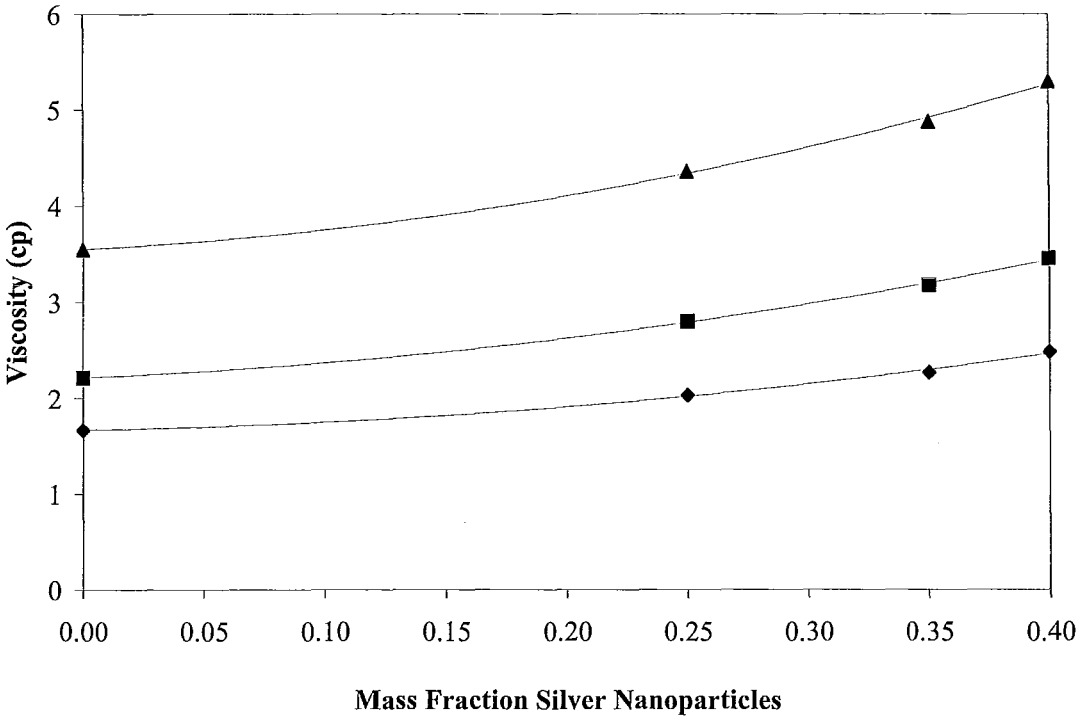

Figure 3.1: Ink viscosity as a function of silver nanoparticle mass fraction for inks with a solvent ratio of 5 (♦), 2 (■) and 1 (▲). Error is ± 0.04 cp

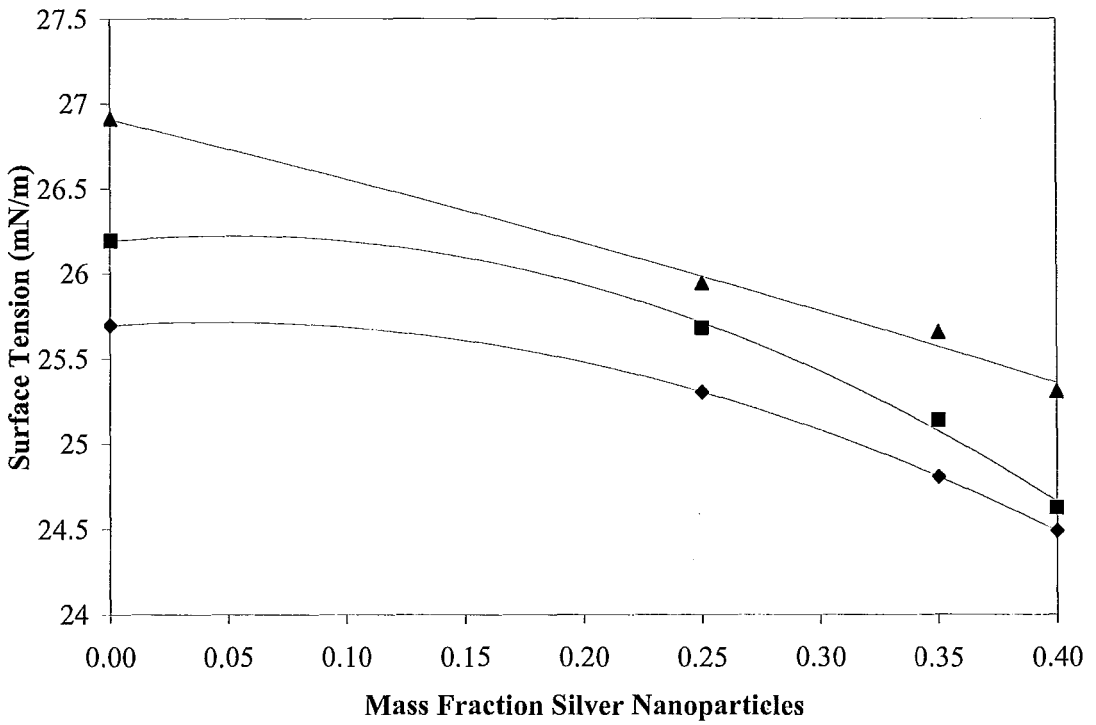

Figure 3.2: Ink surface tension as a function of silver nanoparticle mass fraction for inks with a solvent ratio of 5 (♦), 2 (■) and 1 (▲). Error is ± 1 mN/m

It is clear silver nanoparticle concentration has only a minimal effect on both viscosity and surface tension. In the above figures it can be seen that as silver nanoparticle concentration increases from 0% to 40% viscosity only increases from 1.7cp to 2.5cp for a solvent ratio of 5 and from 3.6cp to 5.3cp for a solvent ratio of 1. For the same change in silver nanoparticle concentration surface tension only decreases from 25.7mN/m to 24.5mN/m for a solvent ratio of 5 and from 26.9 mN/m to 25.3 mN/m for a solvent ratio of 1.

Similarly, solvent ratio had a minor effect on surface tension and viscosity. As solvent ratio was changed from 5 to 1 the viscosity increased by only about 2.5cp, regardless of silver nanoparticle concentration. For the same change in solvent ratio surface tension was increased by only 0.8mN/m regardless of silver nanoparticle concentration.

3.3.2 Conductivity

Conductivity is a unique variable. It was found that for this system it could be treated as either on or off. That is to say printed lines were found to be either very highly conductive or functionally non-conductive. This made it very difficult to analyze using the equations described earlier for design of experiments analysis, as each run could only be given an output variable of one or zero.

Since this output variable could not be analyzed using these equations, it was decided instead that this would instead be used as qualitative variable on which the constraints of the non-linear optimization would be based. Since the first and foremost requirements of printed electrodes is that they be conductive, this was thought to be an excellent choice. Table 3.4 shows the results of this analysis for all runs. The development of constrains based on this data is discussed in the next section of this chapter.

Table 3.4: Conductivity of lines printed using various combinations of high and low settings for silver mass fraction, solvent ratio, substrate surface energy, substrate temperature and dot-to-dot spacing.

			D/T = 5		D/T = 1	
			Ag = 25%	Ag = 40%	Ag = 25%	Ag = 40%
HMDS	T = 30C	DS = 20	No	Yes	No	Yes
		DS = 40	No	No	No	Yes
	T = 60C	DS = 20	No	Yes	Yes	Yes
		DS = 40	No	No	No	Yes
OTS	T = 30C	DS = 20	No	Yes	Yes	Yes
		DS = 40	No	No	No	Yes
	T = 60C	DS = 20	No	No	Yes	Yes
		DS = 40	No	No	Yes	Yes

3.3.3 Line Width

The width of each line printed using the experimental conditions listed in table 3 was measured using a surface profilometer. The results were then used to perform the calculations listed above to determine the β coefficients which would be used to form an optimization equation for this result. Since there are five input variables to this system, 32 coefficients are required to adequately represent the influence of each variable and all

potential variable interaction. These calculated coefficients are shown in table 3.5 in order of significance. As described earlier, a 95% confidence interval is developed for each coefficient. All coefficients whose interval contains zero are considered to be insignificant. The raw data used to make these calculations is also shown in table 3.5. The final calculated coefficients are shown in table 3.6.

Table 3.5: Raw data showing line width obtained for each experimental run outlined in table 3. Error in line width is ± 4.12μm

Mass Fraction Ag	Dodecane/ Terpineol Ratio	Substrate	Substrate Temperature	Drop Spacing	Line Width (μm)
0.25	5	HMDS	30	20	143
0.25	5	HMDS	30	40	100.5
0.25	5	HMDS	60	20	178.5
0.25	5	HMDS	60	40	115
0.25	1	HMDS	30	20	187
0.25	1	HMDS	30	40	128.5
0.25	1	HMDS	60	20	135
0.25	1	HMDS	60	40	98
0.4	5	HMDS	30	20	191.5
0.4	5	HMDS	30	40	136
0.4	5	HMDS	60	20	131.5
0.4	5	HMDS	60	40	96
0.4	1	HMDS	30	20	174
0.4	1	HMDS	30	40	127
0.4	1	HMDS	60	20	126
0.4	1	HMDS	60	40	96.5
0.25	5	OTS	30	20	238.5
0.25	5	OTS	30	40	144
0.25	5	OTS	60	20	162
0.25	5	OTS	60	40	101.5
0.25	1	OTS	30	20	144
0.25	1	OTS	30	40	84.5
0.25	1	OTS	60	20	131.5
0.25	1	OTS	60	40	81
0.4	5	OTS	30	20	198.5
0.4	5	OTS	30	40	141.5

0.4	5	OTS	60	20	137
0.4	5	OTS	60	40	96
0.4	1	OTS	30	20	125
0.4	1	OTS	30	40	119
0.4	1	OTS	60	20	127
0.4	1	OTS	60	40	88.5

Table 3.6: Value of coefficients in the equation describing the effect of silver nanoparticle concentration, solvent ratio, substrate surface energy, substrate temperature and dot-to-dot spacing on printed line width. Numbers associated with coefficients indicate variables or variable interactions. 1 = silver nanoparticle concentration; 2 = solvent ratio; 3 = substrate surface energy; 4 = substrate temperature; 5 = dot-to-dot spacing.

Coefficient	Value	Significant?
β_0	133.86	Yes
β_{34}	-22.02	Yes
β_{24}	16.80	Yes
β_4	-10.86	Yes
β_{12}	-9.20	Yes
β_{45}	-7.80	Yes
β_{12345} (error)	-6.89	No
β_2	5.83	No
β_{134}	-5.45	No
β_{35}	5.27	No
β_1	5.17	No
β_{234}	-4.61	No
β_{2345}	3.98	No
β_{125}	3.55	No
β_5	3.08	No
β_3	-2.73	No
β_{135}	-2.64	No
β_{1345}	2.64	No
β_{15}	-2.48	No
β_{245}	-2.45	No
β_{345}	-2.33	No
β_{235}	2.02	No
β_{14}	-1.55	No
β_{123}	-1.55	No
β_{1234}	-1.30	No
β_{13}	1.11	No

β_{1245}	-1.11	No
β_{124}	-1.05	No
β_{23}	-0.52	No
β_{145}	-0.52	No
β_{25}	-0.20	No
β_{1235}	-0.05	No

From the above data, it is evident that there are several variables and variable interactions which have a significant influence over the line width. These results show that a single variable can indeed have contrasting effects on a single variable. Substrate temperature, for instance, is shown to be positively correlated with line width when interacting with solvent ratio (β_{24}) but also negatively as a single variable (β_4) and when interacting with substrate surface energy (β_{34}). This is true for several of the variables. Silver nanoparticle concentration, for instance, is positively related to line width as an individual variable, but negatively related as an interaction with solvent ratio. Although the information obtained through this study is invaluable for determining and understanding the influence of all variables on line width, the presence of these conflicting influences make anything further than qualitative descriptions incredibly difficult. For this reason, this section will deal only with these qualitative observations. Quantitative optimization based on non-linear optimization of the above coefficients will be discussed later in the chapter.

3.3.3.1 Influence of Silver Nanoparticle Concentration on Printed Line Width

From the above data it is evident that silver nanoparticle concentration has a significant influence through the following coefficients:

1) β_1 (= 5.17): Independently, silver nanoparticle concentration is positively correlated with printed line width, meaning that as silver nanoparticle concentration is increased, the printed line width is also increased.
2) β_{12} (= -9.20): The interaction of silver nanoparticle concentration and solvent ratio is negatively correlated with printed line width. This indicates that if the product of silver nanoparticle concentration and solvent ratio is positive (both are -1 or both are +1) the result is a decrease in line width. Conversely if the product is negative (the variables have opposite sign) the result will be an increase in line width.

3.3.3.2 Influence of Solvent Ratio on Printed Line Width

From the above data it is evident that solvent ratio has a significant influence through the following coefficients:

1) β_{24} (= 16.80): The interaction of solvent ratio and substrate temperature is positively correlated with printed line width, indicating that if the product of these two variables is positive the result is an increase in printed line width.
2) β_{12} (= -9.20): The correlation of solvent ratio and silver nanoparticle concentration was discussed in the above section. It is clear that there is a

negative correlation with printed line width.

3.3.3.3 Influence of Substrate Surface Energy on Printed Line Width

From the above data it is evident that substrate surface energy has a significant influence through the following coefficient:

1) β_{34} (= -22.02): The interaction of substrate surface energy and substrate temperature is negatively correlated with printed line width.

3.3.3.4 Influence of Substrate Temperature on Printed Line width

From the above data it is evident that substrate temperature has a significant influence through the following coefficients:

1) β_{34} (= -22.02): The interaction of substrate surface energy and substrate temperature is negatively correlated with printed line width.
2) β_{24} (= 16.80): The interaction of solvent ratio and substrate temperature is positively correlated with printed line width.
3) β_4 (= -10.86): Independently, substrate temperature is negatively correlated with printed line width.
4) β_{45} (= -7.80): The interaction of substrate temperature and dot-to-dot spacing is negatively correlated with printed line width.

3.3.3.5 Influence of Dot-to-Dot Spacing on Printed Line Width

From the above data it is evident that dot-to-dot spacing has a significant influence through the following coefficient:

1) β_{45} (= -7.80): The interaction of substrate temperature and dot-to-dot spacing is negatively correlated with printed line width.

3.3.4 Line Thickness

The thickness of each line printed using the experimental conditions shown in table 3 was measured using a surface profilometer. This was used to calculated the coefficients for the optimization equation for line thickness. Again, there were thirty two coefficients involved in this equation. The raw data for this study is shown in table 3.7. The calculated value of the coefficients is shown in table 3.8.

Table 3.7: Raw data showing line thickness obtained for each experimental run outlined in table 3. Error in line thickness is ± 26.3μm

Mass Fraction Ag	Dodecane/ Terpineol Ratio	Substrate	Substrate Temperature	Drop Spacing	Thickness (A)
0.25	5	HMDS	30	20	404.08
0.25	5	HMDS	30	40	313
0.25	5	HMDS	60	20	810.39
0.25	5	HMDS	60	40	679.91
0.25	1	HMDS	30	20	844.16
0.25	1	HMDS	30	40	643.87
0.25	1	HMDS	60	20	1050.29
0.25	1	HMDS	60	40	805.02
0.4	5	HMDS	30	20	1044.31
0.4	5	HMDS	30	40	908.24
0.4	5	HMDS	60	20	1585.14
0.4	5	HMDS	60	40	1197.35

0.4	1	HMDS	30	20	1297.8
0.4	1	HMDS	30	40	1262.64
0.4	1	HMDS	60	20	1737.05
0.4	1	HMDS	60	40	1216.8
0.25	5	OTS	30	20	1407.82
0.25	5	OTS	30	40	896.85
0.25	5	OTS	60	20	1315.57
0.25	5	OTS	60	40	1242.38
0.25	1	OTS	30	20	1712.55
0.25	1	OTS	30	40	1731.6
0.25	1	OTS	60	20	1837.74
0.25	1	OTS	60	40	2009.93
0.4	5	OTS	30	20	1024.45
0.4	5	OTS	30	40	854.21
0.4	5	OTS	60	20	1771.44
0.4	5	OTS	60	40	1401.35
0.4	1	OTS	30	20	1464.7
0.4	1	OTS	30	40	1168.75
0.4	1	OTS	60	20	1761.59
0.4	1	OTS	60	40	1226.02

Table 3.8: Value of coefficients in the equation describing the effect of silver nanoparticle concentration, solvent ratio, substrate surface energy, substrate temperature and dot-to-dot spacing on printed line thickness. Numbers associated with coefficients indicate variables or variable interactions. 1 = silver nanoparticle concentration; 2 = solvent ratio; 3 = substrate surface energy; 4 = substrate temperature; 5 = dot-to-dot spacing.

Coefficient	Value	Significant?
β_0	1207.09	Yes
β_{134}	-164.85	Yes
β_1	-145.28	Yes
β_{12345} (error)	122.82	No
β_{1234}	-120.93	No
β_{14}	119.34	No
β_{1345}	-100.17	No
β_{25}	97.21	No
β_{124}	91.81	No
β_{23}	85.34	No
β_{24}	-84.63	No
β_3	73.13	No

β_{35}	71.80	No
β_{123}	67.64	No
β_{2}	-65.41	No
β_{145}	-63.90	No
β_{5}	59.57	No
β_{135}	-53.28	No
β_{13}	-50.24	No
β_{34}	-48.53	No
β_{125}	39.00	No
β_{4}	37.53	No
β_{245}	-36.61	No
β_{2345}	-27.30	No
β_{345}	23.92	No
β_{234}	23.34	No
β_{15}	23.23	No
β_{235}	-23.21	No
β_{12}	19.85	No
β_{1245}	19.78	No
β_{45}	-8.75	No
β_{1235}	8.03	No

3.3.4.1 Influence of Silver Nanoparticle Concentration on Printed Line Thickness

From the above data it is evident that silver nanoparticle concentration has a significant influence through the following coefficients:

1) β_{134} (= -164.85): The interaction of silver nanoparticle concentration, substrate surface energy and substrate temperature is negatively correlated with printed line thickness.
2) β_{1} (= -145.28): Independently, silver nanoparticle concentration has a negative correlation with printed line thickness

3.3.4.2 Influence of Substrate Surface Energy on Printed Line Thickness

From the above data it is evident that substrate surface energy has a significant influence through the following coefficient:

1) β_{134} (= -164.85): The interaction of silver nanoparticle concentration, substrate surface energy and substrate temperature is negatively correlated with printed line thickness.

3.3.4.3 Influence of Substrate Temperature on Printed Line Thickness

From the above data it is evident that substrate temperature has a significant influence through the following coefficient:

1) β_{134} (= -164.85): The interaction of silver nanoparticle concentration, substrate surface energy and substrate temperature is negatively correlated with printed line thickness.

3.3.5 Center to Edge Height Ratio

The center to edge height ratio was calculated for each run outlined in table 3. This data was used to calculate the coefficients for the optimization equation. The raw data for this study is shown in table 3.9, and the calculated coefficients are listed in table 3.10.

Table 3.9: Raw data showing center to edge height ratio obtained for each experimental run outlined in table 3. Error in center to edge height ratio is ± 0.084μm

Mass Fraction Ag	Dodecane/ Terpineol Ratio	Substrate	Substrate Temperature	Drop Spacing	hc/he
0.25	5	HMDS	30	20	1.3
0.25	5	HMDS	30	40	1.126
0.25	5	HMDS	60	20	0.639
0.25	5	HMDS	60	40	0.604
0.25	1	HMDS	30	20	1.48
0.25	1	HMDS	30	40	1.36
0.25	1	HMDS	60	20	1.15
0.25	1	HMDS	60	40	1.08
0.4	5	HMDS	30	20	1.02
0.4	5	HMDS	30	40	1.11
0.4	5	HMDS	60	20	0.7
0.4	5	HMDS	60	40	0.909
0.4	1	HMDS	30	20	1.39
0.4	1	HMDS	30	40	1.25
0.4	1	HMDS	60	20	1
0.4	1	HMDS	60	40	1.26
0.25	5	OTS	30	20	0.964
0.25	5	OTS	30	40	0.957
0.25	5	OTS	60	20	0.955
0.25	5	OTS	60	40	0.908
0.25	1	OTS	30	20	1.42
0.25	1	OTS	30	40	1.26
0.25	1	OTS	60	20	0.91
0.25	1	OTS	60	40	0.98
0.4	5	OTS	30	20	0.87
0.4	5	OTS	30	40	1.01
0.4	5	OTS	60	20	0.748
0.4	5	OTS	60	40	0.848
0.4	1	OTS	30	20	1.3
0.4	1	OTS	30	40	1.4
0.4	1	OTS	60	20	1.08
0.4	1	OTS	60	40	1.1

Table 3.10: Value of coefficients in the equation describing the effect of silver nanoparticle concentration, solvent ratio, substrate surface energy, substrate temperature and dot-to-dot spacing on center to edge height ratio. Numbers associated with coefficients indicate variables or variable interactions. 1 = silver nanoparticle concentration; 2 = solvent ratio; 3 = substrate surface energy; 4 = substrate temperature; 5 = dot-to-dot spacing.

Coefficient	Value	Significant?
β_0	1.07	Yes
β_{12345}	0.09	No
β_{345}	-0.09	No
β_{134}	0.07	No
β_{1245}	-0.07	No
β_{234}	-0.06	No
β_4	-0.06	No
β_{35}	-0.05	No
β_2	-0.05	No
β_1	-0.05	No
β_{14}	-0.04	No
β_{123}	0.03	No
β_3	-0.03	No
β_{34}	-0.03	No
β_{13}	0.03	No
β_{2345}	0.03	No
β_{235}	-0.03	No
β_{23}	-0.03	No
β_{1234}	0.02	No
β_{15}	0.02	No
β_{1345}	0.02	No
β_5	0.02	No
β_{124}	0.02	No
β_{45}	0.02	No
β_{135}	0.02	No
β_{125}	0.02	No
β_{1235}	0.01	No
β_{24}	-0.01	No
β_{145}	0.01	No
β_{12}	0.01	No
β_{245}	0.00	No
β_{25}	0.00	No

Interestingly, no variables or variable interactions were found to have significant influence over the center to edge ratio. Instead this ratio is predicted to remain constant regardless of variable settings. This is due to previous optimization study on the solvents selection for the ink formulation, wherein minimizing coffee ring effect was already taken into account.

3.3.6 Final Conclusions Based on DOE Study

Based on the above data conclusions can be drawn regarding which variables and variable interactions have the greatest influence over printed line width, line thickness and center to edge ratio. This information is crucial to the ability to both optimize the system and troubleshoot the system. It is important to recall that the coefficient describing the interaction of all five variables is considered to be representative of the amount of error in the study. Thus any variable with lower influence than this variable was considered insignificant.

From table 6, one can see that the three most influential terms over printed line width are the interaction of substrate surface energy and substrate temperature (β=-22); the interaction of solvent ratio and substrate temperature (β = 16); and the independent influence of substrate temperature (β = -11). Based on this data, it is evident that to decrease the width of inkjet printed silver nanoparticle lines, one must ensure that the product of surface energy and substrate temperature is +1, the product of solvent ratio and surface temperature is -1, and that substrate temperature remains at +1. Because we

know this final fact, we can then deduce that substrate surface energy must have a value of +1 (HMDS modified) and solvent ratio must have a value of -1 (1:1).

From table 8, one can see that the two influential terms regarding printed line thickness are the interaction of silver mass fraction, substrate surface energy and substrate temperature (β = -165) and the independent influence of silver mass fraction (β = -145). Based on this data, we can see that in order to maximize line thickness, one must set the silver mass fraction to a value of -1 and the product of silver mass fraction, substrate surface energy and substrate temperature to -1. Because these terms involve interactions of three variables, it is very difficult to determine the optimal values. Thus computer optimization is used to determine the optimal variable settings. This is shown in the next section.

3.4 Non-Linear Optimization

Having determined the influence of each variable and all variable interaction on the width, thickness and center to edge height ratio of printed lines, a non-linear optimization program was developed such that the optimal input variable setting could be determined. This optimization was performed independently for each output variable. In order to accomplish the optimization we required both a set of constraints and an objective function for each output variable.

3.4.1 Development of Variables for Optimization Study

In order to successfully perform an optimization of these output variables, one must first develop the input variables to be used. In this case, each of our input variables can be chosen to be either **+1** or **-1**. Since our variables must be one of two choices, our system closely resembles a binary system. However in a binary system one is given the choice between zero and one. Thus if we are to use binary variables in this optimization, we must map them to our allowable values before they are used in the objective function. This was accomplished using equation (9). Using this equation it is evident that if a value of **+1** is chosen for the binary variable (x^b) this will be mapped to **+1**, whereas if a value of **0** is chosen for the binary variable it will be mapped to **-1**.

$$x_i = 2x_i^{\,b} - 1 \quad \textit{where} \quad x_i^{\,b} \in \textit{binary} \tag{9}$$

3.4.2 Development of Constraints for Optimization

As mentioned earlier, it was decided that the conductivity data would be used to form the constraints for the optimization. This decision was based on the fact that the first and foremost goal of this study was to print lines which were conductive. Any optimization of resolution and film uniformity must not have any adverse effects on conductivity. With this in mind, constraints were developed such that they would force the optimization program to choose only combinations of variables which resulted in conductive lines. For the reader's convenience, the conductivity data is shown here again in table 3.11.

Table 3.11: Conductivity of lines printed using various combinations of high and low settings for silver mass fraction, solvent ratio, substrate surface energy, substrate temperature and dot-to-dot spacing.

			D/T = 5		D/T = 1	
			Ag = 25%	Ag = 40%	Ag = 25%	Ag = 40%
HMDS	T = 30C	DS = 20μm	No	Yes	No	Yes
		DS = 40μm	No	No	No	Yes
	T = 60C	DS = 20μm	No	Yes	Yes	Yes
		DS = 40μm	No	No	No	Yes
OTS	T = 30C	DS = 20μm	No	Yes	Yes	Yes
		DS = 40μm	No	No	No	Yes
	T = 60C	DS = 20μm	No	No	Yes	Yes
		DS = 40μm	No	No	Yes	Yes

The first constraint applied to this optimization is that if the silver nanoparticle concentration is 25%, the solvent ratio (D/T) must be 1. As is evident from table 3.11 no combination of variables which includes 25% silver concentration and a solvent ratio of 5 results in a conductive line. Thus this constraint was used to block this combination.

The second constraint applied to the optimization is that if the silver nanoparticle concentration is 25%, the dot-to-dot spacing must be 20μm. This constraint was chosen due to the fact that any variable combination which includes a silver nanoparticle concentration of 25% and a dot-to-dot spacing of 40μm results in a non-conductive line.

The third constraint applied to this optimization is that if the solvent ratio is equal to 5, then dot-to-dot spacing spacing must be 20μm. This was chosen because no line printed with at dot-to-dot spacing of 40μm and a solvent ratio of 5 was found to be conductive.

The final constrain applied to this optimization is that if solvent ratio is 1 and the substrate is HMDS modified and the substrate temperature is 30°C then the silver nanoparticle concentration must be 40%. This was chosen because lines printed onto HMDS modified substrates with a solvent ratio of 1 and a silver concentration of 25% were found to be non-conductive regardless of dot-to-dot spacing.

The total effect of these constraints is to block out almost all combinations of variables which result in non-conductive lines. This can be seen in table 3.12, where combinations of variables which have been blocked out by constraints are shaded with grey.

Table 3.12: Conductivity data for experiments performed with different combinations of variable settings. Variable setting combinations disallowed by constraints are shown shaded in grey.

			D/T = 5		D/T = 1	
			Ag = 25%	Ag = 40%	Ag = 25%	Ag = 40%
HMDS	T = 30C	DS = 20	No	Yes	No	Yes
		DS = 40	No	No	No	Yes
	T = 60C	DS = 20	No	Yes	Yes	Yes
		DS = 40	No	No	No	Yes
OTS	T = 30C	DS = 20	No	Yes	Yes	Yes
		DS = 40	No	No	No	Yes
	T = 60C	DS = 20	No	No	Yes	Yes
		DS = 40	No	No	Yes	Yes

In order to apply these constraints in the optimization program, the must first be converted into mathematical inequalities. When doing this it is essential that the inequality block only those combinations that are desired. The inequalities used in this optimization to represent these constraints are shown in equations 10 – 13.

Constraint #1: *If* x_1 (silver nanoparticle concentration) = **-1** (25%), *then* x_2 (solvent ratio) = **-1** (D/T = 1).

$$x_1 - x_2 \geq 0 \tag{10}$$

The reader can verify that all combinations of x_1 and x_2 satisfy this inequality except x_1 = **-1** and x_2 = **1**.

Constraint #2: *If* x_1 (silver nanoparticle concentration) = **-1** (25%), *then* x_5 (dot-to-dot spacing) = **-1** (20μm).

$$x_1 - x_5 \geq 0 \tag{11}$$

The reader can verify that all combinations of x_1 and x_2 satisfy this inequality except x_1 = **-1** and x_5 = **1**.

Constraint #3: *If* x_2 (solvent ratio) = **1** (D/T = 5), *then* x_5 (dot-to-dot spacing) = **-1** (20μm).

$$-x_2 - x_5 \geq 0 \tag{12}$$

The reader can verify that all combinations of x_1 and x_2 satisfy this inequality except x_1 = **1** and x_5 = **1**.

Constraint #4: *If* x_2 (solvent ratio) = **-1** (D/T = 1) *and* x_3 (substrate surface energy) = **1** (HMDS modified) *and* x_4 (substrate temperature) = **-1** (30°C) *then* x_1 (silver nanoparticle concentration) = **1** (40%).

$$-x_1 - x_2 + x_3 - x_4 \leq 3 \tag{13}$$

The reader can verify that all combinations of x_1 and x_2 satisfy this inequality except $x_1 = \mathbf{-1}, x_2 = \mathbf{-1}, x_3 = \mathbf{1}, x_4 = \mathbf{-1}$.

3.4.3 Development of Objective Equations

The objective equations for these optimizations are fairly simple to develop. An objective equation describes mathematically the goal of the optimization. The algorithm used for the optimization then chooses settings for the input variables which move as far in the direction of this goal as possible.

In the case of printed line width, our goal in the optimization is to choose a combination of variable settings which yields conductive lines which are as narrow as possible. Since our DOE study has already yielded an equation which describes the influence of each variable and all variable interactions on the printed line width, our objective function in this case is simply to minimize this equation. This can be seen in equation (14) where the β values shown are those from table 5.

$$\begin{aligned} LW = {} & \beta_0 + \beta_1 x_1 + \beta_2 x_2 + \beta_3 x_3 + \beta_4 x_4 + \beta_5 x_5 + \\ & \beta_{12} x_1 x_2 + \beta_{13} x_1 x_3 + \beta_{14} x_1 x_4 \beta_{15} x_1 x_5 + \beta_{23} x_2 x_3 + \\ & \beta_{24} x_2 x_4 + \beta_{25} x_2 x_5 + \beta_{34} x_3 x_4 + \beta_{35} x_3 x_5 + \\ & \beta_{45} x_4 x_5 + \beta_{123} x_1 x_2 x_3 + \beta_{124} x_1 x_2 x_4 + \beta_{125} x_1 x_2 x_5 + \\ & \beta_{134} x_1 x_3 x_4 + \beta_{135} x_1 x_3 x_5 + \beta_{145} x_1 x_4 x_5 + \\ & \beta_{234} x_2 x_3 x_4 + \beta_{235} x_2 x_3 x_5 + \beta_{245} x_2 x_4 x_5 + \\ & \beta_{345} x_3 x_4 x_5 + \beta_{1234} x_1 x_2 x_3 x_4 + \beta_{1235} x_1 x_2 x_3 x_5 \\ & + \beta_{1245} x_1 x_2 x_4 x_5 + \beta_{1345} x_1 x_3 x_4 x_5 + \\ & \beta_{2345} x_2 x_3 x_4 x_5 + \beta_{12345} x_1 x_2 x_3 x_4 x_5 \end{aligned} \tag{14}$$

Objective

min LW

With respect to printed line thickness the goal of the optimization is to set the variable values such that the printed lines are as thick as possible to ensure the lines to be conductive. Again, the DOE has already yielded an equation which describes the total influence of each variable on the line thickness. The objective function for this case is simply to maximize this equation. This can be seen in equation (15), where the β values shown are those from table 6.

$$\begin{aligned} LT = {} & \beta_0 + \beta_1 x_1 + \beta_2 x_2 + \beta_3 x_3 + \beta_4 x_4 + \beta_5 x_5 + \\ & \beta_{12} x_1 x_2 + \beta_{13} x_1 x_3 + \beta_{14} x_1 x_4 \beta_{15} x_1 x_5 + \beta_{23} x_2 x_3 + \\ & \beta_{24} x_2 x_4 + \beta_{25} x_2 x_5 + \beta_{34} x_3 x_4 + \beta_{35} x_3 x_5 + \\ & \beta_{45} x_4 x_5 + \beta_{123} x_1 x_2 x_3 + \beta_{124} x_1 x_2 x_4 + \beta_{125} x_1 x_2 x_5 + \\ & \beta_{134} x_1 x_3 x_4 + \beta_{135} x_1 x_3 x_5 + \beta_{145} x_1 x_4 x_5 + \\ & \beta_{234} x_2 x_3 x_4 + \beta_{235} x_2 x_3 x_5 + \beta_{245} x_2 x_4 x_5 + \\ & \beta_{345} x_3 x_4 x_5 + \beta_{1234} x_1 x_2 x_3 x_4 + \beta_{1235} x_1 x_2 x_3 x_5 \\ & + \beta_{1245} x_1 x_2 x_4 x_5 + \beta_{1345} x_1 x_3 x_4 x_5 + \\ & \beta_{2345} x_2 x_3 x_4 x_5 + \beta_{12345} x_1 x_2 x_3 x_4 x_5 \end{aligned} \tag{15}$$

Objective

max LT

The objective function for the optimization of center to edge height ratio requires some manipulation. In this case the goal of our optimization is to print lines with a center to edge height ratio as close to 1 as possible. Since this is neither a minimization nor a maximization, we need to create an equation which will either move towards infinity or towards zero as center to edge height ratio moves towards 1. This can be seen in equation (16), where the β values shown are those from table 7.

$$CE = \beta_0 + \beta_1 x_1 + \beta_2 x_2 + \beta_3 x_3 + \beta_4 x_4 + \beta_5 x_5 + \beta_{12} x_1 x_2 + \beta_{13} x_1 x_3 + \beta_{14} x_1 x_4 \beta_{15} x_1 x_5 + \beta_{23} x_2 x_3 + \beta_{24} x_2 x_4 + \beta_{25} x_2 x_5 + \beta_{34} x_3 x_4 + \beta_{35} x_3 x_5 + \beta_{45} x_4 x_5 + \beta_{123} x_1 x_2 x_3 + \beta_{124} x_1 x_2 x_4 + \beta_{125} x_1 x_2 x_5 + \beta_{134} x_1 x_3 x_4 + \beta_{135} x_1 x_3 x_5 + \beta_{145} x_1 x_4 x_5 + \beta_{234} x_2 x_3 x_4 + \beta_{235} x_2 x_3 x_5 + \beta_{245} x_2 x_4 x_5 + \beta_{345} x_3 x_4 x_5 + \beta_{1234} x_1 x_2 x_3 x_4 + \beta_{1235} x_1 x_2 x_3 x_5 + \beta_{1245} x_1 x_2 x_4 x_5 + \beta_{1345} x_1 x_3 x_4 x_5 + \beta_{2345} x_2 x_3 x_4 x_5 + \beta_{12345} x_1 x_2 x_3 x_4 x_5 \quad (16)$$

Objective

$$\min \left| 1 - 10^{(1-CE)} \right|$$

3.4.4 Full Optimization Schemes

The full schemes used for the optimization of printed line width, printed line thickness and center to edge height ratio are shown in schemes 1 – 3. These schemes were inputted into GAMS optimization software, and solved as a mixed integer non-linear programming problem using the CONOPT solver.

Variables

$$\left.\begin{matrix} x_1^{\,b} \\ x_2^{\,b} \\ x_3^{\,b} \\ x_4^{\,b} \\ x_5^{\,b} \end{matrix}\right\} \textit{binary variables}$$

$$\left.\begin{matrix} x_1 \\ x_2 \\ x_3 \\ x_4 \\ x_5 \end{matrix}\right\} \textit{converted binary varaibles}$$

$LW\}$ *Line Width*

Constraints

$$x_1 - x_2 \geq 0$$
$$x_1 - x_5 \geq 0$$
$$-x_2 - x_5 \geq 0$$
$$-x_1 - x_2 + x_3 - x_4 \leq 3$$

Equations

$$x_1 = 2x_1^{\,b} - 1$$
$$x_2 = 2x_2^{\,b} - 1$$
$$x_3 = 2x_3^{\,b} - 1$$
$$x_4 = 2x_4^{\,b} - 1$$
$$x_5 = 2x_5^{\,b} - 1$$

$$LW = \beta_0 + \beta_1 x_1 + \beta_2 x_2 + \beta_3 x_3 + \beta_4 x_4 + \beta_5 x_5 + \beta_{12} x_1 x_2 + \beta_{13} x_1 x_3 + \beta_{14} x_1 x_4 \beta_{15} x_1 x_5 + \beta_{23} x_2 x_3 + \beta_{24} x_2 x_4 + \beta_{25} x_2 x_5 + \beta_{34} x_3 x_4 + \beta_{35} x_3 x_5 + \beta_{45} x_4 x_5 + \beta_{123} x_1 x_2 x_3 + \beta_{124} x_1 x_2 x_4 + \beta_{125} x_1 x_2 x_5 + \beta_{134} x_1 x_3 x_4 + \beta_{135} x_1 x_3 x_5 + \beta_{145} x_1 x_4 x_5 + \beta_{234} x_2 x_3 x_4 + \beta_{235} x_2 x_3 x_5 + \beta_{245} x_2 x_4 x_5 + \beta_{345} x_3 x_4 x_5 + \beta_{1234} x_1 x_2 x_3 x_4 + \beta_{1235} x_1 x_2 x_3 x_5 + \beta_{1245} x_1 x_2 x_4 x_5 + \beta_{1345} x_1 x_3 x_4 x_5 + \beta_{2345} x_2 x_3 x_4 x_5 + \beta_{12345} x_1 x_2 x_3 x_4 x_5$$

Objective

min LW

Scheme 3.1: Optimization of line width using data from DOE study

Variables

$$\left.\begin{matrix} x_1^{\,b} \\ x_2^{\,b} \\ x_3^{\,b} \\ x_4^{\,b} \\ x_5^{\,b} \end{matrix}\right\} \textit{binary variables}$$

$$\left.\begin{matrix} x_1 \\ x_2 \\ x_3 \\ x_4 \\ x_5 \end{matrix}\right\} \textit{converted binary varaibles}$$

$$LT\} \quad \textit{Line Thickness}$$

Constraints

$$x_1 - x_2 \geq 0$$
$$x_1 - x_5 \geq 0$$
$$-x_2 - x_5 \geq 0$$
$$-x_1 - x_2 + x_3 - x_4 \leq 3$$

Equations

$$x_1 = 2x_1^{\,b} - 1$$
$$x_2 = 2x_2^{\,b} - 1$$
$$x_3 = 2x_3^{\,b} - 1$$
$$x_4 = 2x_4^{\,b} - 1$$
$$x_5 = 2x_5^{\,b} - 1$$

$$LT = \beta_0 + \beta_1 x_1 + \beta_2 x_2 + \beta_3 x_3 + \beta_4 x_4 + \beta_5 x_5 + \beta_{12} x_1 x_2 + \beta_{13} x_1 x_3 + \beta_{14} x_1 x_4 \beta_{15} x_1 x_5 + \beta_{23} x_2 x_3 +$$
$$\beta_{24} x_2 x_4 + \beta_{25} x_2 x_5 + \beta_{34} x_3 x_4 + \beta_{35} x_3 x_5 + \beta_{45} x_4 x_5 + \beta_{123} x_1 x_2 x_3 + \beta_{124} x_1 x_2 x_4 + \beta_{125} x_1 x_2 x_5 +$$
$$\beta_{134} x_1 x_3 x_4 + \beta_{135} x_1 x_3 x_5 + \beta_{145} x_1 x_4 x_5 + \beta_{234} x_2 x_3 x_4 + \beta_{235} x_2 x_3 x_5 + \beta_{245} x_2 x_4 x_5 + \beta_{345} x_3 x_4 x_5 +$$
$$\beta_{1234} x_1 x_2 x_3 x_4 + \beta_{1235} x_1 x_2 x_3 x_5 + \beta_{1245} x_1 x_2 x_4 x_5 + \beta_{1345} x_1 x_3 x_4 x_5 + \beta_{2345} x_2 x_3 x_4 x_5 + \beta_{12345} x_1 x_2 x_3 x_4 x_5$$

Objective

$$\max \quad LT$$

Scheme 3.2: Optimization of line thickness using data from DOE study

Variables

$$\left.\begin{matrix} x_1^{\,b} \\ x_2^{\,b} \\ x_3^{\,b} \\ x_4^{\,b} \\ x_5^{\,b} \end{matrix}\right\} \textit{binary variables}$$

$$\left.\begin{matrix} x_1 \\ x_2 \\ x_3 \\ x_4 \\ x_5 \end{matrix}\right\} \textit{converted binary varaibles}$$

CE Center to edge edge height ratio

Constraints

$$x_1 - x_2 \geq 0$$
$$x_1 - x_5 \geq 0$$
$$-x_2 - x_5 \geq 0$$
$$-x_1 - x_2 + x_3 - x_4 \leq 3$$

Equations

$$x_1 = 2x_1^{\,b} - 1$$
$$x_2 = 2x_2^{\,b} - 1$$
$$x_3 = 2x_3^{\,b} - 1$$
$$x_4 = 2x_4^{\,b} - 1$$
$$x_5 = 2x_5^{\,b} - 1$$

$$CE = \beta_0 + \beta_1 x_1 + \beta_2 x_2 + \beta_3 x_3 + \beta_4 x_4 + \beta_5 x_5 + \beta_{12} x_1 x_2 + \beta_{13} x_1 x_3 + \beta_{14} x_1 x_4 \beta_{15} x_1 x_5 + \beta_{23} x_2 x_3 + \beta_{24} x_2 x_4 + \beta_{25} x_2 x_5 + \beta_{34} x_3 x_4 + \beta_{35} x_3 x_5 + \beta_{45} x_4 x_5 + \beta_{123} x_1 x_2 x_3 + \beta_{124} x_1 x_2 x_4 + \beta_{125} x_1 x_2 x_5 + \beta_{134} x_1 x_3 x_4 + \beta_{135} x_1 x_3 x_5 + \beta_{145} x_1 x_4 x_5 + \beta_{234} x_2 x_3 x_4 + \beta_{235} x_2 x_3 x_5 + \beta_{245} x_2 x_4 x_5 + \beta_{345} x_3 x_4 x_5 + \beta_{1234} x_1 x_2 x_3 x_4 + \beta_{1235} x_1 x_2 x_3 x_5 + \beta_{1245} x_1 x_2 x_4 x_5 + \beta_{1345} x_1 x_3 x_4 x_5 + \beta_{2345} x_2 x_3 x_4 x_5 + \beta_{12345} x_1 x_2 x_3 x_4 x_5$$

Objective

$$\min \left| 1 - 10^{(1-CE)} \right|$$

Scheme 3.3: Optimization of Center to edge height ratio using data from DOE study

3.4.5 Results of Optimization Studies

The above optimizations were performed using several initial guesses for the variables such that the optimal variable values determined could be considered to be accurate. Each optimization resulted in a combination of variable values which was optimized for a single output variable. For instance the optimization performed on line width was completely independent of the optimizations performed for line thickness and center to edge height ratio. The optimal variable settings which were determined for all optimizations are shown in table 3.13.

Table 3.13: Optimal variable settings determined by optimizing system for various output variables

Variable	Output Variable		
	Line Width	**Line Thickness**	**Center to Edge Height Ratio**
Silver Nanoparticle Concentration	25%	25%	25%
Solvent Ratio	1:1	1:1	1:1
Substrate Surface Energy	HMDS	OTS	OTS
Substrate Temperature	60°C	30°C	30°C
Dot-to-Dot Spacing	20μm	20μm	20μm
Objective Function	**75μm**	**1224.9A**	**1.07**

Based on the above results, it is evident that the optimal variable settings for line thickness and center to edge height ratio are the same, whereas those for line width are slightly different.

3.4.6 Determining the Optimal Variable Setting

In order to determine which of the above sets of variable values is indeed the optimal for the system, one must revisit the overall goals of this study. Recall that the hope was to optimize the process such that highly conductive, highly resolute electrodes with excellent film uniformity could be inkjet printed. Based on the constraints system which was developed we know that both of the variable settings described above result in conductive lines. Therefore we must choose the variable setting which will provide the greatest resolution and the highest film uniformity.

Since line width is directly related to printing resolution and line thickness is not, the apparent choice of variable setting would be to use that determined by optimizing line width. This decision can be verified by inputting these variable settings into the optimization equation for center to edge height ratio determined in section 3.5. When this is done, we can see that these variable settings result in a predicted center to edge height ratio of 1.29 – still an excellent ratio. Thus by using the variable settings determined by the line width optimization we achieve conductive lines with the highest possible resolution and excellent film uniformity.

Given all of this information, it was decided that the optimal variable settings for inkjet printing silver nanoparticle ink for the fabrication of electrodes are those obtained when optimizing the process for line width. These can be seen in table 3.14.

Table 3.14: Optimal variable setting for inkjet printing silver nanoparticle ink for fabrication of source and drain electrodes of OTFT devices.

Variable	Optimal Setting
Silver Nanoparticle Concentration	25%
Solvent Ratio	1:1
Substrate Surface Energy	HMDS Modified Substrate
Substrate Temperature	60°C
Dot-to-Dot Spacing	20μm

3.5 Fabrication of OTFT Devices

Having determined the optimal variable setting for inkjet printing silver nanoparticles, it was then necessary to show that these printed electrodes could be integrated into OTFTs to yield high performance devices. Two different devices were fabricated.

The first was an OTFT fabricated in the standard manner for testing. Silver nanoparticles were printed onto a heavily doped n-type silicon wafer (gate) with a 200nm SiO_2 layer (dielectric). After the printed lines were annealed, the substrate was modified with octyltrichlorosilane (OTS-8) and the electrodes were modified with octanethiol. These modifications have been shown to greatly improve the performance of OTFT devices. PQT – 12 was then spin coated over the entire wafer. Figure 3.3 shows the final transistor. From this image it is clear that the silver nanoparticle ink can be printed to yield highly resolute lines with no edge roughness.

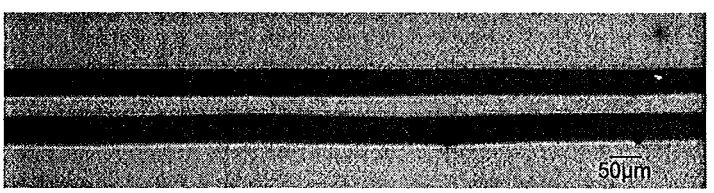

Figure 3.3: Organic thin film transistor fabricated using printed silver nanoparticle ink for source and drain electrodes. Electrodes were printed onto heavily doped n-type

silicon wafer (gate) with a 200nm SiO_2 layer (dielectric). After the printed lines were annealed PQT – 12 was spin coated onto the wafer.

Figure 3.4a shows the drain current vs. gate voltage curve for the transistor shown in figure 3.3. Figure 3.4b shows the drain current vs. source voltage for a range of gate voltages. Through these images it is evident that there is minimal contact resistance in our transistor. Furthermore the mobility of the device was calculated to be $0.11 cm^2/Vs$ and the on/off current ratio was found to be 10^7. These values are in line with what has been previously reported for devices fabricated using PQT – 12 and vacuum evaporated silver, indicating no performance is lost due to inkjet printing fabrication.

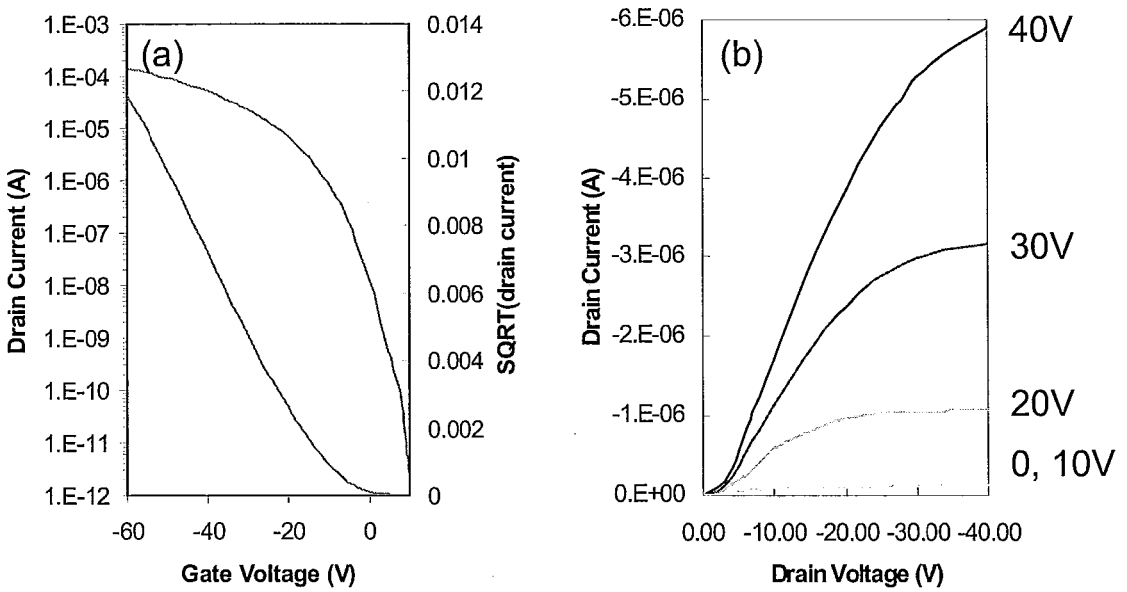

Figure 3.4: Drain current vs. gate voltage (a) and drain current vs. drain voltage for a variety of gate voltages (b). Data is for the device shown in figure 3.3.

The second device fabricated using silver nanoparticle ink was a top-gate transistor. This was fabricated to illustrate the potential for an all-inkjet printed OTFT.

To fabricate this device source and drain electrodes were first printed onto a glass substrate. Following annealing of the silver, PQT-12 semiconductor was then inkjet printed into the channel. Following annealing of the PQT-12, a PVP dielectric was spin coated onto over the semiconductor. This was then thermally cross-linked. Finally a silver nanoparticle gate was printed and annealed on top of the gated semiconductor. A schematic of this fabrication process can be seen in figure 3.5. A picture of an actual device taken using an optical microscope can be seen in figure 3.6.

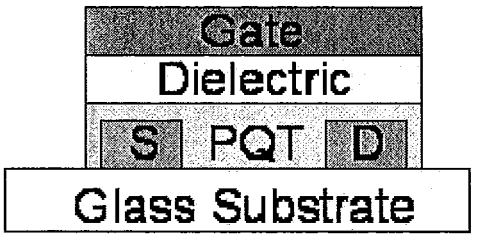

Figure 3.5: Schematic showing method of fabricating top-gate organic thin film transistors

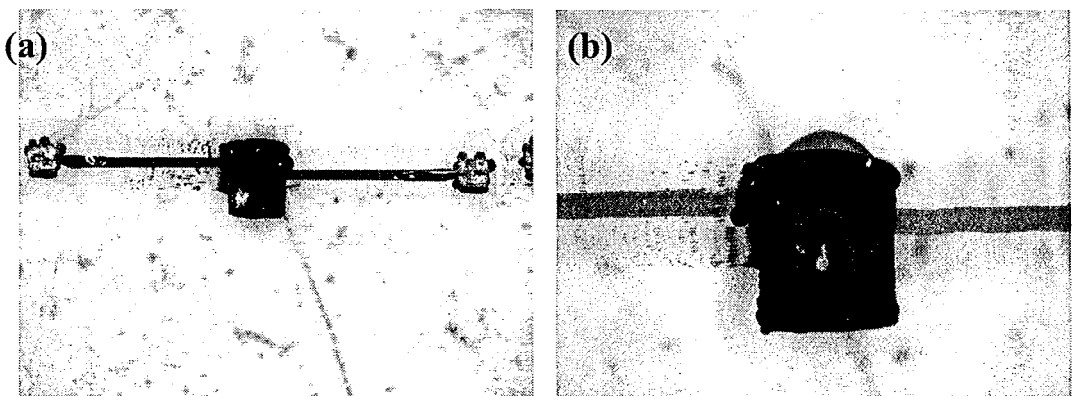

Figure 3.6: Top gate transistor fabricated using all solution processing methods. Silver nanoparticles were inkjet printed for the source, drain and gate electrodes, PQT-12 was inkjet printed for the semiconductor and PVP was spin coated for the dielectric.

The devices fabricated using this un-optimized printing process yielded very poor performance. The mobility of the device shown in figure 6 was only about 10^{-4} and the on/off current ratio was only about 10^{2}. This was not unexpected, however, as there are many issues which still need to be optimized for the successful fabrication of all solution processed OTFTs. This device was fabricated simply as a proof of concept illustrating that this was indeed possible.

3.6 Conclusions and Recommendations

The process of silver source and drain electrode fabrication using inkjet printed silver nanoparticle ink was optimized using a design of experiments study followed by a non-linear optimization study. This was found to be a very effective method for determining the complete influence of each input variable on a variety of output variables including line width, line thickness, center-to-edge height ratio and conductivity.

The optimized process was used to print electrodes for OTFT devices. Devices fabricated using silicon wafer as the gate with a silicon dioxide dielectric and PQT-12 semiconductor were found to yield excellent mobility and on/off current ratio. All solution processed top-gate devices were also fabricated and were shown to be functional, although the performance of these devices needs to be improved.

A great deal of work remains in this field. Ideally these silver nanoparticles will be used to fabricate all-inkjet printed OTFTs. For this to occur, a study similar to the one performed here should be carried out on the process of inkjet printing the semiconductor

and dielectric components of the OTFT. This will allow each component to be printed with a high degree of resolution, film uniformity and performance.

Furthermore, a great deal of work must still be performed to allow for seamless integration of all of these components into one device. There currently remains some incompatibility between the silver electrodes and the organic semiconductor. Also, it is difficult to deposit the organic dielectric without creating 'pinholes', which in turn cause shorts in the devices and decrease the device yield. These, among many issues, must be addressed if inkjet printed OTFTs are indeed to be commercialized.

Although there remain many issues, this study has shown that there also remains great promise in this field. By approaching these problems from an engineering standpoint it is likely that the problems facing this technology can indeed be overcome.

3.7 References

1. Klauk, H. *et al.* High-mobility polymer gate dielectric pentacene thin film transistors. *J. Appl. Phys.* **92**, 5259-5263 (2002).

2. Kato, Y. *et al.* High mobility of pentacene field-effect transistors with polyimide gate dielectric layers. *Appl. Phys. Lett.* **84**, 3789-3791 (2004).

3. Rogers, J. A., Bao, Z., Dodabalapur, A. & Makhija, A. Organic smart pixels and complementary inverter circuits formed on plastic substrates by casting and rubber stamping. *Electron Device Letters, IEEE* **21**, 100-103 (2000).

4. Gundlach, D. J., Lin, Y. Y., Jackson, T. N., Nelson, S. F. & Schlom, D. G. Pentacene organic thin-film transistors-molecular ordering and mobility. *Electron Device Letters, IEEE* **18**, 87-89 (1997).

5. Servet, B. *et al.* Polymorphism and Charge Transport in Vacuum-Evaporated Sexithiophene Films. *Chemistry of Materials* **6**, 1809-1815 (1994).

6. Parashkov, R. *et al.* All-organic thin-film transistors made of poly(3-butylthiophene) semiconducting and various polymeric insulating layers. *J. Appl. Phys.* **95**, 1594-1596 (2004).

7. Nur, H. M., Song, J. H., Evans, J. R. G. & Edirisinghe, M. J. Ink-jet printing of gold conductive tracks. **13**, 213-219 (2002).

8. Wu, Y., Li, Y. & Ong, B. S. A Simple and Efficient Approach to a Printable Silver Conductor for Printed Electronics. *J. Am. Chem. Soc.* **129**, 1862-1863 (2007).

9. Wu, Y., Li, Y. & Ong, B. S. Printed Silver Ohmic Contacts for High-Mobility Organic Thin-Film Transistors. *J. Am. Chem. Soc.* **128**, 4202-4203 (2006).

10. Gamerith, S. *et al.* Direct Ink-Jet Printing of Ag-Cu Nanoparticle and Ag-Precursor Based Electrodes for OFET Applications. *Advanced Functional Materials* **17**, 3111-3118 (2007).

11. Mallick, K., Witcomb, M. J. & Scurrell, M. S. Directional assembly of polyaniline functionalized gold nanoparticles. *Journal of Physics: Condensed Matter*, 196225 (2007).

12. Sanaur, S., Whalley, A., Alameddine, B., Carnes, M. & Nuckolls, C. Jet-printed electrodes and semiconducting oligomers for elaboration of organic thin-film transistors. *Organic Electronics,* **7**, 423-427 (2006).

13. Wu, Y., Li, Y., Liu, P., Gardner, S. & Ong, B. S. Studies of Gold Nanoparticles as Precursors to Printed Conductive Features for Thin-Film Transistors. *Chem. Mater.* **18**, 4627-4632 (2006).

14. Szczech, J. B., Megaridis, C. M., Zhang, J. & Gamota, D. R. INK JET PROCESSING OF METALLIC NANOPARTICLE SUSPENSIONS FOR ELECTRONIC CIRCUITRY FABRICATION. *Nanoscale and Microscale Thermophysical Engineering* **8**, 327 (2004).

15. Kim, D., Jeong, S., Park, B. K. & Moon, J. Direct writing of silver conductive patterns: Improvement of film morphology and conductance by controlling solvent compositions. *Appl. Phys. Lett.* **89**, 264101 (2006).

16. Noguchi, Y., Sekitani, T. & Someya, T. Organic-transistor-based flexible pressure sensors using ink-jet-printed electrodes and gate dielectric layers. *Appl. Phys. Lett.* **89**, 253507 (2006).

17. Li, Y., Wu, Y. & Ong, B. S. Facile Synthesis of Silver Nanoparticles Useful for Fabrication of High-Conductivity Elements for Printed Electronics. *J. Am. Chem. Soc.* **127**, 3266-3267 (2005).

18. Chong-an Di, Gui Yu, Yunqi Liu, Yunlong Guo, Ying Wang, Weiping Wu,Daoben Zhu,. High-Performance Organic Field-Effect Transistors with Low-Cost Copper Electrodes. *Adv Mater* **9999**, NA (2008).

19. Sunho Jeong, Kyoohee Woo, Dongjo Kim, Soonkwon Lim, Jang Sub Kim, Hyunjung Shin, Younan Xia,Jooho Moon,. Controlling the Thickness of the Surface Oxide Layer on Cu Nanoparticles for the Fabrication of Conductive Structures by Ink-Jet Printing. *Advanced Functional Materials* **18**, 679-686 (2008).

20. Arias, A. C. *et al.* All jet-printed polymer thin-film transistor active-matrix backplanes. *Appl. Phys. Lett.* **85**, 3304-3306 (2004).

21. Macgregor, J. Chemical Engineering 4C03 Course Notes. (2007).

22. Swartz, C. Chemical Engineering 752 Course Notes. (2008).

23. T. H. J. van Osch, J. Perelaer, A. W. M. de Laat,U.S.Schubert,. Inkjet Printing of Narrow Conductive Tracks on Untreated Polymeric Substrates. *Adv Mater* **20**, 343-345 (2008).

Chapter 4

A Novel Method for the Fabrication of Defect-Free Inkjet Printed Source and Drain Electrodes with >10μm Channel Length

This part of work has been organized into a paper to be submitted to Nature - Materials. It has been submitted to Xerox for review to obtain permission to publish.

4.1 Introduction

4.1.1 The Challenge of Decreasing Channel Length

The preceding two chapters have demonstrated that inkjet printing is an excellent method for the fabrication of source and drain electrodes for organic thin film transistor (OTFT) devices. This study has shown that through optimization of printer settings and ink formulation one can inkjet print lines which are very narrow, have excellent film uniformity, and are highly conductive. This study has also shown effective methods for reducing the channel length of these devices through manipulating the ink viscosity. Although this method has yielded excellent results, further work in this area is required if inkjet printed OTFTs are to compete with traditional inorganic thin film transistors.

The channel length is an important parameter for a number of reasons. It is the distance which charge carriers must travel between the source and drain electrodes. Clearly the shorter the distance, the more responsive and higher performing the device will be. Smaller channel length also allows for decreased overall device dimensions,

which in turn allows for more individual transistors to be placed in a certain area. This allows for higher powered and more complex devices to be fabricated.

Traditionally, various methods such as photolithography, ion sputtering and chemical etching are used to create very narrow channel lengths. Unfortunately these methods are very complex, expensive and often require high pressure, temperature or other harsh environments. Other groups have demonstrated the use of lasers to ablate a channel into a single electrode.[1, 2] However this is costly, complicated and not compatible with a roll-to-roll fabrication system. Clearly these are not compatible with the low cost and simple fabrication methods required for OTFT fabrication.

One method which has generated some interest is the use of surface energy driven self alignment. In this method, patterns of low surface energy are applied to a substrate.[3] These areas of low surface energy drive inkjet printed ink into preformed patterns, allowing feature sizes of less than 1μm to be obtained. Unfortunately this pre-patterning technique still requires some form of lithography. As an alternative, Sirringhaus *et al.*[4] have demonstrated a self alignment technique which can be used to obtain sub micrometer channel lengths. In this technique, a single electrode is printed and surface-modified with a fluorinated monolayer. When a second electrode is printed such that it slightly overlaps the first, the low surface energy of the modified original electrode causes it to dewet from the surface, forming a very narrow gap. Although this method is simpler than others, it still requires an undesirable intermediate processing step for the modification.

4.1.2 Purpose of this Study

In this study, we sought to develop a self alignment technique for fabricating source and drain electrodes in OTFT devices which requires no intermediate processing steps and results in very reproducible channel lengths as low as 10μm. This method uses a hydrophobic boundary around printed electrodes which is formed during the printing process. Ink subsequently printed in the vicinity of the original electrode is repelled by this boundary creating a narrow channel. Furthermore, this self alignment method compensates for small printing errors or irregularities in the original printed electrode allowing for transistor arrays to be printed with very narrow channel length distribution.

4.2 Materials and Methods

For this study, a silver nanoparticle ink developed at the Xerox Research Center of Canada was used. These nanoparticles have an average diameter of 5nm and are capped with hexadecylamine to increase their stability in solution. For printing, these silver nanoparticles are dispersed in a mixture of dodecane and terpineol. The exact formulation of the ink was 2 parts silver nanoparticles with 2 parts dodecane and 1 part terpineol (by weight).

The surface modification agent used for this study was the hexadecylamine used to stabilize the silver nanoparticles. When in solution, an equilibrium is reached between stabilizer adhered to the silver nanoparticles and free stabilizer. Free stabilizer is able to adhere to the plasma cleaned glass, which drastically reduces its surface energy. To demonstrate this, plasma cleaned glass was dip coated with a 3% hexadecylamine

solution in toluene and allowed to dry. As shown in figures 4.1a and b, the water contact angle on the modified substrate is significantly higher than that on the plasma cleaned glass (78.3° and 25°, respectively) confirming that hexadecylamine was indeed able to lower the surface energy of the glass.

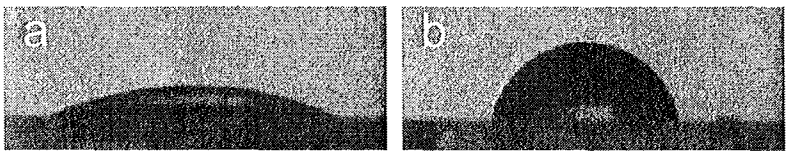

Figure 4.1: The water contact angle of plasma cleaned glass (a) is shown to increase from 25° to 78° when the surface is modified with hexadecylamine (b).

Glass substrates used for printing were washed using isopropyl alcohol, plasma cleaned for 3 minutes under air, rinsed with deionized water, rinsed with IPA, then dried with compressed and filtered air. Some substrates were then modified further by first dip coating in a 3% solution of hexadecylamine in toluene then drying at 60 °C for 30 seconds.

To print source and drain electrodes, a Dimatix DMP-2800 drop-on-demand inkjet printer equipped with a 10pL print head was used. For printing of silver nanoparticle, ink the substrate was heated to 60 °C. Drop velocity was set to 5 m/s by controlling the nozzle voltage.

Channel lengths were characterized using an optical microscope equipped with software which contained digital calipers. Device fabrication was characterized using a Keithly 3-point semiconductor testing system.

4.3 Results and Discussion

4.3.1 Scheme for Self Alignment Technique

Our method takes advantage of the dynamics of a droplet impacting a solid surface during printing. Upon impact, the kinetic energy contained within the droplet drives it to spread to some maximum radius R_m after which the surface tension of the ink and the surface energy of the substrate drive the droplet to recede to some final radius, R_f. We hypothesized that it may be possible to include a surface modification agent in the ink which would modify the substrate during this spreading, resulting in a hydrophobic boundary surrounding any printed feature. This hydrophobic boundary would then repel any ink subsequently deposited in the proximity of the original printed feature, resulting in a self aligned channel. A schematic of this method is illustrated in figure 4.2.

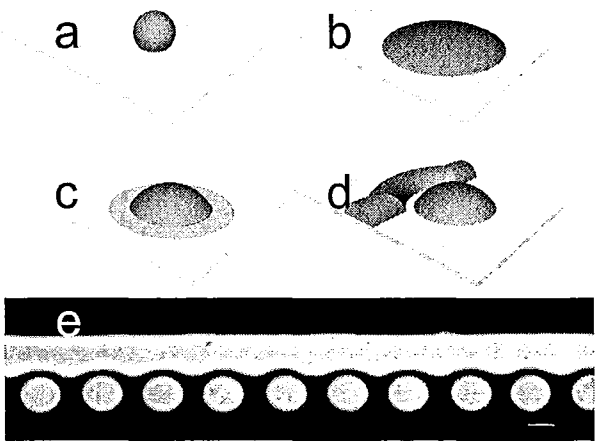

Figure 4.2: Schematic illustrating the method used for self alignment. Droplets ejected from the inkjet printer impact the surface (a) and spread to a maximum radius R_m (b). The surface tension of the ink and the surface energy of the substrate then cause the ink to recede to some final radius R_f during which hexadecylamine is deposited on the substrate (c). Subsequent ink deposited in the proximity of the original feature is repelled

by the hydrophobic boundary layer (d). This repulsion is evident in the optical microscope image shown (e).

4.3.2 Verification of Substrate Modification

The ability of hexadecylamine to create a low surface energy boundary around electrodes through the inkjet printing process was demonstrated by printing two silver lines 5mm apart. A 4μm droplet of water was then placed between the lines. This water spread easily on the plasma cleaned glass between the lines but was held a distance of 50μm away from the printed lines. This confirmed that a hydrophobic boundary around the electrode was indeed created during the printing process. This can be seen schematically in figure 3a and in an image taken from an optical microscope in figure 4.3b.

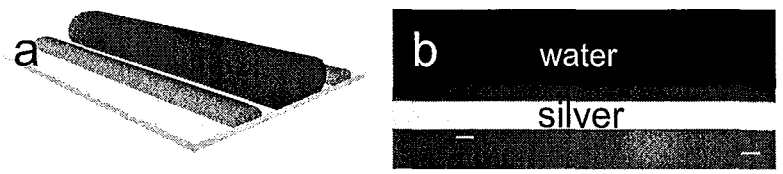

Figure 4.3: To show that free hexadecylamine within the silver nanoparticle ink also modified the surface, two lines were printed 5mm apart and 4μL of water was dropped between them (a). It is evident from the optical microscope image (b) that a 50μm hydrophobic boundary exists around the printed silver.

4.3.3 Fabrication of Source and Drain Electrodes with Self Aligned Channel

Having demonstrated that our method effectively creates a hydrophobic boundary surrounding the printed silver nanoparticle features, we then sought to demonstrate that

this could be useful for fabrication of source and drain electrodes with very small channel length. Two lines were printed such that their ends overlap for 500 μm, with the second line being printed immediately after the first was completed (approximately two seconds later). It is evident in figure 4.4a that the second line was clearly repelled by the first line, resulting in a very narrow (12 μm) channel. This result was found to be consistent and reproducible. Importantly, no additional delay was required to allow the hexadecylamine to adhere to the glass. This allows for rapid, roll to roll fabrication of these electrodes. To demonstrate that this self alignment was indeed caused by selective surface modification, the same pattern was printed on glass substrates which had been previously modified with hexadecylamine. As can be seen in figure 4.4b, no self alignment is observed in this case.

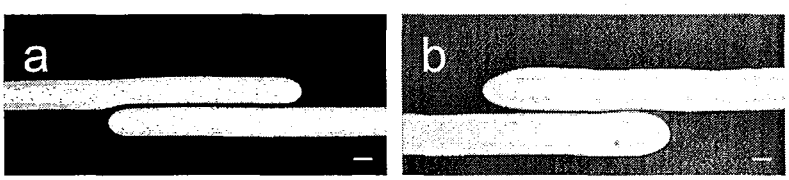

Figure 4.4: When overlapping silver is printed on plasma cleaned glass it is evident that this hydrophobic boundary causes the second electrode to be repelled creating a narrow channel (a). When the same two electrodes are printed on hexadecylamine modified glass no repulsion is seen (b).

4.3.4 Demonstration of Improved Channel Length Reproducibility

A 10x10 array of source and drain electrodes was then printed using this new ink formulation with a commercial ink containing no hexadecylamine as a control experiment for comparison. These can be seen in figures 4.5a and b. The channel lengths of the 100 transistors in these arrays were measured at three locations for each

transistor. These measurements were plotted as histograms, shown in figure 4.5c and d. It is clear that the arrays printed using our new ink formulation showed greatly reduced channel length distribution. This is due to the self correcting attributes associated with the self alignment technique. Misfired droplets which occurred during printing had little influence since the subsequent printed features self-aligned a constant distance away from them, allowing for a consistent channel length in spite of printing errors.

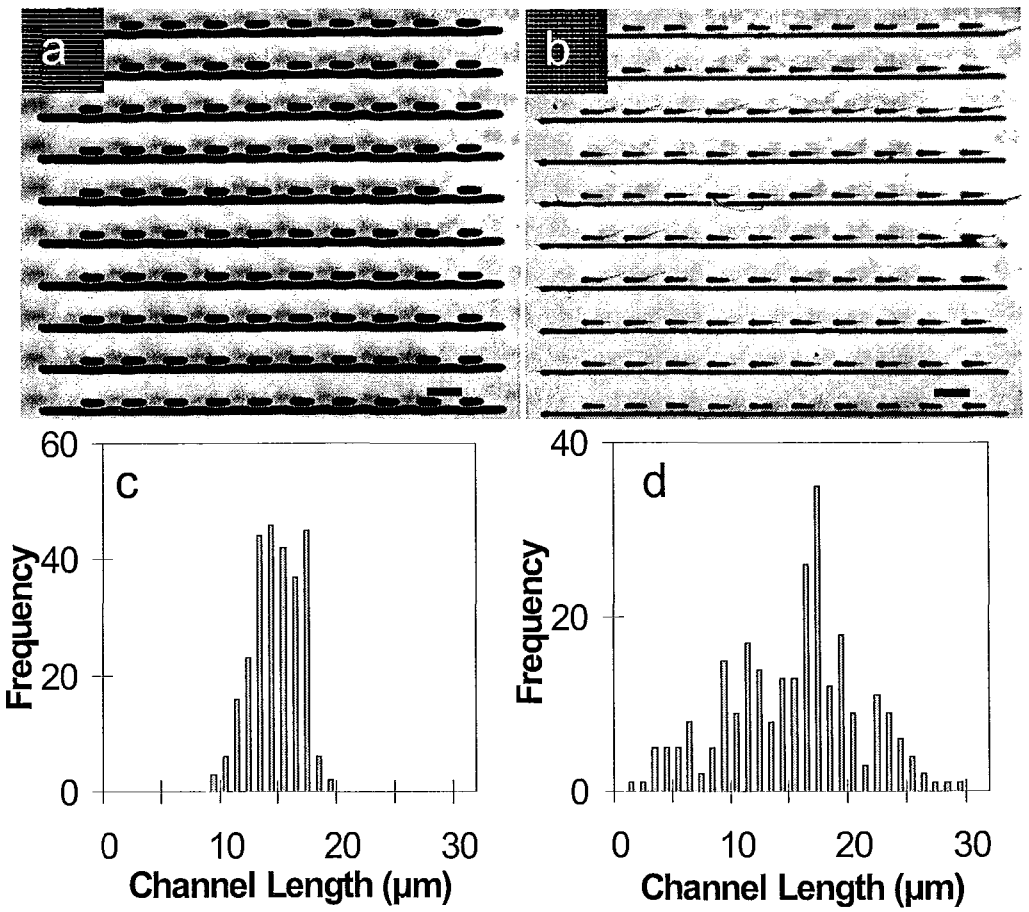

Figure 4.5: Optical microscope images of 10x10 transistor arrays printed using our new self aligning ink (a) and a commercial ink (b). Histograms showing distribution of channel lengths for transistors printed with new ink (c) and commercial ink (d). Scale bar in (a) and (b) indicates 300µm.

4.3.5 Fabrication of OTFT Devices

As already discussed, the use of this new method for fabricating self-aligned source and drain electrodes causes the substrate between the electrodes (the channel) to be modified with hexadecylamine. In order for this method to be useful for OTFT fabrication, it is necessary that the hexadecylamine in the channel not detract from the device performance. Previous work has shown that modification of the substrate onto which the semiconductor is deposited can have a very significant influence on device performance. Specifically it has been shown that hydrophobic modifications can cause a large improvement in the mobility of devices. For this reason, it was expected that this new method would, in fact, improve device performance. To investigate this, an array of 50 OTFTs was fabricated using this new method for inkjet printing source and drain electrodes. These electrodes were printed onto heavily doped n-type silicon (gate) with a 200nm SiO_2 layer (dielectric). After annealing, poly(3,3'''-didodecylquarter-thiophene) (PQT–12) was inkjet printed into the channel. These devices were found to have an average mobility of 0.02 cm^2/Vs. Previous reports have shown the mobility of devices fabricated on unmodified SiO_2 to be 0.0004 cm^2/Vs[5] indicating that our process improves the device performance by nearly two orders of magnitude. Furthermore, when the silicon wafer was plasma cleaned after source drain fabrication (to remove hexadecylamine) then modified with octyltrichlorosilane (OTS–8) and octanethiol, the mobility was improved to an average of 0.07cm^2/Vs with some devices showing mobility as high as 1.0cm^2/Vs and on/off ratios of 10^6.

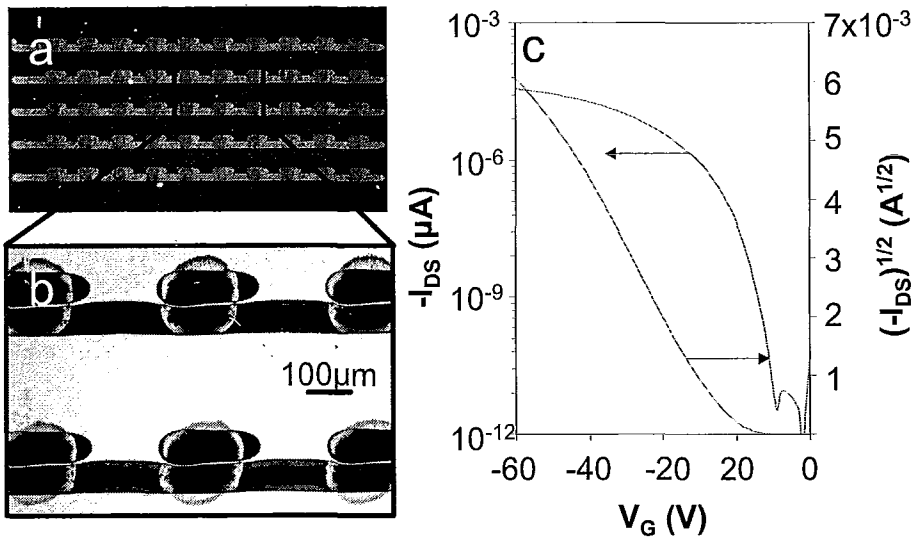

Figure 4.6: 10x5 OTFT array fabricated using inkjet printed silver source and drain electrodes and inkjet printed PQT–12 semiconductor (a). When magnified one can see the narrow and consistent channel achieved using this printing method (b). Shown is the drain current vs. gate voltage curve for a device fabricated on OTS–8 modified substrate. Devices fabricated in this manner showed very high mobility and on/off ratio.

4.4 Conclusion

Our work has demonstrated a facile method for fabrication of source and drain electrodes with very reproducible narrow channel length without the need for any intermediate processing steps. The use of hexadecylamine as a stabilizer for silver nanoparticles allows a hydrophobic boundary around electrodes to be formed during the printing process. This boundary repels subsequently deposited ink to a consistent distance from the original electrode. Since this method relies on self alignment, it is also able to automatically compensate for small printing errors, allowing for large defect-free source drain arrays to be printed with a very narrow distribution of channel length.

Furthermore we have demonstrated that electrodes fabricated with this method can be used to fabricate OTFT devices with very high mobility and on/off ratio. This study takes a large stride towards the development of roll-to-roll all inkjet printing fabrication of OTFT devices.

4.5 References

1. Ko, S. H., Chung, J., Pan, H., Grigoropoulos, C. P. & Poulikakos, D. Fabrication of multilayer passive and active electric components on polymer using inkjet printing and low temperature laser processing. *Sensors and Actuators A: Physical* **134**, 161-168 (2007).

2. Ko, S. H. et al. Laser based hybrid inkjet printing of nanoink for flexible electronics Ser. 5713, SPIE, (2005).

3. Wang, J. Z., Zheng, Z. H., Li, H. W., Huck, W. T. S. & Sirringhaus, H. Dewetting of conducting polymer inkjet droplets on patterned surfaces. *Nat Mater* **3**, 171-176 (2004).

4. Zhao, N. *et al.* Self-aligned inkjet printing of highly conducting gold electrodes with submicron resolution. *J. Appl. Phys.* **101**, 064513 (2007).

5. Wu, Y. *et al.* Controlled orientation of liquid-crystalline polythiophene semiconductors for high-performance organic thin-film transistors. *Appl. Phys. Lett.* **86**, 142102 (2005).

Chapter 5

Contributions, Perspective and Recommendations for Future Research

5.1 Contributions to the Field

This work has contributed to the field of printed organic thin film transistors in a number of ways. Here we investigated the inkjet printing of conductive inks for fabrication of the source and drain electrodes of these devices. For this purpose, silver based inks have thus far proven to be the best option Gold based inks have proven to be prohibitively expensive and copper based inks still require a great deal of material development before they become viable in devices. With regard to silver inks, there are generally two forms used – silver precursor inks and silver nanoparticle inks.

Previous to this study, the majority of research in this field had been performed from a material science perspective. This current work has approached this study from an engineering perspective with the goal of optimization and improvement of the inkjet printing process. As a result of this work, the resolution of the printing process was greatly improved for electrodes fabricated from both silver precursor and silver nanoparticle inks. The line width and channel length of source and drain electrodes fabricated using silver precursor ink were 40μm and 50μm, respectively. Line width and channel length for electrodes fabricated using silver nanoparticle ink were 50μm and 40μm, respectively. Furthermore, these electrodes could be printed with an excellent film thickness uniformity – a trait which is very desirable in these applications.

This work has made several significant contributions to this field. These are outlined below.

5.1.1 Improved Understanding of the Influence of Dot-to-Dot Spacing, Substrate Temperature, Surface Energy, and Ink Properties on Inkjet Printed Films

Prior to this work, the majority of research concentrating on inkjet printing fabrication of conductive components for OTFTs had focused on controlling film morphology and uniformity via the solvent composition of the ink. This neglected several important aspects of inkjet printing and left many questions unanswered about the influence of other key variables. This study has addressed such questions and has established good understanding of the influences of both individual variables and their interactions.

It was found during this study that solvent composition not only had a strong influence on film uniformity, but also on printed line width. This is an important discovery, as it allows for an additional degree of freedom when attempting to improve printing resolution. The resolution was also found to be influenced by dot-to-dot spacing, as was intuitively expected, as well as by ink viscosity and substrate surface roughness.

It was also found that film uniformity could be optimized via controlling the dot-to-dot spacing. It was found that the width of the line (controlled by dot-to-dot spacing) had a strong influence over the migration of solute in the ink during annealing. This is the first time such a correlation has been made.

5.1.2 Optimization of Inkjet Printing Process for Fabrication of Electrodes with Silver Nanoparticle Ink

A major portion of this work was devoted to optimization of the printing process for fabrication of source and drain electrodes from silver nanoparticle ink. Although many groups have demonstrated successful inkjet printing of silver nanoparticle inks, none had shown an effective and thorough method for optimization of this process.

Using data acquired in the previous portion of this work, five variables were chosen as having a major influence over the printing process. These variables were silver nanoparticle mass fraction, solvent ratio in the ink, substrate surface energy, substrate temperature, and dot-to-dot spacing. The design of experiments (DOE) method was used to derive a set of experimental runs such that the results would allow us to elicit the independent influence of each variable on the process as well as the influence of their interactions on the system.

The above experiments resulted in a set of mathematical equations which could be used to approximate the center-to-edge height ratio, line width or line thickness based on the values of five variables listed above. These equations were non-linear and complex, and so a non-linear optimization program was written such that the variable settings that would yield optimal line width, line thickness and center-to-edge height ratio could be determined. The constraints used in this program were derived based on the conductivity data acquired from the experiments. This allowed for the optimal variable setting to be obtained.

This portion of the work represents a highly valuable contribution to this field for two reasons. Firstly, it allowed for a robust optimization of a process which is already very industrially relevant. Inkjet printed silver nanoparticle ink is one of the most promising methods for fabricating electrodes. Having this process optimized allows the yield and reliability of this process to increase. Secondly, this portion presented an ideal method for optimizing the inkjet printing process of all other components for OTFTs, as well as other inkjet printing fabrication projects.

5.1.3 Development of Method for Defect Free Inkjet Printing of Source and Drain Electrodes with Self-Aligned and Very Narrow Channel

Although only a small portion of this work, perhaps the most important contribution to the field is the development of the method for the fabrication of self aligned source and drain electrodes which requires no intermediate processing steps. One of the greatest challenges facing the inkjet printing process is methods for printing electrodes with a very narrow channel. This is difficult because ejected droplets spreading upon impact on the surface create a limit to the channel length when using inkjet printing.

Here, we presented a mechanism for overcoming this obstacle using self-alignment. By using a silver nanoparticle ink containing free alkylamine stabilizer, a hydrophobic boundary is created around the first printed electrode. This boundary is formed due to the alkylamine adhering to the plasma cleaned glass when the ink spreads and recedes upon impact. The second electrode is then printed such that it overlaps the first one. However this hydrophobic boundary repels the ink resulting in a very narrow and uniform channel.

Because this method relies on self-alignment, it also automatically corrects slight printing errors, allowing for large transistor arrays to be printed with a very small distribution of channel length. Furthermore this process requires no additional processing, and can be easily incorporated into a roll-to-roll process.

5.2 Perspective

The field of printed organic thin film transistors holds a great deal of potential. By allowing for low-cost low-energy fabrication of transistor devices on a variety of substrate materials, this field promises to revolutionize the microelectronics industry. Devices could be fabricated on flexible polymeric substrates, and could be incorporated into low-end disposable applications without significantly increasing their costs.

One of the greatest obstacles in the path towards the commercialization of this technology lies with fabrication methods. Although inkjet printing has been shown to be an excellent candidate for this purpose, there are many challenges which must first be overcome. Firstly, a thorough and robust understanding of the process must be obtained such that the process can be easily optimized or modified with little down time. Secondly, the process must allow for adequate resolution such that these devices can successfully compete with traditional inorganic devices. Thirdly, and most significantly, this fabrication method must allow for successful integration of all components such that devices have high performance and yield.

This project has demonstrated that the first two obstacles can be overcome. By completing an engineering based optimization of the inkjet printing process, a complete

and thorough understanding of the inkjet printing process was obtained. The influence of several important variables over key output variables is ascertained. Furthermore, the inkjet printing process for fabrication of source and drain electrodes from silver nanoparticles was optimized such that sufficient resolution and performance was obtained. Resolution was further improved via the use of a novel one-step inkjet printing and self-assembly method for source and drain electrode fabrication.

One of the greatest remaining challenges is the development of methods for improving the integration of the semiconductor, dielectric, source and drain electrodes. Although there are many challenges involved in achieving this, the author is confident that it is very possible. As a result of this work, the promise of all-inkjet printed OTFTs has taken several steps towards becoming reality.

5.3 Recommendations for Future Research

5.3.1 Optimization of the Inkjet Printing Process for Fabrication of Dielectric and Semiconductor Components

In order for printed organic thin film transistors to become a reality it is necessary that all components of OTFTs be able to inkjet printed successfully. Although some groups have demonstrated inkjet printing of semiconductors, a full optimization which examines methods of improving resolution, registration and molecular orientation has not been completed. Furthermore, an efficient method for printing the dielectric must also be established. This layer is critical to the performance of the device, as it is involved in controlling the molecular orientation of the semiconductor and also has a strong influence

over the threshold voltage of the device. Currently, very few groups have demonstrated successful inkjet printing of this component. The difficulty here lies in the need for a dielectric layer which is as thin as possible while remaining defect-free. Unfortunately, as thickness decreases the probability of the presence of 'pinholes' in the layer increases. It may be that spin coating or dip coating would be a viable alternative, as these techniques are able to yield more reliable thickness and uniformity. However if these methods are to be adopted, novel techniques need to be devised to integrate them into the roll-to-roll process.

5.3.2 Optimization of Complete Device Fabrication

Despite all of the great successes that have been realized in the field of printed organic thin film transistors, one major milestone which has yet to be reached is the demonstration of a high performance device fabricated entirely from inkjet printing. Although some groups have demonstrated devices which have many components inkjet printed, all of these have relied on some form of intermediate surface modification or etching to provide the required resolution and performance. There are a number of reasons why this has proven to be so difficult.

One major hindrance is the electrical incompatibility between silver electrodes and organic semiconductors. Although silver is inexpensive and relatively stable, its work function is mismatched to that of most organic semiconductors. For this reason, the electrodes are often modified with some sort of alkylthiol group after annealing. These alkylthiols have been shown to greatly improve the compatibility between these

components, and thus greatly increase the performance of the device. Unfortunately, this is a step which requires additional processing away from the inkjet printing. This may be overcome via the addition of organic surface modifiers to the silver nanoparticle ink. These modifiers would migrate to the surface during annealing, performing essentially the same function as the alkylthiols. Alternatively, silver nanoparticles could be fabricated with different stabilizers which could bridge the incompatibility. This is an essential step towards obtaining all-inkjet printed OTFTs.

Another great challenge lies in depositing the dielectric layer such that it is very thin yet also defect free. Furthermore it is necessary that this layer have as little surface roughness as possible such that subsequent layers can be easily deposited on top of it. This is very difficult to do using inkjet printing, as there is always a small degree of solute migration and droplet splashing which occurs. During the course of this study, some work was performed in this area, and it was found that by adding certain high boiling-point components the surface roughness could be adequately controlled. Although this was not thoroughly investigated here, some promising results were shown. Alternatively, as mentioned above, methods such as spin coating or dip coating could be used. The downside to these methods is they use more material than is required, and they complicate the overall device fabrication process by adding an additional step. However, this is definitely an area that is ripe for investigation.